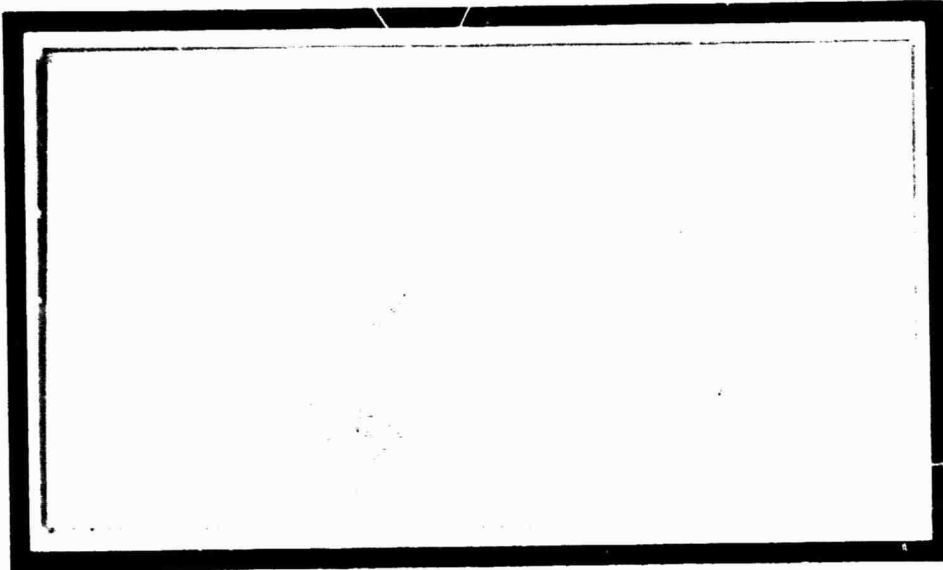


General Disclaimer

One or more of the Following Statements may affect this Document

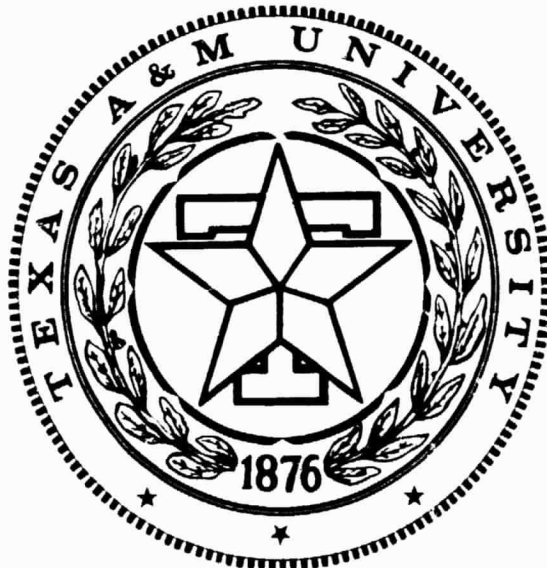
- This document has been reproduced from the best copy furnished by the organizational source. It is being released in the interest of making available as much information as possible.
- This document may contain data, which exceeds the sheet parameters. It was furnished in this condition by the organizational source and is the best copy available.
- This document may contain tone-on-tone or color graphs, charts and/or pictures, which have been reproduced in black and white.
- This document is paginated as submitted by the original source.
- Portions of this document are not fully legible due to the historical nature of some of the material. However, it is the best reproduction available from the original submission.

CR 167 840
c.1



(NASA-CR-167840) PROCEEDINGS OF THE
NASA/MPRIA WORKSHOP: PATTERN RECOGNITION
Progress Report (Texas A&M Univ.) 237 p
HC A11/MP A01 CSCI 09B

M83-23073
THRU
M83-23082
Unclas
09828
G3/63



DEPARTMENT OF MATHEMATICS

TEXAS A&M UNIVERSITY
COLLEGE STATION, TEXAS

PROCEEDINGS OF THE NASA/MPRIA WORKSHOP:
PATTERN RECOGNITION

Texas A&M University
College Station, Texas
February 3-4, 1983

Prepared for
Earth Resources Research Division
NASA/Johnson Space Center
Houston, Texas 77058

by

L. F. Guseman, Jr.
Principal Investigator
Department of Mathematics
Texas A&M University
College Station, Texas 77843

under

NASA Contract NAS 9-16664

"Mathematical Pattern Recognition
and Image Analysis Program"

TABLE OF CONTENTS

Introduction - L. F. Guseman, Jr.	1
Agenda	3
Participants and Other Attendees	5
Papers:	
Textural Edge Detection and Sensitivity Analysis K. Sam Shanmugan	7
The Influence of Sensor and Flight Parameters on Texture in Radar Images - V. S. Frost, K. S. Shanmugan, and J. C. Holtzman	27
Aspects of Simulation for Rectification Studies E. M. Mikhail and Fidel D. Paderes, Jr.	59
Image Matching Using Hough Transforms Larry S. Davis and Azriel Rosenfeld	73
Subpixel Registration Accuracy and Modelling Laveen N. Kanal	109
Improving Spatial Modelling in Remote Sensing A. H. Strahler, W. R. Tobler and C. E. Woodcock	159
Approaches to Image Registration and Segmentation Grahame Smith	187
Reduction and Utilization of Speckle Noise in SAR Imagery Daniel Held	197
Progress in the Scene-to-Map Registration Task David D. Dow	207
Appendix	223
Fundamental Research Data Base	225

INTRODUCTION

by

L. F. Guseman, Jr.

The organizational meeting for the NASA Fundamental Research Program in "Mathematical Pattern Recognition and Image Analysis" (MPRIA) was held at the NASA/Johnson Space Center in August, 1982. At this meeting each of the fifteen principal investigators briefly outlined the goals of their particular proposed research efforts. Most of the efforts (those outside NASA) had just been funded (July 16, 1982), and investigations were just getting underway.

In order to gain a better understanding of and stimulate discussions between the individual research efforts, it was decided to conduct two technical workshops at Texas A&M University about six months into the program. The first workshop was held January 27-28, 1983 and consisted of investigators from the "Mathematics/Statistics" areas. The second workshop was held February 3-4, 1983 and consisted of investigators from the "Pattern Recognition" areas.

Each of the workshops was conducted in an informal manner. Most of the time was spent in lively technical discussions about each of the research efforts. Additional time was spent discussing the availability of data sets. Dr. R. P. Heydorn announced the availability of a data tape that has been compiled for use by the research teams. Details concerning the content and format of the tape are discussed in the document entitled "Fundamental Research Data Base" appearing in the Appendix of these proceedings.

Agendas and lists of participants for the workshops appear in their respective Proceedings.

NASA/MPRIA WORKSHOP: PATTERN RECOGNITION

Texas A&M University
February 3-4, 1983
Room 308, Rudder Tower

Thursday, February 3:

8:00 - 8:30	Coffee and donuts
8:30 - 8:45	Opening Remarks L. F. Guseman, Jr., TAMU
8:45 - 9:15	Remote Sensing Fundamental Research Program: An Overview Howard Hogg, NASA Headquarters
9:15 - 10:30	Textural Edge Detection in the Frequency Domain K. S. Shanmugan, University of Kansas
10:30 - 10:45	Break
10:45 - 12:00	Aspects of Simulation for Rectification Studies E. M. Mikhail and Fidel Paderes, Purdue University
12:00 - 1:00	Lunch
1:00 - 2:15	Image Matching Using Hough Transforms L. S. Davis and Azriel Rosenfeld, University of Maryland
2:15 - 2:30	Break
2:30 - 3:45	Subpixel Registration Accuracy and Modelling L. N. Kanal, LNK Corporation
3:45 - 4:00	Break
4:00 - 5:15	Discussion and Symposium Planning

PRECEDING PAGE BLANK NOT FILMED

NASA/MPRIA WORKSHOP: PATTERN RECOGNITION cont.

Friday, February 4:

8:00 - 8:30	Coffee and donuts
8:30 - 9:45	Spatial Scene Modelling Alan H. Strahler, Hunter College and W. R. Tobler, UC Santa Barbara
9:45 - 10:15	Break
10:15 - 11:30	Approaches to Image Registration and Segmentation Grahame Smith, SRI International
11:30 - 1:00	Lunch
1:00 - 2:15	Reduction and Utilization of Speckle Noise in SAR Imagery Daniel N. Held, Jet Propulsion Laboratory
2:15 - 2:30	Break
2:30 - 4:00	Progress in the Scene-to-Map Registration Task David D. Dow, National Space Technology Labs

NASA/MPRIA WORKSHOP: PATTERN RECOGNITION

February 3-4, 1983

Participants and Other Attendees:

L. S. Davis
Computer Vision Laboratory &
Computer Science Center
University of Maryland
College Park, MD 20742

David Dow
NASA/National Space Technology
Laboratories
Earth Resources Laboratory
NSTL Station, MS 39529

L. F. Guseman, Jr.
Department of Mathematics
Texas A&M University
College Station, TX 7843

Daniel Held
Jet Propulsion Laboratory
4800 Oak Grove
Pasadena, CA 91103

Richard P. Heydorn/SG3
NASA/Johnson Space Center
Houston, TX 77058

Howard Hogg/EI.4
Chief, Earth Resources Branch
NASA Headquarters
Washington D. C. 20546

Laveen N. Kanal
L.N.K. Corporation
302 Notley Court
Silver Spring, MD 20904

R. Kent Lenington/C31
Lockheed E.M.S.Co.
1830 Space Park Drive
Houston, TX 77058

R. B. MacDonald/SG
Chief, Earth Resources Research
Division
NASA/Johnson Space Center
Houston, TX 77058

E. M. Mikhail
School of Civil Engineering
Purdue University
West Lafayette, IN 47907

Fidel D. Paderes, Jr.
School of Civil Engineering
Purdue University
West Lafayette, IN 47907

K. S. Shanmugan
Remote Sensing Laboratory
University of Kansas
Lawrence, KS 77044

Grahame Smith
Artificial Intelligence Center
S.R.I. International
333 Ravenswood Avenue
Menlo Park, CA 94025

Alan H. Strahler
Department of Geology & Geography
Hunter College
695 Park Avenue
New York, NY 10021

Muralidhara Subbarao
Computer Vision Laboratory &
Computer Science Center
University of Maryland
College Park, MD 20742

L N83 23074

D/

7

TEXTURAL EDGE DETECTION AND SENSITIVITY ANALYSIS

by

K. Sam Shanmugan

Department of Electrical Engineering and
Remote Sensing Laboratory
University of Kansas
Lawrence, Kansas 66045

PRECEDING PAGE BLANK NOT FILMED

PAGE 6 INTENTIONALLY BLANK

TEXTURAL EDGE DETECTION:

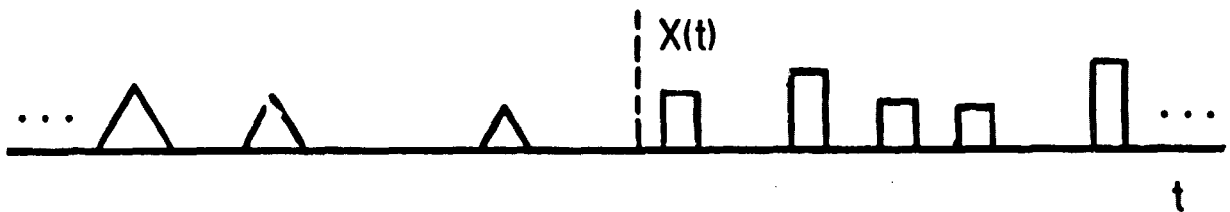
- Develop an optimum (global) textural edge detection operator based on statistical models for texture.

SENSITIVITY ANALYSIS:

- Analyze the effects of the imaging process on the textural patterns of a scene as it appears in the image -- i. e., separate scene-induced textural patterns from sensor-induced textural patterns.

TEXTURAL EDGE DETECTION

- Texture
 - Primitive Elements
 - Structural Arrangement

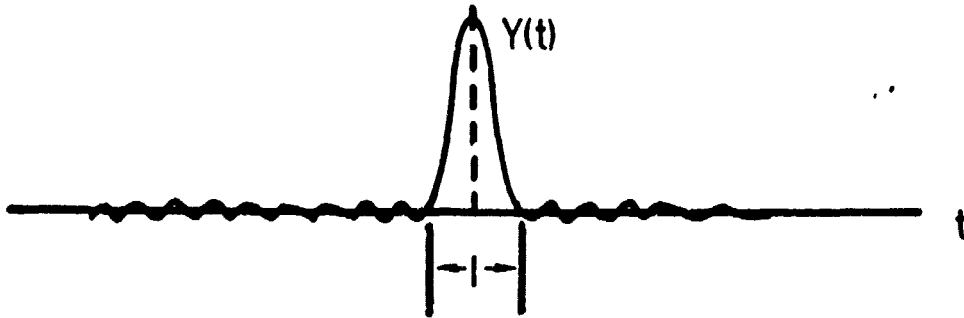
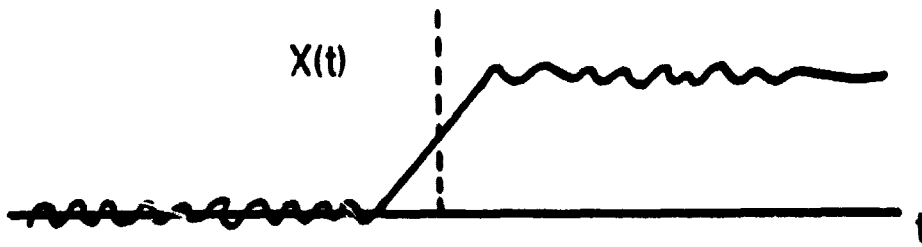


- Textural Edge Detection Operators:

- Local Operators
- Global Operators
- Optimum

- Let $X(t) = X_1(t) [1 - u(t-t_0)] + X_2(t) u(t-t_0) + n(t)$

Want to process $X(t)$ using a LTIV operator and produce $Y(t)$ that best approximates $\delta(t-t_0)$. $X_1(t)$ and $X_2(t)$ represent random process models for two textural classes that form a boundary at $t = t_0$.

OPTIMUM TONAL EDGE DETECTION OPERATOR:

Find $h(t)$ such that $\alpha = \frac{\int_{-1/2}^{1/2} y^2(t) dt}{\int_{-\infty}^{\infty} y^2(t) dt}$ is maximized,

subjected to the constraints

- (1) $|H(f)| = 0$ for $|f| > B$
- (2) $h(t)$ is LTIV

OPTIMUM TONAL EDGE DETECTION OPERATOR• Soln:

$$y(t) = a_1 \psi_1(c, t), \quad c = B/2$$

$$H(\omega) = y(\omega) / X(\omega)$$

$$\approx \omega^2 e^{-c\omega^2}, \quad |f| < B$$

(edge model used: unit step and exponential)

- An approach similar to the one described above can be used to derive an optimum textural edge detection operator.
- In order to derive an optimum textural edge detection operator we need:
 - random field models for texture
 - edge models
 - performance measure
 - frequency domain models for textural fields
 - $H(\omega) = y(\omega) / F(G_{x_1}(f); G_{x_2}(f))$

FREQUENCY DOMAIN DESCRIPTION OF
MARKOV TEXTURAL FIELD MODELS

$$X(t) = \sum_{-\infty}^{\infty} A_i p_{m_i}(t-t_i)$$

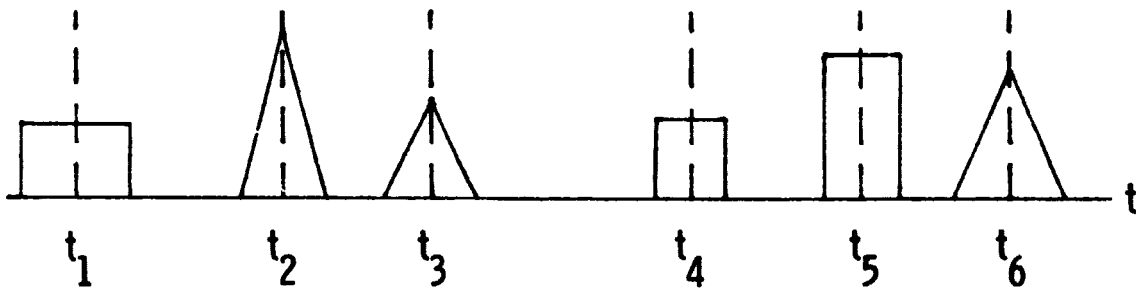
ORIGINAL PAGE IS
OF POOR QUALITY

$\{A_i\}$ = Amplitude sequence

p_1, p_2, \dots, p_N : N primitive elements

$\{m_i\}$; $m_i \in [1, 2, \dots, N]$ indicates which one of the N primitives is present at the i -th location

$\{t_i\}$: Location of the i -th primitive



• Want to find $G_X(f)$

TEXTURAL FIELD MODELSASSUMPTIONS:ORIGINAL PAGE IS
OF POOR QUALITY1. a. $\{t_i\}$ - uniformly distributed locations1. b. $\{t_i\}$ - Poisson sequence with an exponential
distribution for inter-location distance2. a. $\{A_i\}$: Constant2. b. $\{A_i\}$: Correlated sequence3. a. p_1, p_2, \dots, p_N : deterministic shapes3. b. p_1, p_2, \dots, p_N : random processes4. a. $\{m_i\}$: Independence sequence $\{m_i\}$: Homogeneous markov sequence

COMPLETED MODEL:ORIGINAL PAGE IS
OF POOR QUALITY $\{t_i\}$: uniformly distributed $\{A_i\}$: constant p_1, p_2, \dots, p_N : deterministic $\{m_i\}$: markov $P \{ \text{occurrence of } p_k \} = \pi_k$ $P \left(\text{occurrence of } p_i \text{ followed by } p_j \text{ after } n \text{ locations} \right) = p_{ij}$

$$X(t) = \sum_{-\infty}^{\infty} p_{m_i}(t - mT_s)$$

 T_s = average spacing between elements

$$\begin{aligned} G_X(f) = & \frac{1}{T_s} \sum_{n=-\infty}^{\infty} \left| \sum_{j=1}^N \pi_j S_j\left(\frac{n}{T_s}\right) \right|^2 \delta\left(f - \frac{n}{T_s}\right) \\ & + \frac{1}{T_s} \sum_{j=1}^N \pi_j \left| S_j'(f) \right|^2 \\ & + \frac{2}{T_s} \operatorname{Re} \left\{ \sum_{j=1}^N \sum_{k=1}^N \pi_j S_j'^*(f) S_k'(f) Q_{jk}(f) \right\} \end{aligned}$$

where:

$$S_k(f) = F \{ p_k(t) \}$$

$$S_k'(f) = F \left\{ p_k(t) - \sum_{j=1}^M \pi_j p_j(t) \right\}$$

$$Q_{jk}(f) = \sum_{n=1}^{\infty} p_{jk}(n) \exp(-i 2 \pi n f T_s)$$

SPECIAL CASE:ORIGINAL PAGE IS
OF POOR QUALITY

$N = 2$; $\{m_i\}$ - Independence sequence; equal probability

$$G_x(f) = \frac{1}{T_s} \sum_{n=-\infty}^{\infty} \left| p S_1\left(\frac{n}{T_s}\right) + q S_2\left(\frac{n}{T_s}\right) \right|^2 \delta\left(f - \frac{n}{T_s}\right)$$

$$+ \frac{1}{T_s} p(1-p) \left| S_1'(f) - S_2'(f) \right|^2$$

ORIGINAL PAGE IS
OF POOR QUALITY

RESEARCH PLAN:


- Generalize (2-dimensional, $t = (x, y)$; Poisson)
- Find $F(G_{x_1}(f), G_{x_2}(f))$
(Edge model)
- Test filters on simulated fields
- Develop estimation procedures, test on actual image data

TEXTURAL EDGE DETECTION

Approach:

- Define appropriate measures of performance -
What is "optimum"?
- Develop random field models for different classes
of textures (different means, covariance/co-occurrence
matrices)
- Given $X_1(t)$ and $X_2(t)$ derive the transfer function of
the optimum filter subjected to appropriate constraints
- Modify the transfer function to take into account
the presence of noise in the input image
- Find a sub-optimum filter for a wide class of
textural edges
- Test the filter on natural and synthesized textural
edges

SENSITIVITY OF TEXTURAL FEATURES

- Textural Patterns in an image 
 - scene or target induced
 - sensor induced (due to sensor transfer function, geometry, nature of the illumination, etc.)
- In a LANDSAT-type image, the textural patterns that appear in the image usually represent the textural patterns of the underlying scene (assuming that the illumination variations and shadows are minimum)
- In a SAR image of a scene with significant terrain relief, the textural patterns that appear in the image may be very different than the textural patterns in the underlying scene due to layover, shadowing, fading, etc.
- Objective of the proposed research effort is to develop mathematical models and methodologies for evaluating the effects of the imaging process on the textural patterns of a scene as it appears on the image

SENSITIVITY OF TEXTURAL FEATURES

ORIGINAL PAGE IS
OF POOR QUALITY.

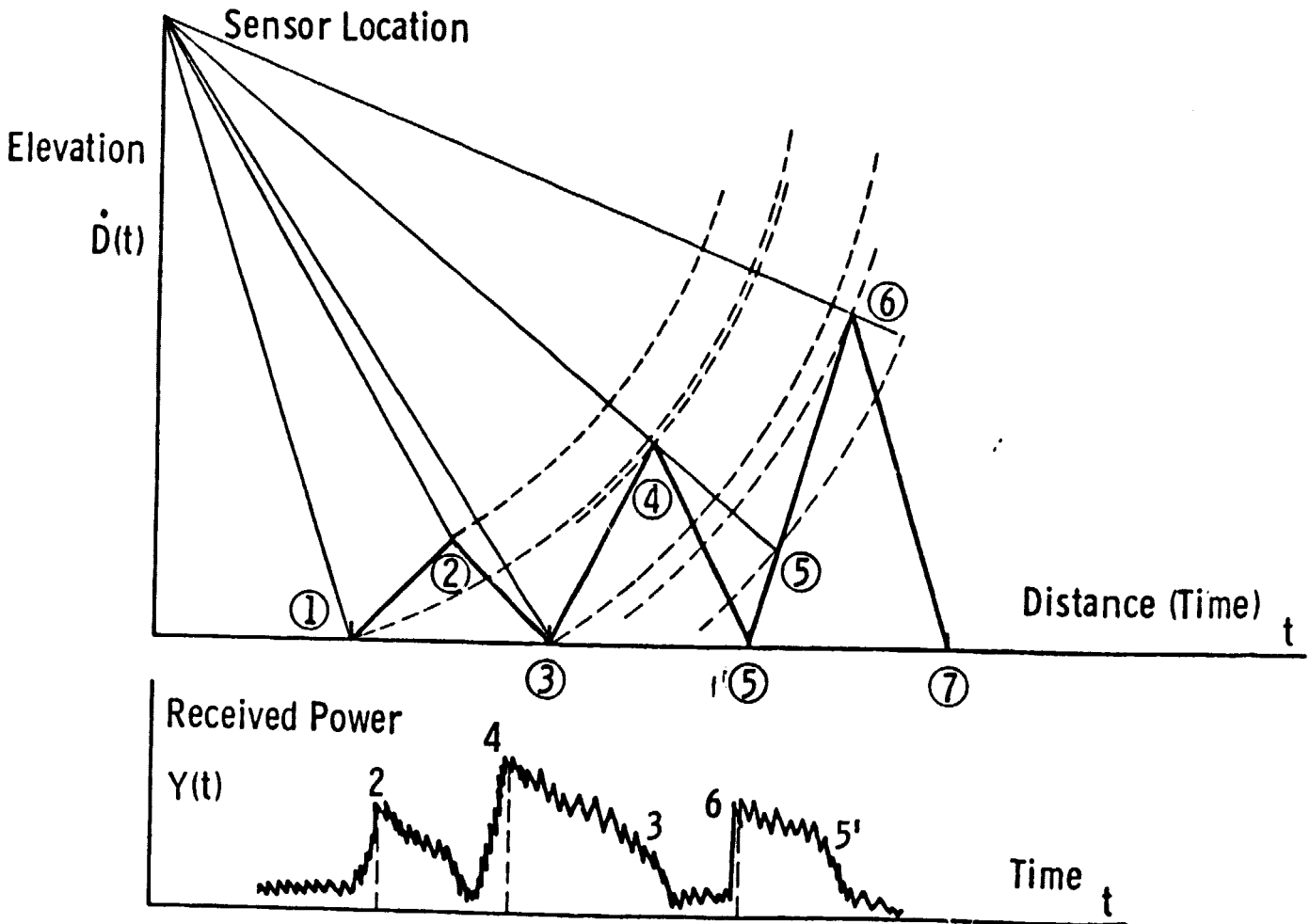
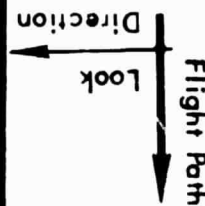
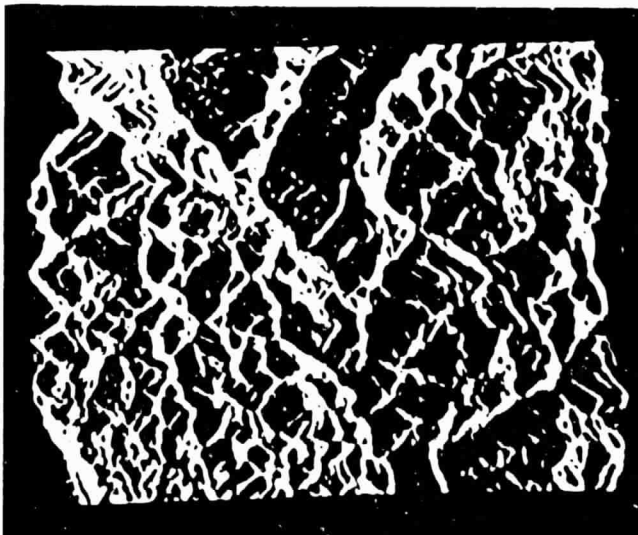
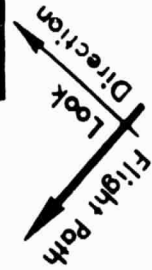
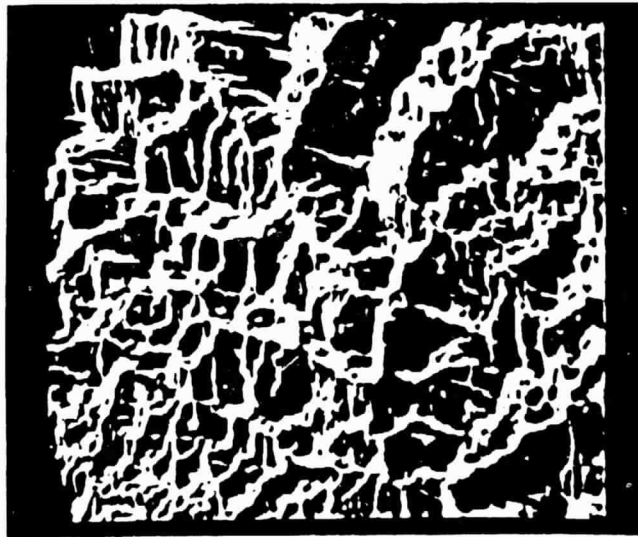
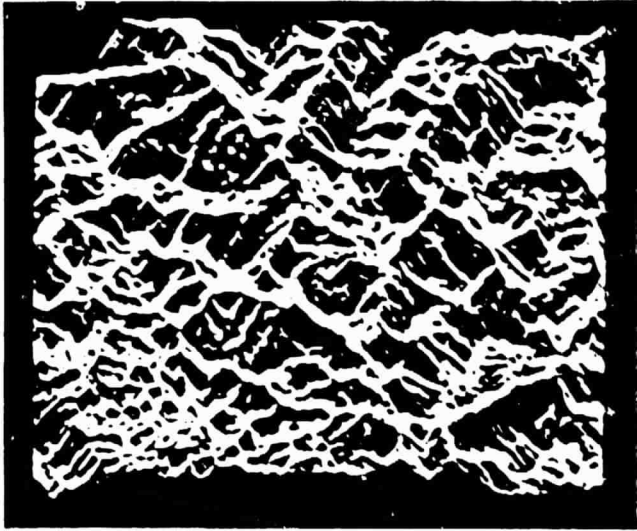
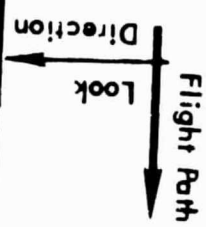
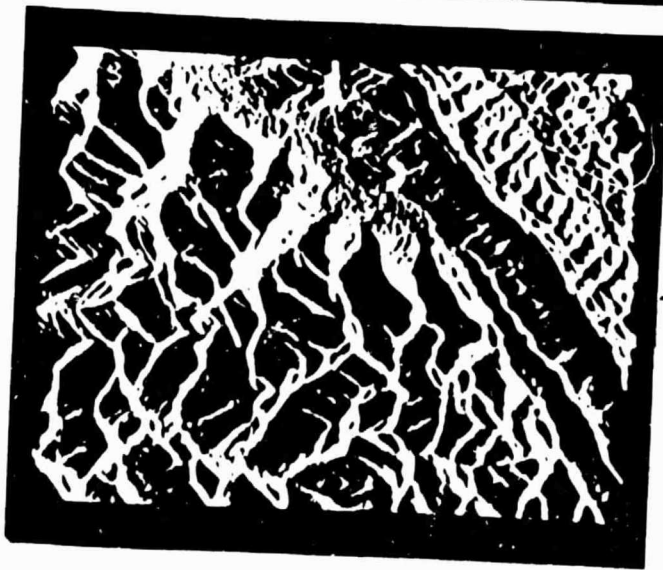
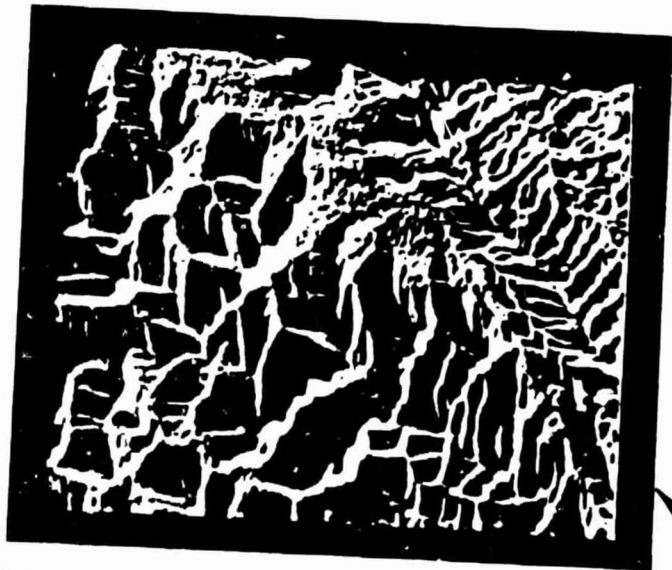
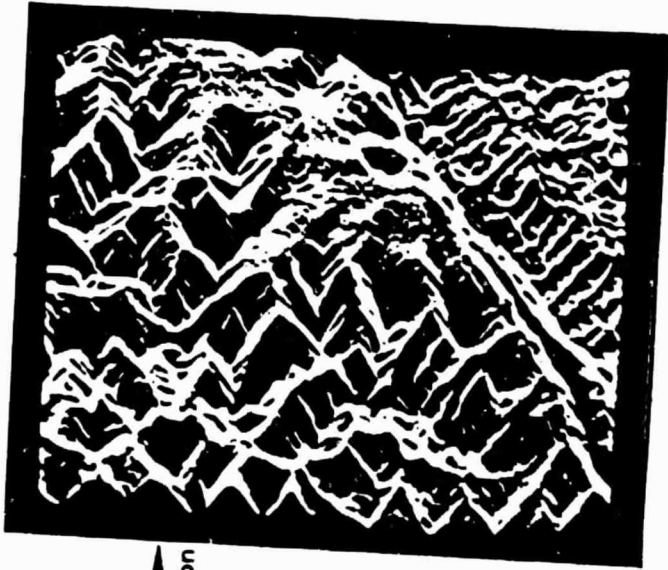
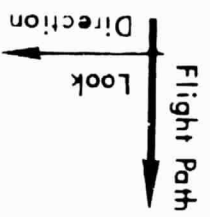
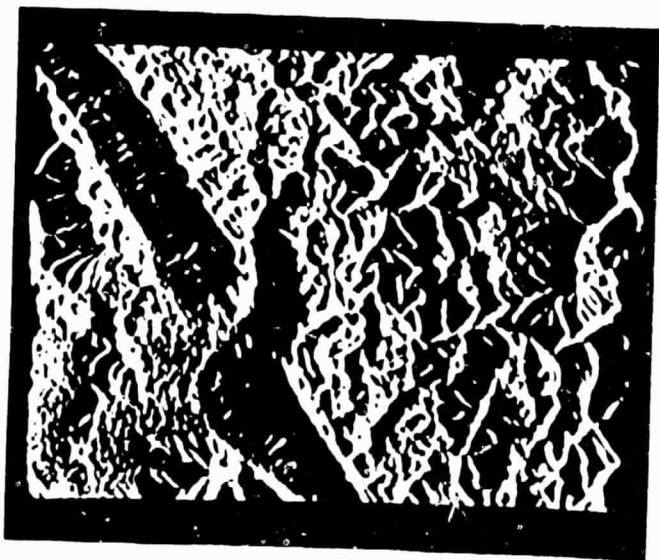
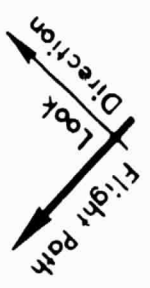
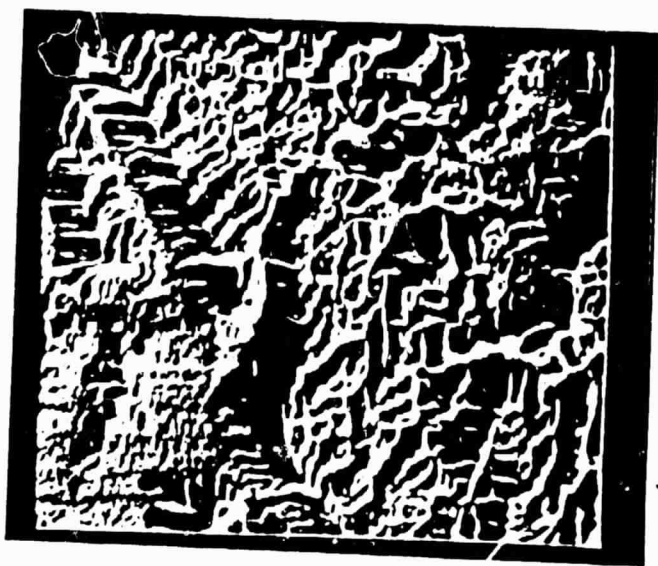
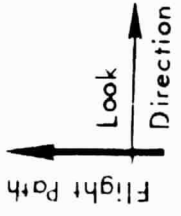
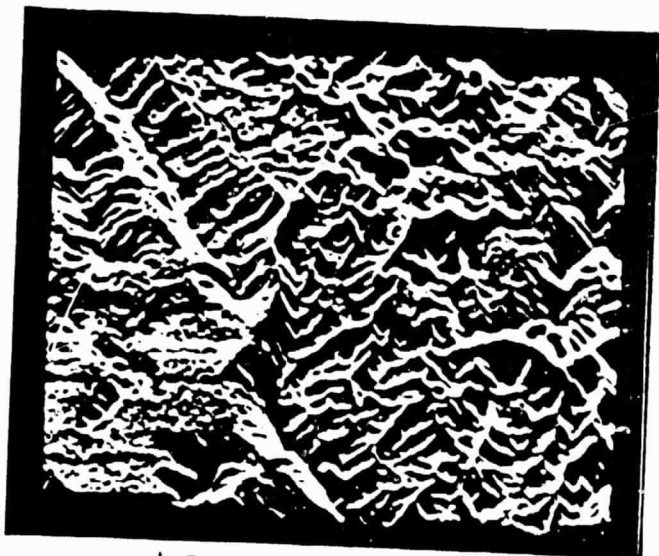


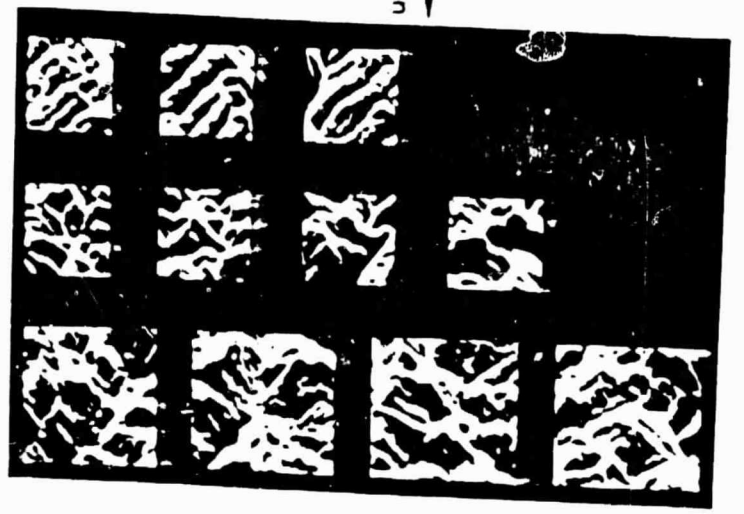
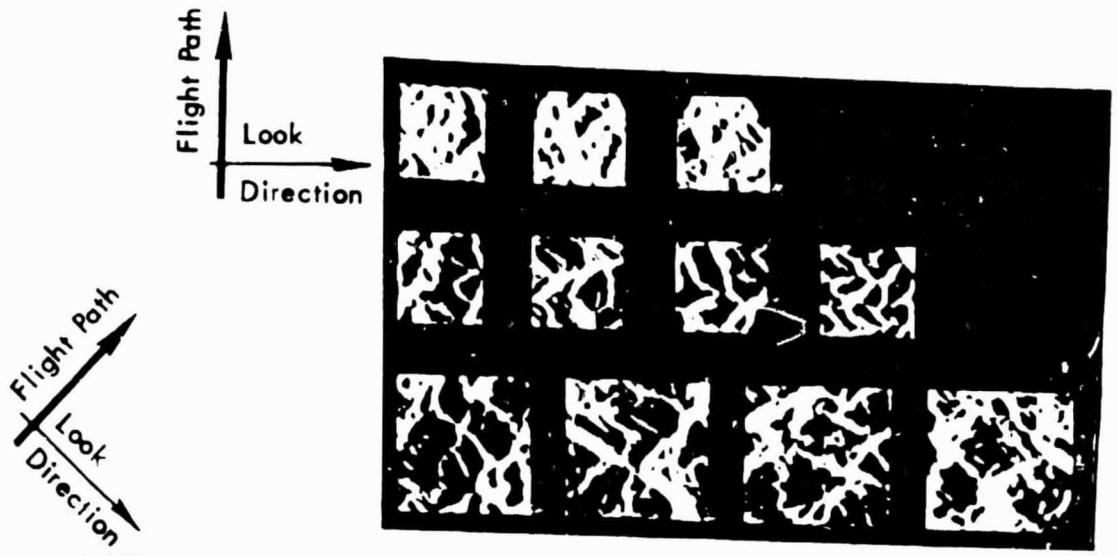
Figure 1. Simplified View of the Radar Imaging Process.







ORIGINAL PAGE IS
OF POOR QUALITY



SENSITIVITY ANALYSIS

Research Plan:

- Develop random process models of terrain elevation, and backscatter variations of typical scene categories (agricultural, forestry, urban areas, hilly and mountainous terrains, water bodies, etc.). The models will be in a parametric form, and the scene texture will be described by the parameter values and the model type.
- Develop simple parametric models for the imaging process of a SAR.
- Using the scene model and the system model, derive the textural properties of the image parametric form.
- For different scene categories, analyze the effect of imaging system parameters on the features (parameter values) of the image textural patterns.
- For different scene categories, compare the separability of the scene textures with the separability of the textural patterns of the corresponding images.
- For the cases where the comparison could not be done by analytical methods, use simulated imagery to study the effects of the imaging system.

[Paper for IEEE Trans. on Geoscience and Remote Sensing]

The Influence of Sensor and Flight Parameters
on Texture in Radar Images

V.S. Frost, K.S. Shanmugan, and J.C. Holtzman

Remote Sensing Laboratory
University of Kansas Center for Research, Inc.
Lawrence, Kansas 66045

Abstract

Texture is known to be important in the analysis of radar images for geologic applications. It has previously been shown that texture features derived from the grey-level co-occurrence matrix (GLCM) can be used to separate large scale texture in radar images. Here the influence of sensor parameters, specifically the spatial and radiometric resolution and flight parameters, i.e., the orientation of the surface structure relative to the sensor, on the ability to classify texture based on the GLCM features is investigated. It was found that changing these sensor and flight parameters greatly affects the usefulness of the GLCM for classifying texture on radar images.

PRECEDING PAGE BLANK NOT FILMED

Manuscript Received _____, Revised _____.
This work was supported by NASA under Contract No. NASA 9-16664.

1. INTRODUCTION

Spectral, textural temporal and contextual features are four important pattern elements used in human interpretation of image data in general and SAR data in particular. Spectral features describe the average band-to-band tonal variations in a multi-band image set, whereas textural features describe the spatial distribution of tonal values within a band. Contextual features contain information about the relative arrangement of image segments belonging to different categories, and temporal features describe changes in image attributes as a function of time. However, when small image areas within, say, a synthetic aperture radar (SAR) image are independently processed on a computer for automated analyses only the tonal and textural features are usually available in making decisions.

In much of the automated procedures for processing radar image data from small areas, such as in crop classification studies, only the average tonal values are used for developing a classification algorithm. Textural features are generally ignored on the basis that the poor resolution of radar imagery does not provide meaningful textural information for such applications since the areal extent of the target is usually small. However, there are many other applications such as the identification of large scale geological formations, land use patterns, etc., where the resolution is more than adequate to provide textural information. Indeed, in these applications, texture is probably the most important image feature. It was previously shown [1] that texture features derived from the grey-level co-occurrence matrix (GLCM) can be used to discriminate texture in radar images. We describe in this paper the influence of sensor and flight parameters on our

ability to quantitatively classify textures in radar images using the GLCM. The effect of spatial and radiometric resolution on texture classification was studied in one experiment. It was found that the classification was very sensitive to these sensor parameters, only the image with the best spatial and radiometric resolutions was quantitatively useful. Another experiment was conducted to determine how different flight paths, i.e., looking at the same terrain from different angles with the same sensor and incidence angle, changed the texture classification. Optical imaging systems rely on the sun to illuminate the scene and thus the sun angle becomes a factor; however, mission profiles for these sensors are usually designed to minimize this effect. For example, the LANDSAT series of sensors uses a high sun angle. On the other hand imaging radars provide their own illumination and it is not clear what effect observing the same geologic structure from different angles will have on the automated analysis.

In the following section the texture features used here to separate different surface structures are briefly described. The sensitivity of these texture features to changes in radiometric and spatial resolution is discussed next. Radar image simulation is then used to evaluate the sensitivity of GLCM texture features to changes in the orientation of the surface structure and the radar. The results of the two studies described in this paper indicate that the usefulness of textural features in automated analysis of radar images is sensitive to changes in the spatial and radiometric resolution of the system as well as the target/sensor geometry.

11. The Texture Features

The textural feature extraction algorithm employed here has been widely used [2-5] for analyzing a variety of photographic images. The procedure is based on the assumption that the texture information in an image block 'I' is contained in the overall or 'average' spatial relationship which the grey tones in the image 'I' have to one another. This relationship can be characterized by a set of grey-level co-occurrence (GLC) matrices. We describe a procedure for computing a set of GLC matrices for a given image block and define a set of numerical textural descriptors (features) that can be extracted from the GLC matrices. These textural features can be used for automated analysis and classification of blocks of radar imagery. Image texture may be viewed as a global pattern arising from a deterministic or random repetition of local subpatterns or primitives. The structure resulting from this repetition could be very useful for discriminating between the contents of the image of a complex scene. A number of approaches have been suggested for extracting features that will discriminate between different textures [2-6]. Of these approaches, it has been found that textural features derived from grey-level co-occurrence matrices (GLCM) are most useful for analyzing the contents of a variety of imagery in remote sensing, biomedical and other applications [7-11]. The GLCM approach to texture analysis is based on the conjecture that the texture information in an image is contained in the overall or average spatial relationship between the grey tones of the image.

The second-order grey-level co-occurrence matrix of an image is defined as follows. Let $f(x,y)$ be a rectangular digital picture defined over the domain $x \in [0, n_x), y \in [0, n_y), x, y \in I$. Let n_g be the number of

grey levels in f . The unnormalized, second-order GLC matrix is a square matrix \bar{P} of dimension n_g . The (i,j) -th entry in \bar{P} , denoted by \bar{P}_{ij} , is a function of the image tonal values and a displacement vector $\bar{d} = (d_1, d_2)$. The entries \bar{P}_{ij} are unnormalized counts of how many times two neighboring resolution cells which are spatially separated by \bar{d} occur on the image, one with grey tone i and the other with grey tone j . That is,

$$\bar{P}_{ij} = \# \left\{ \left((m_1, n_1), (m_2, n_2) \right) \mid f(m_1, n_1) = i, \right. \\ \left. f(m_2, n_2) = j, \text{ and } (m_2, n_2) - (m_1, n_1) = \bar{d} \right\}, \quad (1)$$

where $\#$ denotes the number of elements in the set, the indices m_1, m_2 and n_1, n_2 take on integer values in the intervals $[0, n_x)$, $[0, n_y)$. The normalized GLC matrix \bar{P} with entries p_{ij} is obtained from \bar{P} by dividing each entry in \bar{P} by the total number of paired occurrences. The definition of second-order GLC matrices can be extended to include third- and higher-order GLC matrices. While higher-order GLC matrices may be important in some applications, much of the recent work in texture analysis has been based on second-order GLC matrices.

The second-order GLC matrices are computed for various values of the displacement vector \bar{d} , and features derived from the GLC matrices are used for classifying the contents of an image.

Some of the commonly used textural features derived from the GLC matrix are:

- 1) Uniformity (sum of squares):

$$\sum_{I,J} p_{IJ}^2 \quad (2a)$$

ORIGINAL PAGE IS
OF POOR QUALITY

- 2) Contrast:

$$\sum_I \sum_J (I-J)^2 p_{IJ} \quad (2b)$$

- 3) Correlation:

$$\sum_I \sum_J \frac{(I-\mu_x)(J-\mu_y) p_{IJ}}{\sigma_x \sigma_y} \quad (2c)$$

- 4) Entropy:

$$\sum_I \sum_J p_{IJ} \log p_{IJ} \quad (2d)$$

- 5) Inverse Difference Moment:

$$\sum_I \sum_{\substack{J \\ I \neq J}} (p_{IJ})^p / |I-J|^u \quad (2e)$$

- 6) Maximum Probability:

$$\max_{I,J} p_{IJ} \quad (2f)$$

For a variety of imagery (aerial, micrographic and x-ray) the relationship between these textural features, their values and what they represent in terms of visual perception of texture are reasonably well understood. Using features of the form given above, Haralick and

Shanmugan [5-7] were able to classify a variety of images with over 85% classification accuracy. These features have also been used to separate texture in radar images [1].

III. Texture Analysis of SAR Images with Different Spatial and Radiometric Resolution

Numerical descriptions of texture (specifically those derived from the grey-level co-occurrence matrix (GLCM) as in Section II) have been shown to separate some simple geological features [1]. To efficiently design a spaceborne SAR for geologic exploration it is of interest to determine how the ability to separate geological features using the GLCM desired features varies with important system parameters, e.g., spatial and radiometric resolution.

A limited set of radar images with different spatial and radiometric resolutions were obtained (primarily from the Jet Propulsion Laboratory [12]). These images were generated by appropriate processing of the Seasat-A SAR video signal, and were of a geologically interesting area in Tennessee (Figure 1). The specific areas that were studied are outlined in white. The combinations of spatial and radiometric resolution contained in this data set were (25 m, 4 looks), (50 m, 4 looks), (100 m, 4 looks), (50 m, 2 looks), and (50 m, 1 look). Within the Tennessee test area, five distinct textures were identified (see Table 1 for a description of the geology and topography) and five to seven samples of each texture obtained (see Figure 1). A sample of a texture is an image (in this case 3.4 km x 3.4 km in size) containing only one texture type. Thus for each set of sensor parameters 30 texture samples were obtained, a total of 150 texture samples (images)

were used in this study. For each texture sample a GLCM was calculated and texture features found. Specifically, uniformity, contrast, correlation, entropy, Inver difference moment, and maximum probability were the texture features used here. Following [1] the GLCM were calculated for distances of 1, 2 and 4 at angles of 0° , 45° , 90° , and 135° . The above texture features were calculated for each distance and angle. In addition, the average over all angles for each texture feature was calculated. Thus each texture sample is described by a set of 30 numbers (6 texture features, 4 angles, and the average for each feature).

Scatter diagrams of the numerical values for one pair of texture features are shown in Figure 2. These plots are for distance 4 and result from averaging all four GLCM angles. All five textures can be separated using the correlation and maximum probability (Figure 2) features only for the system with a 25 m spatial resolution and with four independent samples averaged. As either the radiometric resolution is degraded (decreased number of independent samples or looks averaged) or the spatial resolution is degraded the ability to separate these textures is also degraded. This same result was found for other combinations of texture features [13]. In all cases only the images with 25 m, 4 looks could be quantitatively used to separate these textures using the GLCM.

This experiment reinforces the conclusions of our previous work [1]: automatically derived texture features can be used to discriminate texture in radar images of rough terrain. Additionally, this study shows that the ability to use the GLCM to classify texture is strongly dependent upon both the sensor's spatial and radiometric resolution.

Even though the data set used for this study was very limited these results do indicate that the usefulness of textural features for radar image analysis is sensitive to the spatial and radiometric resolutions of the sensor. This should be expected because it is well known that for manual analysis the interpretability of radar images is sensitive to the radiometric and spatial resolutions [14-17]. Thus, this study demonstrated that this sensitivity also exists for automatic analysis.

IV. A Study of the Effect of Look Direction On Texture In SAR Images

For an automatic texture analysis system for radar to be successful, a set of texture features must be found which are invariant to the flight path of the sensor. This invariance is clearly needed because the orientation of the terrain features relative to the sensor's flight path is not known a priori. For the geologic analysis of radar imagery where terrain elevation plays a dominant role the imaging geometry of radar would seem to be a dominant factor. Also the question of invariance is important in the search for 'optimum' sensor configurations. For example, it might be possible to classify certain terrain features at one sensor orientation but not at another. However, because the orientation of the sensor to the terrain features of interest will never be known a priori an optimum sensor configuration might not exist.

The purpose of this section is to describe the results of an experiment which was aimed at determining the sensitivity of GLCM texture features, shown to be valuable as a discriminate, to the sensor flight direction, i.e., the target/sensor orientation. It was found

(given the limitations of the experiment) that the texture features considered here could be classified for one or two target/sensor orientations but not for all the three orientations considered here.

To isolate the effect of sensor look direction it was necessary to use radar simulation [18] to create a set of images with controlled terrain and sensor parameters. Further it was possible using the simulation approach to remove (i.e., not include) the effect of speckle [18]. Therefore, this study focused on how shadow, layover, and range compression changed the image manifestations of complex terrain structure as the look direction of the sensor was varied.

In radar image simulation (for a complete description see [18]), the terrain to be analyzed is represented as a two-dimensional integer array referred to as a data base. This array is stored on a file containing fixed-length records. These correspond directly to rows in the array which contain a fixed number of words (columns). This relationship is shown in Figure 3.

The three data bases used in this study were generated from data received from the U.S. Geological Survey in the form of three digital elevation models. These were received containing elevation values which correspond directly to a 1:24000 (1 inch = 2000 feet) topographical map sampled at 30 meter intervals in both the x and y directions. Let x define columns in our data base and y to refer to rows (see Figure 3). In these data x and y both represent 30 meters on the ground. Thus each elevation value was considered to be valid for an area of 30x30 square meters.

The third dimension of the data base, h, represents the elevation of each cell above a given reference elevation. Each increment in

elevation corresponds to Δh , which describes a scaling factor for determining the quantization of the actual elevation. In the digital elevation models used in this study, the value for Δh was equal to one meter. This led to a convenient one-to-one relationship for the elevations.

The relationship among the values for Δx , Δy and Δh describes the degree to which the elevation changes over an area on the ground. Since only the relative structures of the terrain are of interest in this study, this relationship may be altered as needed. After first removing the reference elevation constant the data was scaled by 0.25. This allowed the Δx and Δy values to represent 7.5 meters, while the value for Δh remained equal to 1 meter.

The simulation of synthetic aperture radar imagery is made possible through the application of a computer program developed at the University of Kansas Remote Sensing Laboratory [18]. This algorithm will simulate the effects of a spaceborne SAR with a look direction parallel to the rows of the data base array. Since the simulation program always processes the data row by row, the only way to achieve a different look direction is to modify, i.e., rotate, the data base. Keeping this in mind, the unmodified data base is defined to be at a look direction angle of 0° . For this study simulated radar imagery was to be generated for the same areas with look directions of 0° , 45° , and 90° . This required that the data bases be correctly oriented before the simulation was performed. For this, computer programs were applied to rotate the original data in order to simulate different look angles. Nine data bases were thus available for simulation (3 terrain models at 3 look directions). These nine data bases were then processed using the

simulation program. The radar parameters used for the simulation were similar to those of the Seasat-A SAR. The altitude of the sensor was considered to be roughly 800 kilometers, and the angle of incidence between the sensor and the first cell of the data base was given to be 20 degrees. For the purposes of this study, it was assumed that all of the terrain data was of one scattering category. The scattering coefficient as a function of incidence angle is shown in Figure 4.

Using these parameters along with the assumed value of 7.5 meters for both along-track and across-track resolutions, radar images were simulated, producing the desired set of controlled images. However, these images are now rotated relative to each other. To eliminate the rotational dependence of the GLCM the simulations were converted to one coordinate system.

Visually the effect of changing the flight path is dramatic. Figure 5a-c contains the simulated radar images for one of the digital terrain models. In Figure 5a the sensor's look direction is from right to left. This is our reference direction and is referred to as the 0° look angle. The simulation of a 45° look angle (i.e., from the upper left to the lower right) is shown in Figure 5b and the 90° simulation (i.e., from top to bottom) is shown in Figure 5c. Similarly, Figures 6a-c and 7a-c contain the image simulations for two other digital terrain models. Close analysis of these images reveals many features which are totally obscured by shadow at one look angle but not at the others as was shown in [17]. Also, the spatial structure changes as the look angle is varied from 0° to 45° to 90° .

Beginning with the 0° look direction three distinct spatial structures, textures, were identified.

TEXTURE 1 contained low relief with some small hills and ridges, maximum relief is about 100-300 feet.

TEXTURE 2 contained elongated ridges and mountains usually separated by steep gradient streams, maximum relief is about 500-700 feet.

TEXTURE 3 contained long, narrow valleys with steep slopes and depths of about 300-400 feet. Valley streams have medium to low gradients.

From each texture, 3 or 4 samples (subimages) were obtained. The same subimages were then sampled from the 45° and 90° look direction simulations. A total of 33 subimages provided the input for this experiment (11 subimages for each look direction). These subimages are shown in Figure 8a-c. The specific research questions addressed by this experiment were (1) can these three textures be classified using GLCM features at any of the three look directions, and (2) can these three textures be classified using GLCM features independent of the look direction, i.e., are the texture features derived from the same spatial structure independent of the look direction of the sensor, thus, can the textures be classified using all three orientations simultaneously.

For each of the 33 subimages described above a GLCM and the resulting texture features were calculated for distances of 4, 6, and 10 at 0°, 45°, 90°, and 135° (these angles will be referred to as GLC angles as opposed to the look direction angle). It was found [13] that distances 4 and 10 showed basically the same trend as 6 so only the distance 6 results will be discussed. Also, it was found that averaging the texture features over the GLC angle as was done previously [1]

**ORIGINAL PAGE IS
OF POOR QUALITY**

destroyed our ability to separate textures one and two. This is expected from their spatial structure. Thus only results from individual GLC angles will be presented. The GLCM texture features were analyzed pair-wise as was also done previously [1].

Analysis of the data qualitatively showed that all three textures could be classified at one or two target/sensor orientations but not at all three simultaneously. For example, Figure 9a-c contains the scattergrams for the maximum probability and contrast texture features at GLC distance 6 and GLC angle of 0° . At a look direction of 0° (Figure 9a) none of the three textures can be separated, while at 45° (Figure 9b) all three textures can be classified. Analysis of other texture pairs shows the same trend, i.e., the textures considered here can be classified for one or two sensor look directions but not at all three [13]. If the texture samples for each terrain structure from all three look directions are combined it becomes obvious that the textures considered here cannot be classified independent of look direction (see Figure 10a-e).

The purpose of this analysis was to determine the sensitivity that GLCM texture features show to changes in the orientation of the surface structure relative to the sensor. Radar image simulation was used to generate a suitable set of images with the effects of the sensor flight path isolated. Within the limitations of this experiment, i.e., three different terrain structures, and three flight directions, it was shown that (1) the GLCM texture features can be used to classify the terrain structures at one or two flight directions but not at all three, and (2) the GLCM texture features cannot be used to classify these terrain structures independent of the flight path. The search of the optimum

set of sensor parameters for geologic applications is thus complicated. That is, the results of this study indicate that the optimum sensor for classifying (using either manual or automatic techniques) surface structure is dependent upon the orientation of the structure to the flight path of the sensor. Because of the monostatistic nature of radar imaging the same surface structure imaged at two different flight angles can (and often do) appear totally dissimilar. A set of sensor parameters optimized to detect these structures at one flight angle might be totally different if the flight angle were changed.

V. CONCLUSIONS AND RECOMMENDATIONS

Texture is an important characteristic of radar images of rough terrain. It was shown that the GLCM derived texture features can be used to classify texture. In this paper we have demonstrated that GLCM derived texture features are sensitive to both sensor and flight parameters. In fact, we lose our ability to classify texture by these features if either the radiometric or spatial resolution is degraded. We also found that these texture features are sensitive to the sensor flight path. We could classify the surface structure for one or two target/sensor orientations but not for all three considered simultaneously. That is, GLCM texture features cannot be used to classify texture independent of the flight path.

While general conclusions on the sensitivity of textural features to system and flight parameters can be made from the results of this study, there is a need to further refine these conclusions, specifically it is recommended that the sensitivity shown here be quantitatively studied. Quantitative results are needed to help guide system design

and flight planning. Two approaches to obtaining quantitative results should be pursued in parallel. First, an analytic study of the relationships among surface, sensor and flight parameters and the GLCM is needed. Second, more radar images should be analyzed. With more data the qualitative discussion of the effects of spatial and radiometric resolution can be extended to a quantitative analysis, for example plots of the 'variance' of each cluster as a function of resolution could then be studied. The ultimate goal of such an analysis would be an expression for the sensitivity of each texture feature as a function of resolution. This study also dealt with only radical changes in the flight direction over a fixed site. Further analysis is now needed to determine the effect of small angle changes, e.g., on the order of 5° . Also this study only considered one angle of incidence. It would be interesting to determine if there exist some incidence angle for which we could classify surface structure independent of the flight angle.

ACKNOWLEDGMENTS

The authors are indebted to the individuals who have contributed to this study, Dr. Josephine Stiles and Mr. Scott Gardner. Also, thanks are expressed to Dr. Dan Held of the Jet Propulsion Laboratory for supplying the SEASAT-A SAR data.

References

- [1] K.S. Shanmugan et al., "Textural Features for Radar Image Analysis," IEEE Trans. on Geoscience and Remote Sensing, vol. GE-19, July 1981, pp. 155-156.
- [2] A. Rosenfeld and E.B. Troy, "Visual Texture Analysis," Computer Science Center, University of Maryland, June 1970.
- [3] R.M. Haralick and D. Anderson, "Texture Tone Study," Remote Sensing Laboratory Technical Report, RSL TR 182-2, University of Kansas Center for Research, Inc., Lawrence, Kansas, 1971.
- [4] R.N. Sutton and E.L. Hall, "Texture Measures for Automatic Classification of Pulmonary Disease," IEEE Trans. on Computers, vol. C-21, no. 7, July 1972, pp. 667-676.
- [5] R.M. Haralick, K. Shanmugan and I. Dinstein, "Textural Features for Image Classification," IEEE Trans. on Systems, Man, and Cybernetics, vol. SMC-3, November 1973, pp. 610-621.
- [6] M.M. Galloway, "Texture Analysis Using Gray Level Run Lengths," Computer Graphics and Image Processing, vol. 4, no. 2, June 1975, pp. 172-199.
- [7] K. Shanmugan and R.M. Haralick, "Computer Classification of Reservoir Sandstones," IEEE Trans. on Geoscience Electronics, vol. GE-11, October 1973, pp. 171-177.
- [8] R.M. Haralick and K. Shanmugan, "Combined Spectral and Spatial Processing of ERTS Imagery," Remote Sensing, vol. 3, June 1974, pp. 3-13.
- [9] R.P. Kruger, W.B. Thomson and F.A. Turney, "Computer Diagnosis of Pneumoconiosis," IEEE Trans. on Systems, Man, and Cybernetics, vol. SMC-4, no. 1, January 1974, pp. 40-49.
- [10] J.S. Weszka, C.R. Dyer and A. Rosenfeld, "A Comparative Study of Texture Measures for Terrain Classification," IEEE Trans. on Systems, Man, and Cybernetics, vol. SMC-6, no. 4, April 1976, pp. 269-285.
- [11] R.W. Connors and C.A. Harlow, "A Theoretical Comparison of Texture Algorithms," IEEE Trans. on Pattern Analysis and Machine Intelligence, vol. PAMI-2, no. 3, May 1980, pp. 204-223.
- [12] J.P. Ford, "Resolution Versus Speckle Relative to Geologic Interpretability of Spaceborne Radar Images: A Survey of User Preference," IEEE Trans. on Geoscience and Remote Sensing, vol. GE-20, no. 4, October 1982, pp. 434-444.

- [13] V.S. Frost et al., "Topics In Radar Image Processing," Remote Sensing Laboratory Technical Report, RSL TR 453-4, University of Kansas Center for Research, Inc., Lawrence, Kansas, June 1982.
- [14] R.K. Moore, "Tradeoff Between Picture Element Dimensions and Noncoherent Averaging In Side-Looking Airborne Radar," IEEE Trans. on Aerospace and Electronic Systems, Vol. AES-15, September 1979, pp. 697-708.
- [15] G.R. DiCaprio and J.E. Wasielewski, "Radar Image Processing and Interpreter Performance," Photogrammetric Engineering and Remote Sensing, vol. 52, no. 8, August 1976, pp. 1043-1048.
- [16] L.J. Porcello, "Speckle Reduction In Synthetic-Aperture Radars," J. Opt. Soc. Am., vol. 66, no. 11, 1976, pp. 1305-1311.
- [17] L.F. Dellwig, B.C. Hanson, N.E. Hardy, J.C. Holtzman, P.L. Hulien, J.R. McCauley, and R.K. Moore, "A Demonstration and Evaluation of the Utilization of Side Looking Airborne Radar for Military Terrain Analysis," Remote Sensing Laboratory Technical Report, RSL TR 288-1, University of Kansas Center for Research, Inc., Lawrence, Kansas, October 1975.
- [18] J.C. Holtzman et al., "Radar Image Simulation," IEEE Trans. on Geoscience and Remote Sensing, vol. GE-16, no. 5, October 1978.

ORIGINAL PAGE IS
OF POOR QUALITY

LIST OF FIGURES

- Figure 1. SEASAT-A SAR Image.
- Figure 2. Scatter Diagrams for Texture Feature Pairs as a Function of Spatial and Radiometric Resolution (Average Over All GLC Angles). Maximum Probability/Correlation.
- Figure 3. Data Base Geometry for Radar Image Simulation.
- Figure 4. Backscattering Function Used In Radar Image Simulations.
- Figure 5. Radar Image Simulations for Three Flight Paths for Site 1.
- Figure 6. Radar Image Simulations for Three Flight Paths for Site 2.
- Figure 7. Radar Image Simulations for Three Flight Paths for Site 3.
- Figure 8. Texture Samples from the Radar Image Simulations.
- Figure 9. Scatter Diagrams for Texture Feature Pairs, Contrast/Maximum Probability, at a 0° GLCM Angle as a Function of Flight Path.
- Figure 10. Scatter Diagrams for Texture Feature Pairs Combining all Flight Paths.

ORIGINAL FILE
OF POOR QUALITY



Figure 1. Seasat-A SAR Image.

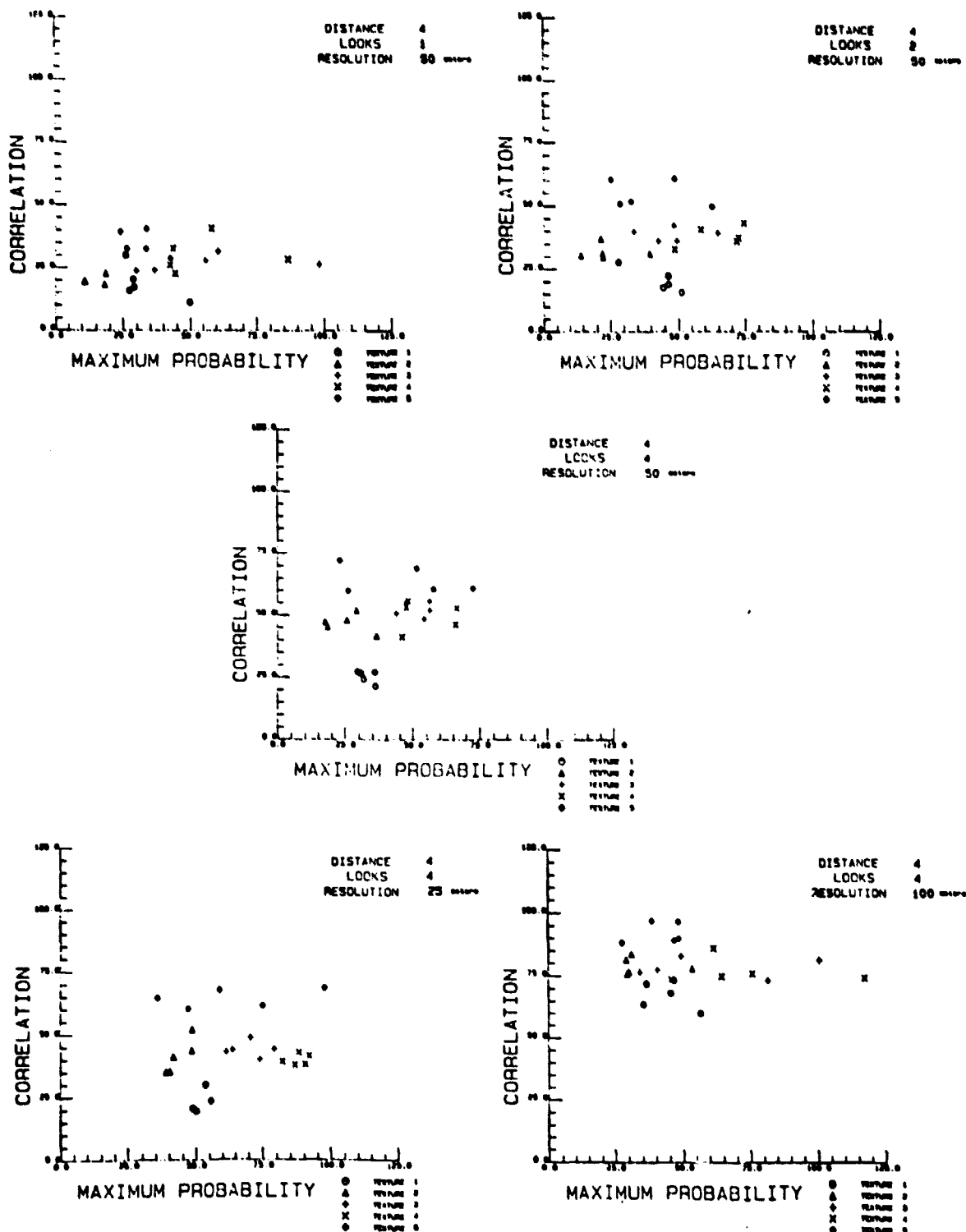


Figure 2. Scatter Diagrams for Texture Feature Pairs as a Function of Spatial and Radiometric Resolution (Average Over All GLC Angles). Maximum Probability/Correlation.

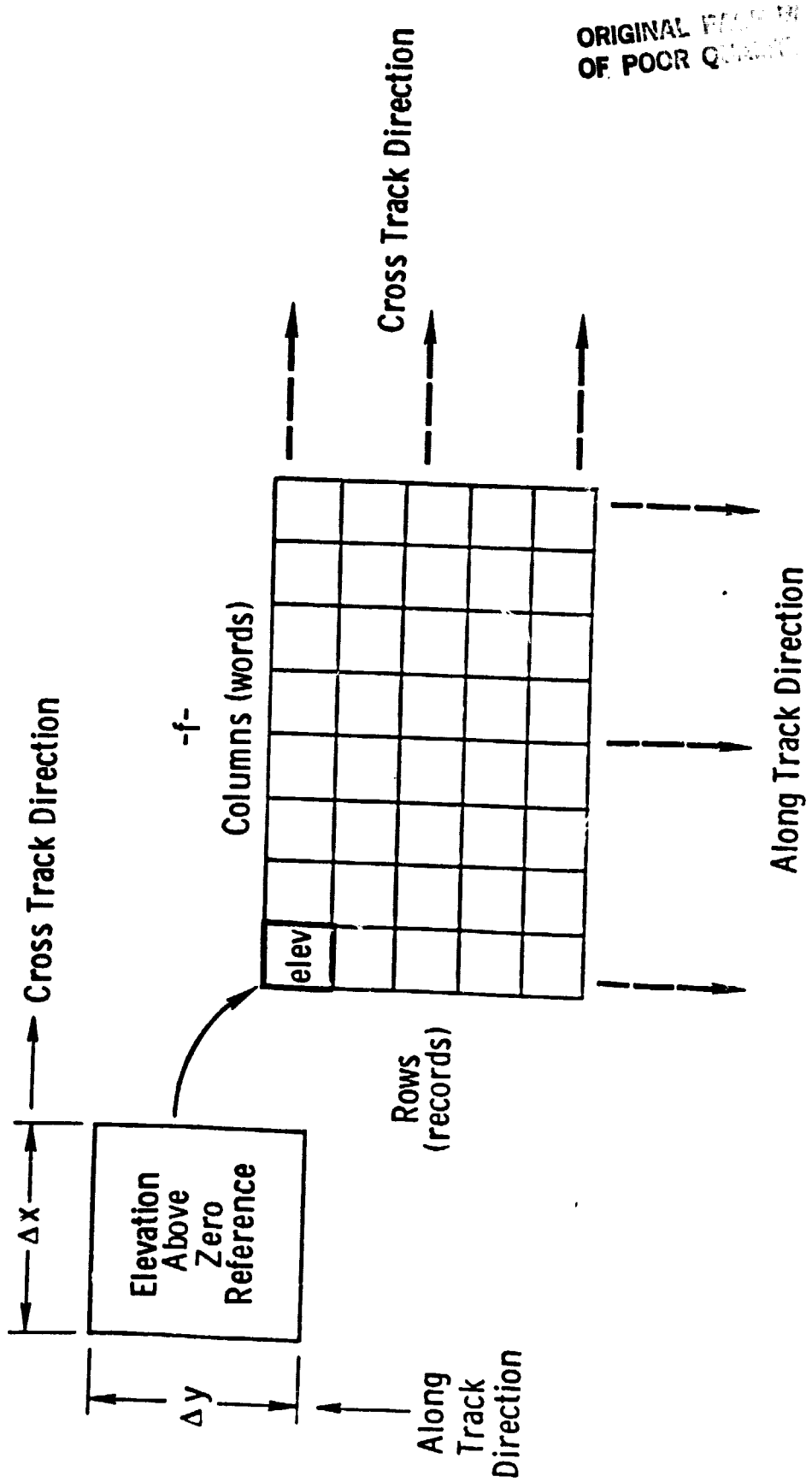


Figure 3. Data Base Geometry for Radar Image Simulation.

ORIGINAL PAGE IS
OF POOR QUALITY.

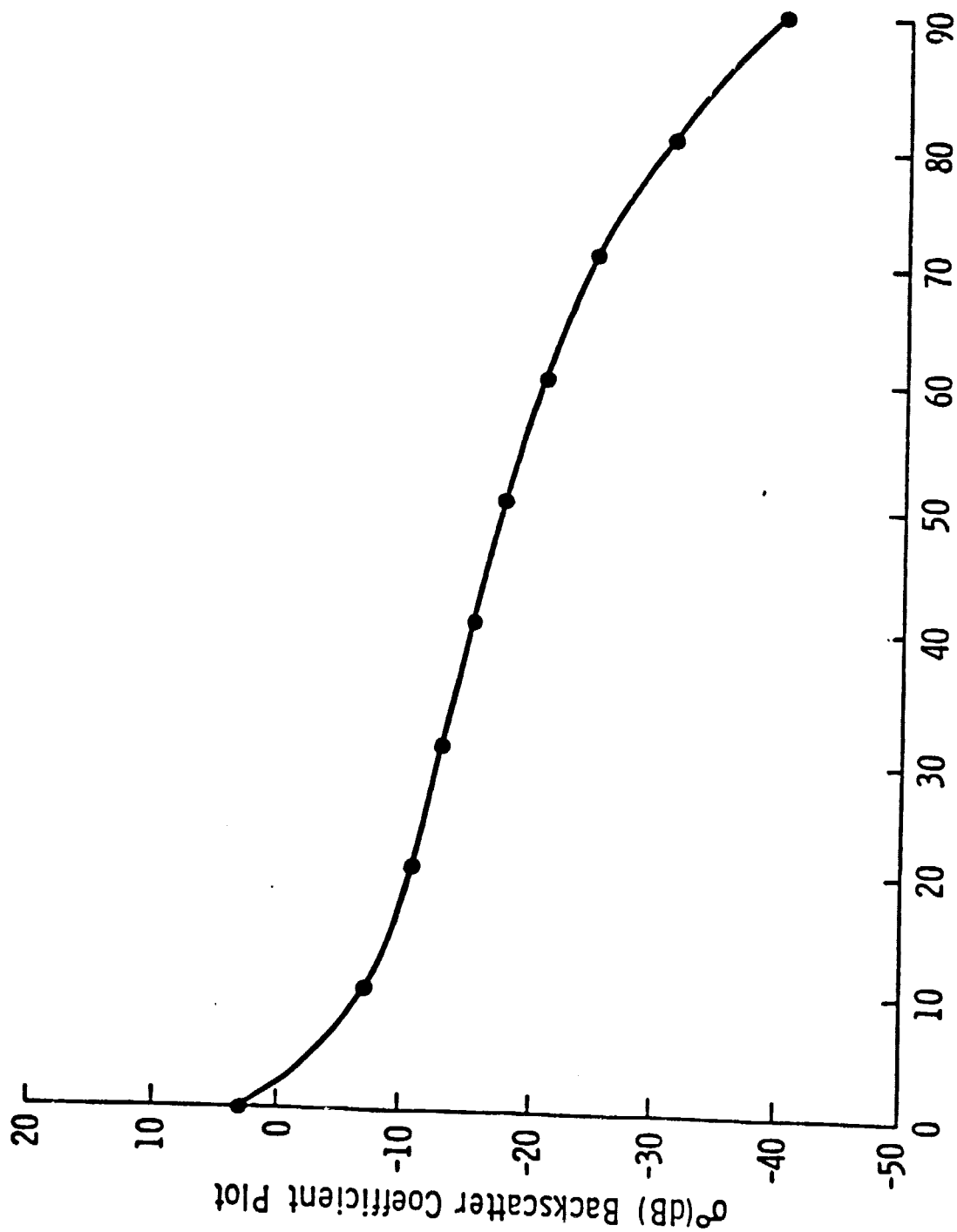


Figure 4. Backscattering Function Used in

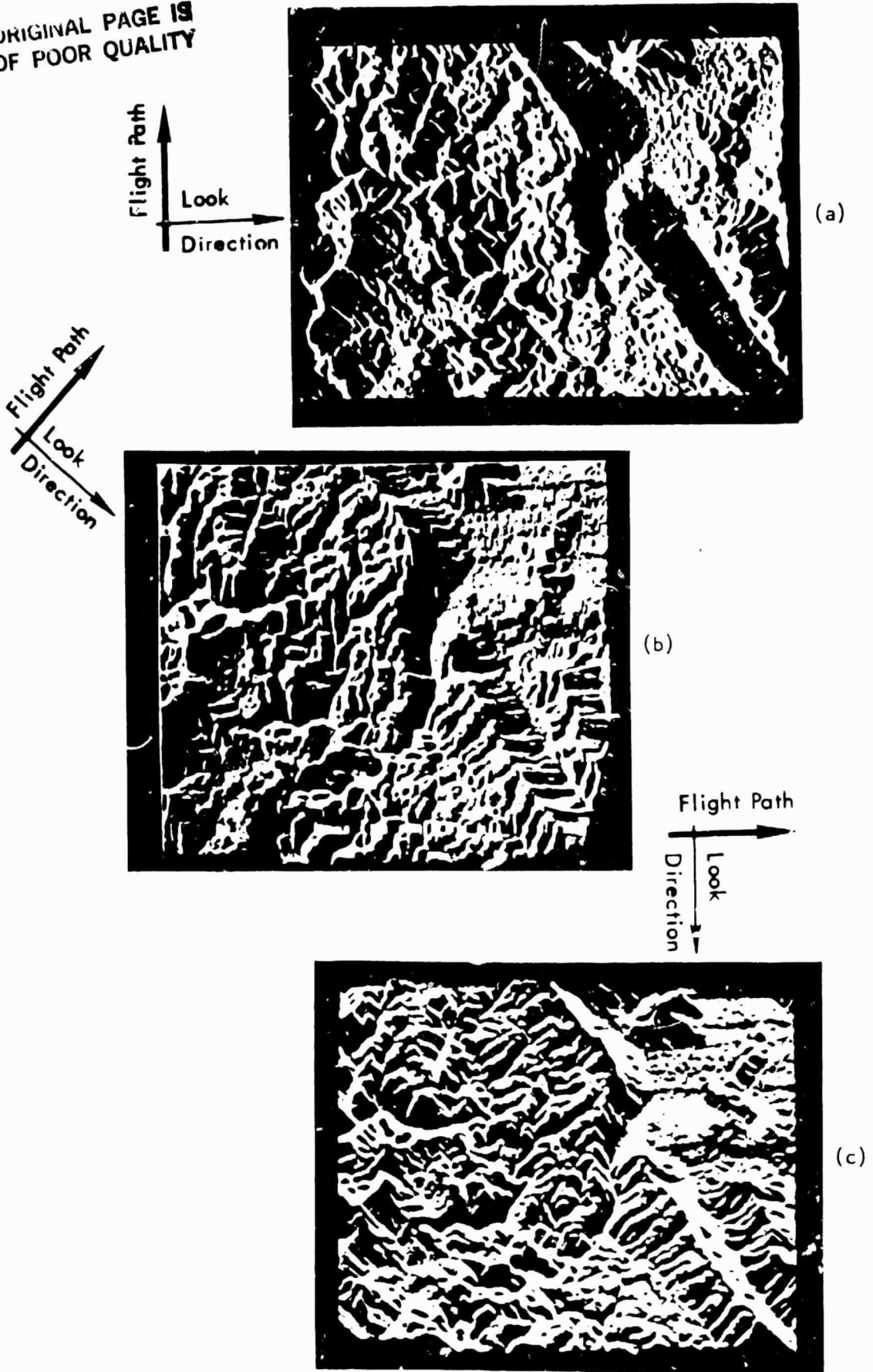
ORIGINAL PAGE IS
OF POOR QUALITY

Figure 5. Radar Image Simulations for Three Flight Paths for Site 1.

ORIGINAL PAGE IS
OF POOR QUALITY

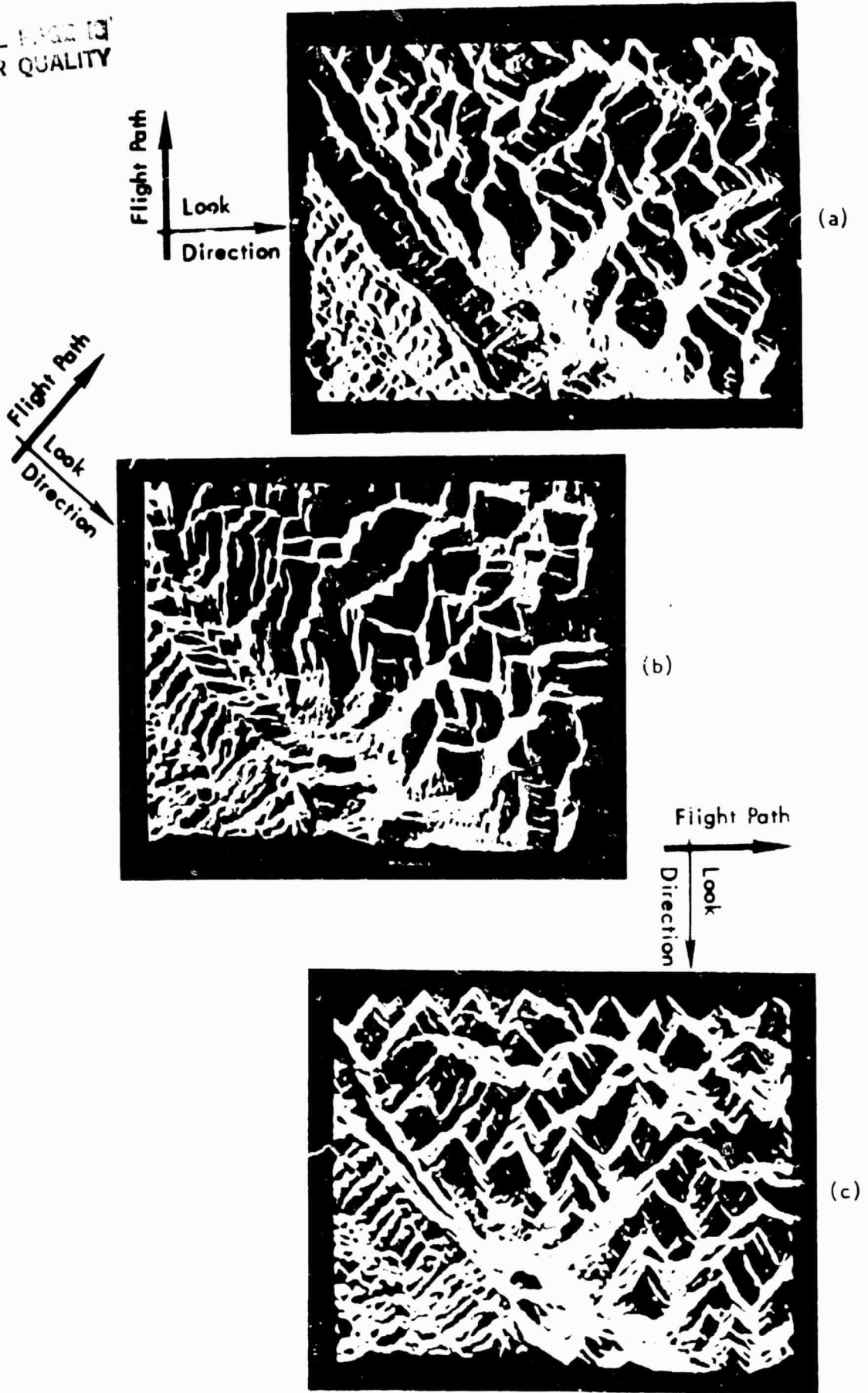


Figure 6. Radar Image Simulations for Three Flight Paths for Site 2.

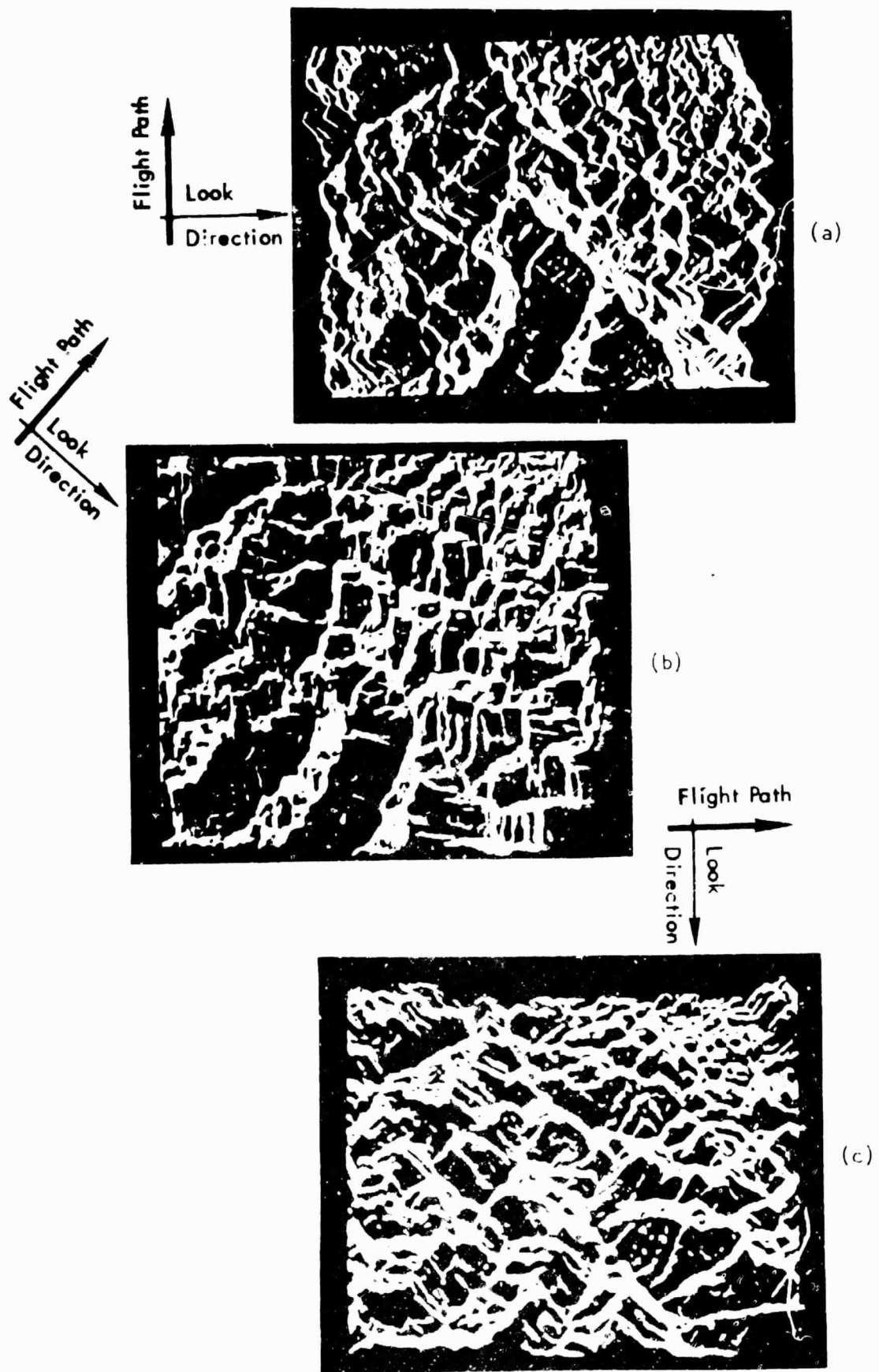


Figure 7. Radar images of a textured surface for three flight paths and look directions.

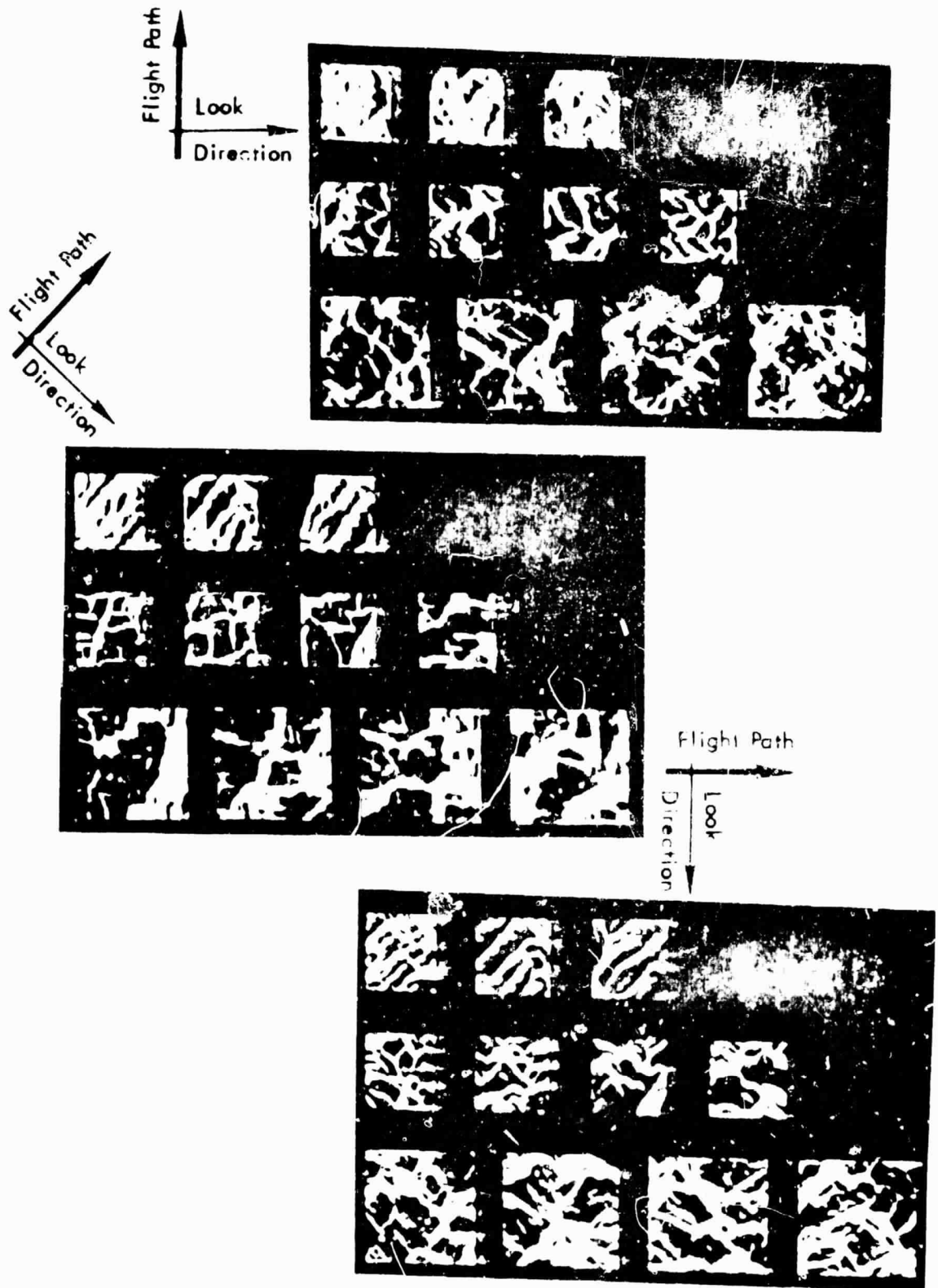
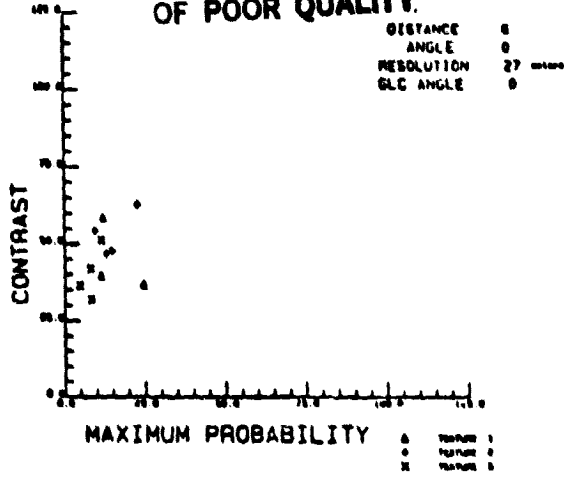
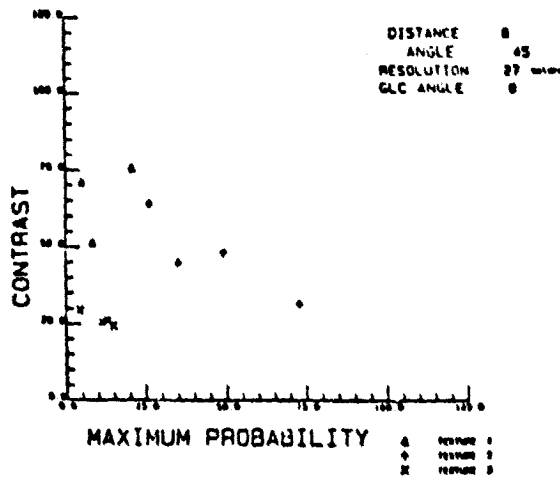


Figure 5. Texture Samples from the *Journal of the American Ceramic Society*, Vol. 10, No. 1, 1967, pp. 1-10.

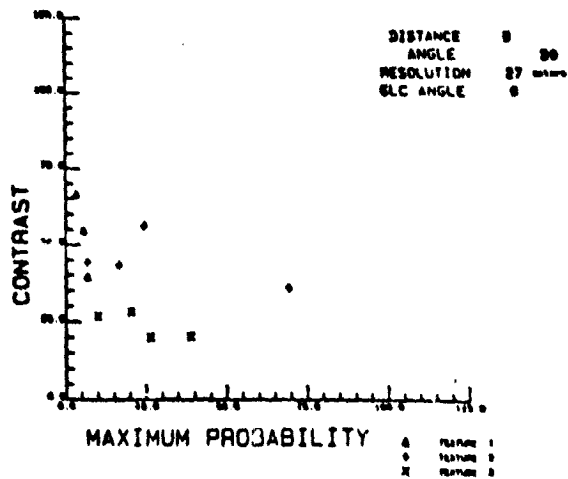
ORIGINAL PAGE IS
OF POOR QUALITY.



(a) 0°



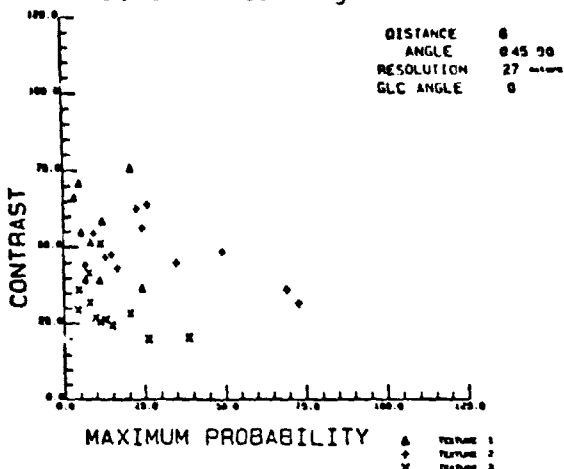
(b) 45°



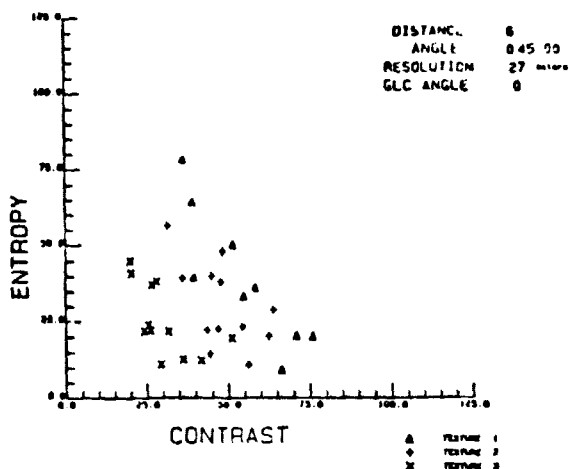
(c) 90°

Figure 9. Scatter Diagrams for Texture Feature Pairs, Contrast/Maximum Probability, at a 0° CLCM Angle as a Function of Flight Path.

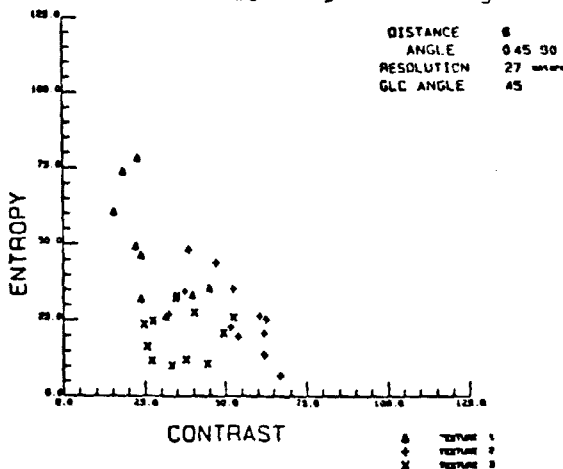
(a) Maximum Probability/Contrast
at a 0° GLCM Angle



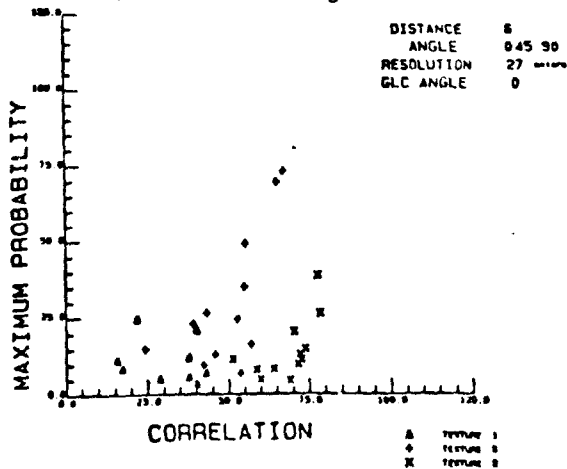
(b) Contrast/Entropy
at a 0° GLCM Angle



(c) Contrast/Entropy
at a 45° GLCM Angle



(d) Correlation/Maximum Probability
at a 0° GLCM Angle



(e) Correlation/Entropy
at a 45° GLCM Angle

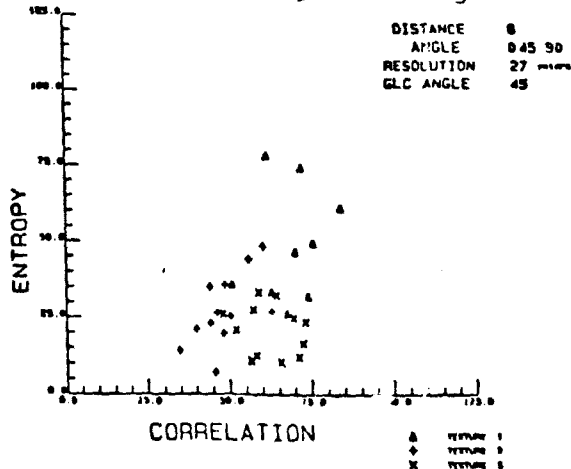


Figure 10: Scatter Diagrams for Texture Feature Pairs
Combining all Flight Paths.

LIST OF TABLES

Table 1. Geology and Topography of the Tennessee Test Area.

ORIGINAL PAGE IS
OF POOR QUALITY.

ORIGINAL PAGE 19
OF POOR QUALITY

	GEOLOGY	TOPOGRAPHY
T ₅	Rocks of the Lower Pennsylvanian Consisting of Alternating Beds of Sandstone and Shale with a Few Beds of Coal.	Mountains and Ridges with Steep Slopes and a Maximum Relief of of About 1500 Feet.
T ₄	Rocks of the Lower to Middle Ordovician Consisting Primarily of Dolomite and Cherty Dolomite with Some Beds of Limestone, Shale, and Sandstone.	Rolling Hills and Several Ridges with a Maximum Relief of 200-300 Feet.
T ₁	See T ₄	Area of Overall Low Relief but with Many Small Hills that are Separated by Several Creeks and Streams.
T ₃	Central Region (See T ₄) Flanked on Either Side by Rocks of the Upper Part of the Middle Cambrian in Beds of Dolomite, Limestone, and Slate.	Rolling Hills and Elongated Ridges Separated by a Trellis Drainage Pattern and Having a Maximum Relief of About 500 Feet.
T ₂	Rocks of the Upper Pre-Cambrian Consisting Primarily of Metasediments.	Mountains and Hills with Steep Slopes and a Maximum Relief of About 1000 Feet.

Table 1

Geology and Topography of the Tennessee Test Area.

ASPECTS OF SIMULATION
FOR RECTIFICATION STUDIES

E. M. MIKHAIL
AND
FIDEL D. PADERES, JR.
SCHOOL OF CIVIL ENGINEERING
PURDUE UNIVERSITY

PRECEDING PAGE BLANK NOT FILMED

58 INTENTIONALLY BLANK

ASPECTS OF SIMULATION FOR RECTIFICATION STUDIES

INTRODUCTION

RECTIFICATION = GROUND POSITION OF PIXEL CENTER

GIVEN PIXEL ROW, COLUMN

- NEED:
1. SATELLITE POSITION
 2. DIRECTION OF IMAGING (OPTICAL) AXIS
 3. INTERNAL GEOMETRY OF SENSOR
 4. ATMOSPHERIC CONDITIONS

1. FROM SATELLITE TRACKING
2. FROM ATTITUDE SENSORS
3. FROM CALIBRATION
4. NEGLECTED

NOT SUFFICIENT FOR SUB-PIXEL ACCURACY
ALTERNATIVE PARAMETER MODELING AND ESTIMATION

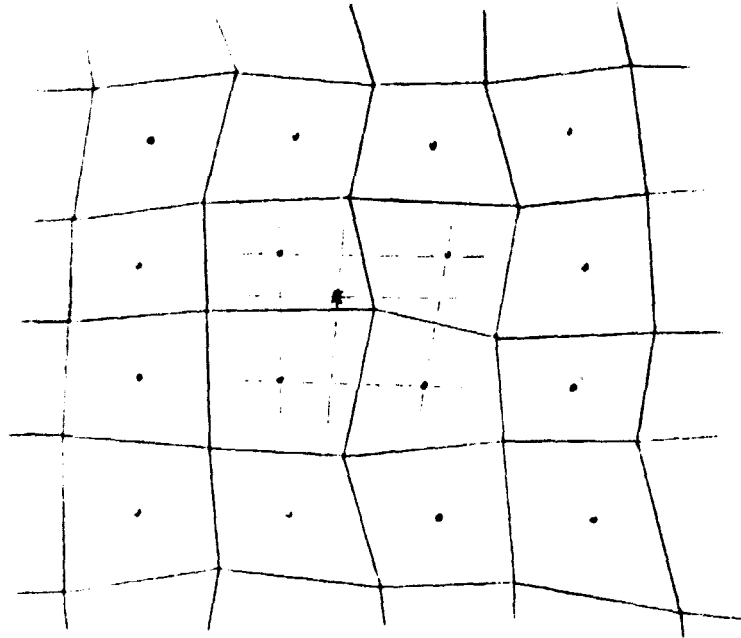


FIGURE 1. GROUND POSITIONS OF PIXELS

- PIXEL CENTER GROUND POSITION
- * OTHER POINT

HEAVY LINES ARE PIXEL BOUNDARIES

DOTTED LINES SHOW INTERPOLATION FOR POSITION
OF A POINT

FACTORS AFFECTING RECTIFICATION ACCURACY

- SENSOR RELATED
 - SCAN NON-LINEARITY
 - SCAN CORRECTOR NON-LINEARITY (TM)
 - BAND-TO-BAND OFFSETS
 - TIMING ERRORS
- PLATFORM ORIENTATION
 - EPIHEMERIS
 - ATTITUDE
- EARTH RELATED FACTORS
 - EARTH SHAPE
 - EARTH ROTATION
 - ATMOSPHERIC REFRACTION (NEGLIGIBLE?)
- GCP'S
 - ACCURACY
 - DENSITY
 - DISTRIBUTION

ORIGINAL PAGE IS
OF POOR QUALITY

MIKAHIL/PADERES

METHODS OF RECTIFICATION

INTERPOLATIVE APPROACH

ARBITRARY MATHEMATICAL FUNCTION RELATING IMAGE
COORDINATES TO RECTIFIED (GROUND) COORDINATES

NO SENSOR/PLATFORM MODELING

PARAMETRIC APPROACH

ATTEMPT AT EFFECTIVE GEOMETRIC MODELING OF
IMAGING PROCESS

PROPER USE OF A-PRIORI INFORMATION

STUDY OF ERRORS AND THEIR EFFECTS IS POSSIBLE
THROUGH SIMULATION

RECTIFICATION/REGISTRATION APPROACHES

INTERPOLATIVE APPROACH TO RECTIFICATION/REGISTRATION

- TYPES

GENERAL TRANSFORMATION

- + 4-PARAMETER ORTHOGONAL
- + 6-PARAMETER AFFINE
- + HIGHER ORDER POLYNOMIAL
- + HARMONIC SERIES

MOVING AVERAGES

- + WEIGHTED MEAN

MESHWISE LINEAR

LINEAR LEAST SQUARES PREDICTION

FINITE ELEMENT METHODS

SPLINES

- CHARACTERISTICS

CONTROL POINTS NECESSARY

NO SENSOR/PLATFORM MODELLING

A-PRIORI INFORMATION NOT USED

ERROR CAUSES AND INTERACTION NOT STUDIED

DEPARTMENT OF PHOTOGRAMMETRY

RECTIFICATION/REGISTRATION APPROACHES 65

PARAMETRIC APPROACH TO RECTIFICATION

- PRESENT IMPLEMENTATION
 - SENSOR GEOMETRY CORRECTION
 - EARTH RELATED SYSTEMATIC ERRORS CORRECTION
 - EPIHEMERIS AND ATTITUDE DATA EXPLOITATION
 - PLATFORM ORIENTATION ESTIMATION USING GCP'S
 - INTERMEDIATE PIXEL POSITION COMPUTATION
- PLATFORM ORIENTATION ESTIMATION
 - FIXED MODEL
 - RANDOM MODEL
- CHARACTERISTICS
 - SENSOR/PLATFORM MODELLING NECESSARY
 - CONTROL POINTS NOT USED SOMETIMES
 - PIXEL ELEVATION ASSUMED KNOWN (SINGLE COVERAGE)
 - GROUND GEOMETRIC CONSTRAINTS NOT EXPLOITED
 - SENSOR/PLATFORM MODELLING INCOMPLETE

ORIGINAL PAGE IS
OF POOR QUALITY

PHOTOMETRIC APPROACH

PROPOSED LANDSAT MSS/TM FRAME RECTIFICATION

- PROBLEM
RECOVERY OF PIXEL GROUND POSITION FROM SINGLE MSS/TM
FRAME
- APPROACH
PARAMETRIC
- MODEL
COLLINEARITY
- IMPLEMENTATION
SENSOR GEOMETRY CORRECTION
PLATFORM ORIENTATION ESTIMATION USING GCP'S
INTERMEDIATE PIXEL POSITION COMPUTATION
- CHARACTERISTICS
SMALLER ANGULAR COVERAGE
BENIGN SPACE ENVIRONMENT
MORE COMPREHENSIVE SENSOR/PLATFORM MODEL
IMPLICIT CORRECTION OF EARTH RELATED SYSTEMATIC ERRORS

ORIGINAL PAGE IS
OF POOR QUALITY

ORIGINAL PAGE IS
OF POOR QUALITY

IMAGING EQUATIONS

$$\begin{bmatrix} X \\ Y \\ Z \end{bmatrix} = s M \begin{bmatrix} U-U_S \\ V-V_S \\ W-W_S \end{bmatrix} = s \begin{bmatrix} M_{11} & M_{12} & M_{13} \\ M_{21} & M_{22} & M_{23} \\ M_{31} & M_{32} & M_{33} \end{bmatrix} \begin{bmatrix} U-U_S \\ V-V_S \\ W-W_S \end{bmatrix}$$

$[X \ Y \ Z]^T$ = IMAGE COORDINATES OF A POINT

$[U \ V \ W]^T$ = COORDINATES OF CORRESPONDING GROUND POINT

$[U_S \ V_S \ W_S]^T$ = SATELLITE COORDINATES AT INSTANT OF
POINT IMAGING IN GROUND COORDINATE
SYSTEM

M = ROTATION MATRIX WHICH BRINGS GROUND COORDINATE
SYSTEM PARALLEL TO IMAGE COORDINATE SYSTEM

s = SCALE FACTOR; VARIES FROM POINT TO POINT

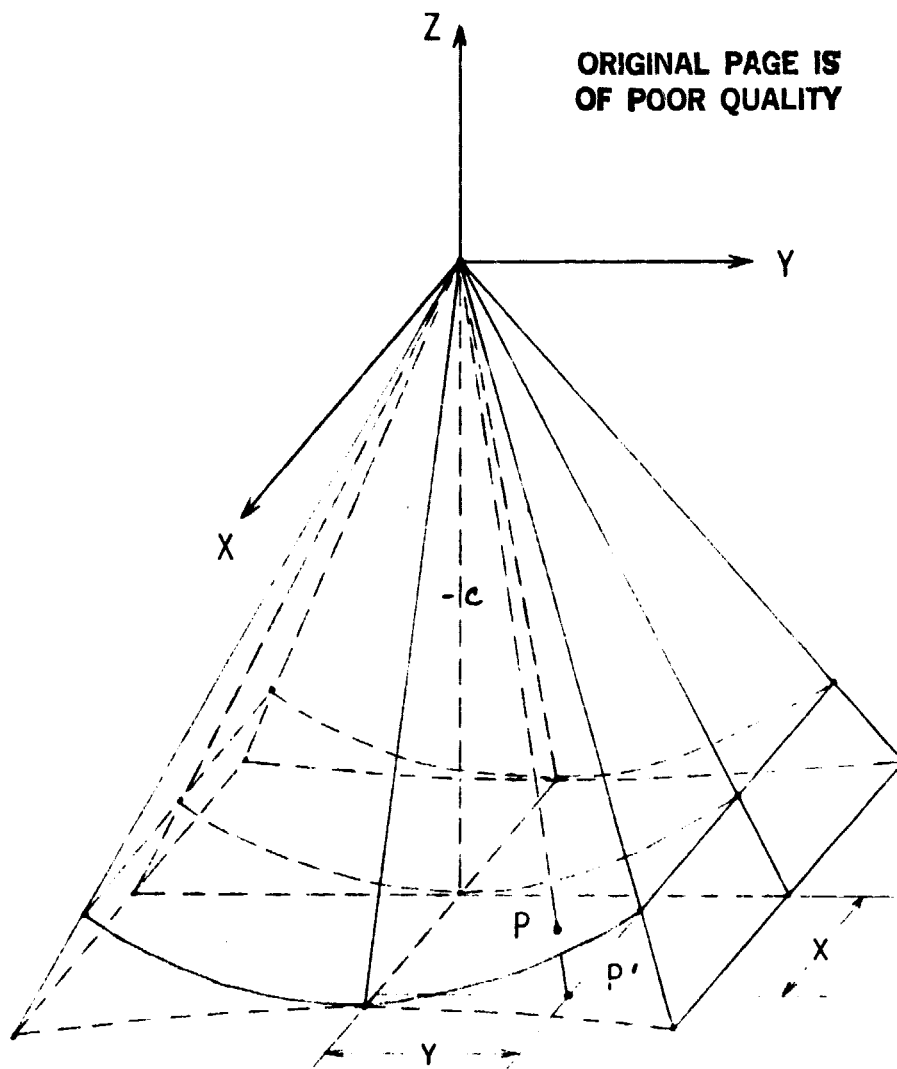


FIGURE 2. INTERNAL GEOMETRY OF SCANNING TYPE
SENSOR

P - A POINT ON IMAGE FRAME

P' - ITS PROJECTION ON A PLANE TANGENT TO
CENTER LINE

C - PRINCIPAL DISTANCE OF SENSOR LENS

COLLINEARITY EQUATIONS FOR SIMULATION

$$\frac{U-U_s}{W-W_s} = \frac{M_{11} X + M_{21} Y + M_{31} Z}{M_{13} X + M_{23} Y + M_{33} Z}$$

$$\frac{V-V_s}{W-W_s} = \frac{M_{12} X + M_{22} Y + M_{32} Z}{M_{31} X + M_{32} Y + M_{33} Z}$$

$[U \ V \ W]^T$ - DEFINED IN RECTANGULAR COORDINATE SYSTEM

$[\phi \ \lambda \ H]^T$ - DEFINED IN GEOGRAPHIC COORDINATE SYSTEM:
 ϕ , LATITUDE; λ , LONGITUDE; H , ELEVATION

FOR SIMULATION

- + ONLY $[U \ V \ W]^T$ UNKNOWN IN COLLINEARITY EQUATION
- + TRANSFORM $[U \ V \ W]^T$ ——— $[\phi, \lambda, H]^T$
- + ASSIGN VALUE TO H
- + SOLVE FOR ϕ, λ

SYNTHETIC DATA

ORIGINAL PAGE IS
OF POOR QUALITY

- GENERATION

MODEL: SATELLITE COLLINEARITY EQUATION
EXPLOIT A-PRIORI KNOWLEDGE OF PARAMETERS
FRAMES WITH DIFFERENT PERTURBATIONS

- VALIDATION PROCEDURE

SELECT REAL IMAGE WITH MANY SUITABLE FEATURES FOR GCP'S
IDENTIFY GCP'S
DIVIDE GCP'S INTO TWO GROUPS
RECTIFY IMAGE USING FIRST GCP GROUP
COMPUTE MSE USING SECOND GCP GROUP
REPEAT USING SYNTHETIC IMAGE SIMILAR GCP CONFIGURATION
COMPARE MSE'S

COLLINEARITY EQUATIONS FOR RECTIFICATION

$$\frac{X}{Z} = \frac{M_{11} (U-U_S) + M_{12} (V-V_S) + M_{13} (W-W_S)}{M_{31} (U-U_S) + M_{32} (V-V_S) + M_{33} (W-W_S)}$$

$$\frac{Y}{Z} = \frac{M_{21} (U-U_S) + M_{22} (V-V_S) + M_{23} (W-W_S)}{M_{31} (U-U_S) + M_{32} (V-V_S) + M_{33} (W-W_S)}$$

+ $[X \ Y \ Z]^T$ AND $[U \ V \ W]^T$ KNOWN (CONTROL POINTS)

+ PARAMETERS DEFINING ROTATION MATRIX AND $[U_S \ V_S \ W_S]^T$
UNKNOWN

+ GIVEN ENOUGH CONTROL POINT PARAMETERS SOLVED FOR BY
LEAST SQUARES

N83 23077 73

D4

Image Matching Using Hough Transforms

Larry S. Davis
and
Azriel Rosenfeld

Computer Vision Lab
University of Maryland

PRECEDING PAGE BLANK NOT FILMED

PAGE 72 INTENTIONALLY BLANK

Hough Transform Techniques

- Efficient matching procedures

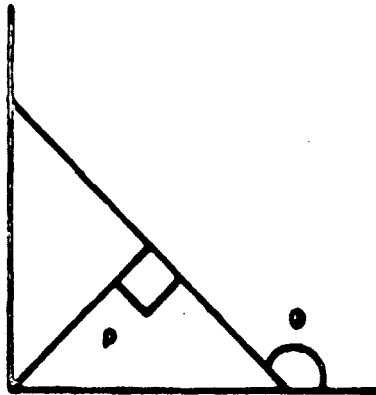
1) Line detection

- find sets of collinear feature points from the set

$$P = \{(X_i, Y_i)\}$$

- Line representation

$$\rho = X \cos \theta + Y \sin \theta$$



- Collinear points lie on a line of particular (ρ, θ)

ORIGINAL PAGE IS
OF POOR QUALITY

Hough transform - array of accumulators

$H(\theta, \rho)$ = number of points in P which lie on the line

$$\rho = X \cos \theta + Y \sin \theta$$

For each $(X, Y) \in P$ do

For $\theta = 0, 2^\circ, 4^\circ, \dots$ do

begin

$$\rho = X \cos \theta + Y \sin \theta$$

$$H(\theta, \rho) = H(\theta, \rho) + 1$$

end

- Peaks in $H(\theta, \rho)$ correspond to large sets of collinear points

while largest $(H) > t$ do

begin

mark largest (H) as a line;

for each $(X, Y) \in P$ which lies on largest (H) do

for $\theta = 0, 2^\circ, 4^\circ, \dots$ do

begin

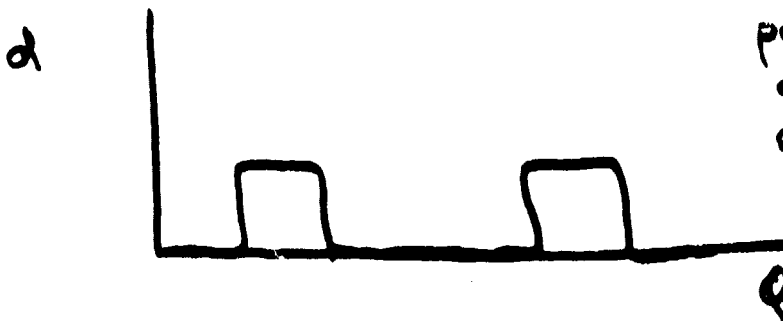
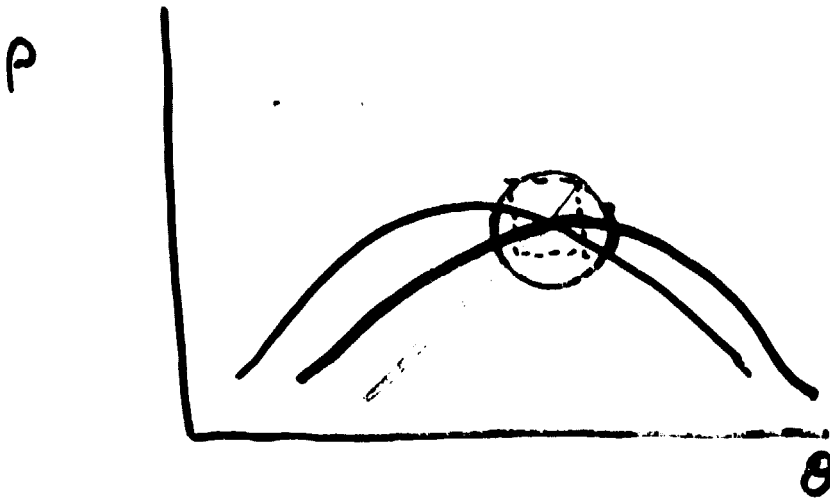
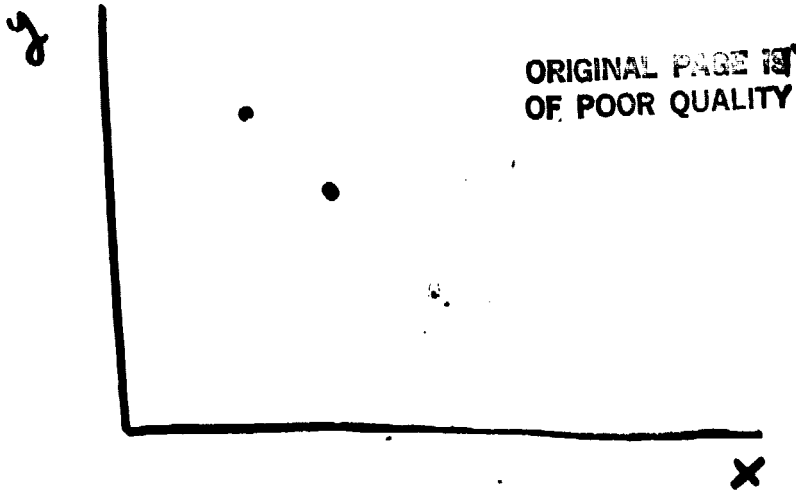
$$\rho = X \cos \theta + Y \sin \theta$$

$$H(\theta, \rho) = H(\theta, \rho) - 1$$

end

Recovering "density" from the Hough transform

76



pair of peaks of equal size separated by π .

ORIGINAL PAGE IS
OF POOR QUALITY

2) Circles (Ballard and Sklansky)

$$(X-h)^2 + (Y-k)^2 = r^2$$

- assume you know r

- want to find (h,k)

For each (X,Y) \in P do

For $\theta = 0, 2\pi, d\theta$ do

begin

$$h = X + r \cos \theta$$

$$k = Y + r \sin \theta$$

$$H(h,k) = H(h,k) + 1$$

end

ORIGINAL PAGE IS
OF POOR QUALITY

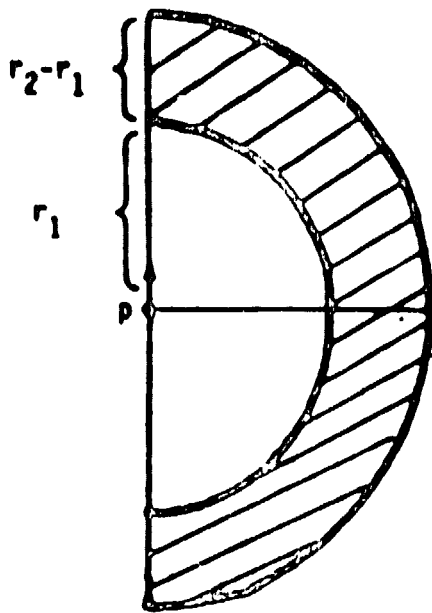
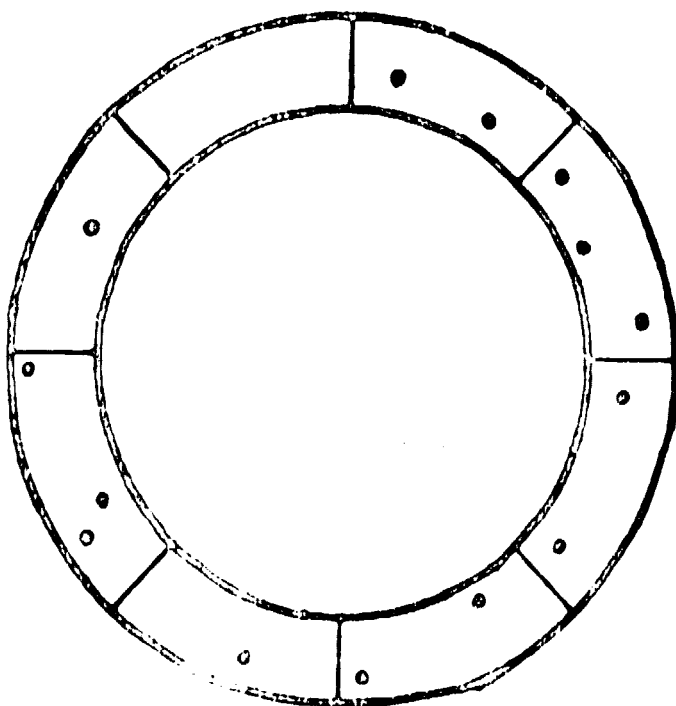


Figure 7. Mash marks show loci of possible circle centers for point p.



i	$D(i)$
1	2
2	3
3	2
4	2
5	1
6	3
7	1
8	0

LARRY S. DAVIS

ORIGINAL PAGE IS
OF POOR QUALITYFIG. 7. Digitized 61×64 orchard image.

3. APPLICATION TO THE DESCRIPTION OF NATURAL IMAGES

In this section we will discuss an application of the procedures described in the preceding section to the description of a set of real textures. As described in the introduction, the problem is to detect trees in aerial photographs of citrus groves, and then to classify the trees as being either healthy or infested. We are concerned here only with the process of tree detection. We will detect trees by first detecting a set of "obvious" trees, and then using the locations of those trees as input to the processes described in the preceding section. These procedures will predict the locations of other trees in the image; these locations can be used by subsequent programs to detect and classify trees not found by the first stage.

The procedures for detecting trees consists of differentiating the image and then using a Hough transform (Kimme *et al.* [11], Shapiro [12]) to find tree centers in the differentiated image.

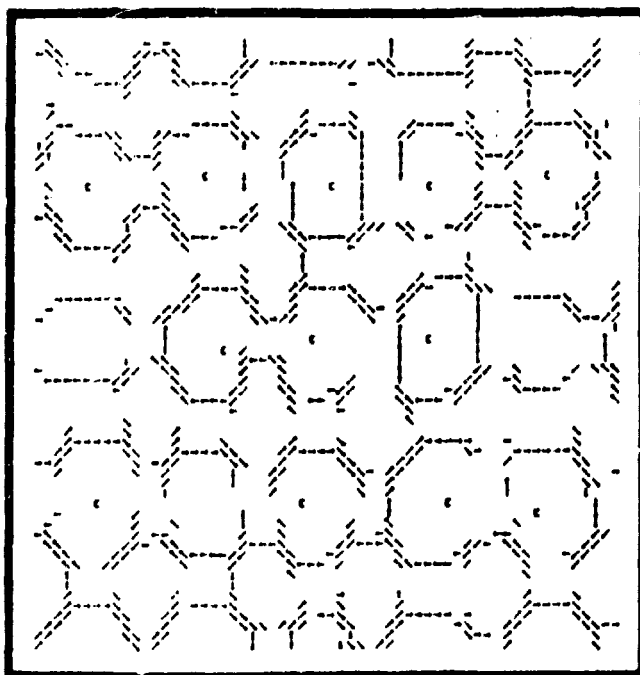


FIG. 8. Circle centers for Fig. 7.

3. Arbitrary Shapes (Ballard, Davis and Yam)



$$B(S) = ((\Delta X_1, \Delta Y_1))_{i=1}^m$$

$$P = ((X_1, Y_1))_{i=1}^n$$

a. Position Invariant matching (Sklansky)

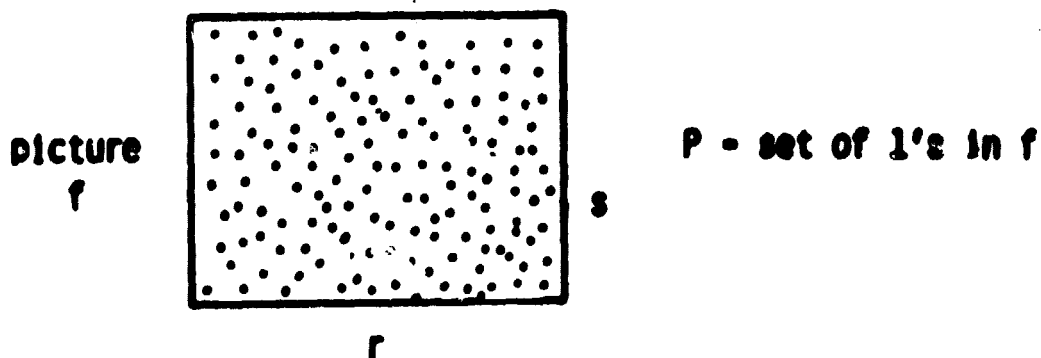
For each $(X, Y) \in P$ do

(1)

for each $(\Delta X, \Delta Y) \in B(S)$ do

$$H(X + \Delta X, Y + \Delta Y) = H(X, Y) + 1$$

Computationally equivalent algorithms:



For each (X, Y) in f

(2)

For each $(\Delta X, \Delta Y)$ in B(S)

$$\begin{aligned} H(X-\Delta X, Y-\Delta Y) &= H(X-\Delta X, Y-\Delta Y) + \theta f(X, Y) \\ \{ H(X, Y) &= H(X, Y) + f(X+\Delta X, Y+\Delta Y) \end{aligned}$$

Algorithm (1) - $O(m \cdot n)$ operations

Algorithm (2) - $O(rsm)$ operations

ORIGINAL PAGE IS
OF POOR QUALITY

b. Rotation invariant matching

- only the magnitude of the vectors in B can be used

For each $(X, Y) \in P$ do

 For each $(\Delta X, \Delta Y) \in B(S)$ do

 For $\theta = 0, 2\pi, d\theta$ do

 begin

$$X' = X + \Delta X \cos \theta$$

$$Y' = Y + \Delta Y \sin \theta$$

$$H(X', Y') = H(X, Y) + 1$$

 end

- each pair $((X, Y), (\Delta X, \Delta Y))$ is used to paint out a circle

in H.

c. Scale invariant matching (S_1, S_2)

For each $(X, Y) \in P$

For each $(\Delta X, \Delta Y) \in B(S)$

For $S = S_1, S_2, \Delta S$

begin

$$X' = X + S \Delta X$$

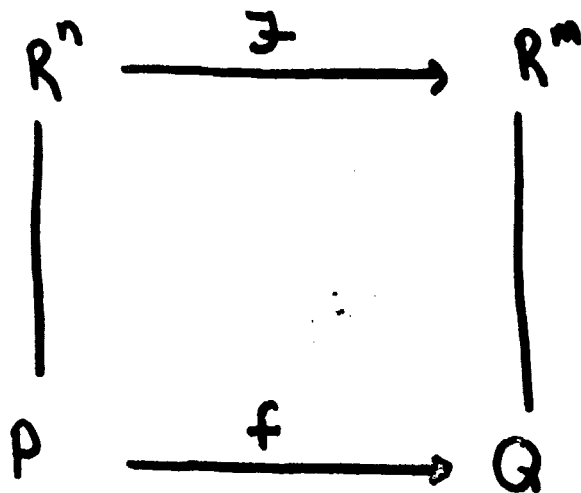
$$Y' = Y + S \Delta Y$$

$$H(X', Y') = H(X, Y) + 1$$

end

Generalized Hough Transforms

84



ORIGINAL PAGE IS
OF POOR QUALITY

P - pattern of interest

Q - pattern of detected features

$$P = \{p_1, \dots, p_r\} \in R^n$$

$$Q = \{q_1, \dots, q_s\} \in R^m$$

$$f(P) = \{f(p_1), \dots, f(p_r)\}$$

Goal: Find $f \in \mathcal{F}$ such that

$$|f(P)| = \#(Q - f(P))$$

is minimal

Ordinarily:

ORIGINAL PAGE IS
OF POOR QUALITY

- \mathcal{F} is defined by a set of parameters
 $\{t_1, \dots, t_n\}$

example

$$\mathcal{F}: \mathbb{R}^2 \rightarrow \mathbb{R}^2$$

$f_{t_1, t_2} \in \mathcal{F}$ is defined by

$$f_{t_1, t_2}(x, y) = (x + t_1, y + t_2)$$

- for computation, \mathcal{F} is reduced to a \mathcal{F}' , a finite subset, by
 - 1) restricting the domains of the t_i
 - 2) quantizing the resulting restricted domains.

Key to the efficiency of the GHT is the ability to efficiently enumerate certain subsets of \mathcal{F} .

Let $p \in P$

ORIGINAL PAGE IS
OF POOR QUALITY

$q \in Q$

Define: $\mathcal{F}_{pq} = \{ f \mid f \in \mathcal{F} \wedge f(p) = q \} \subseteq \mathcal{F}$

In practice, we deal with \mathcal{F}'

$\mathcal{F}'_{pq} = \{ f \mid f \in \mathcal{F}' \wedge \text{dist}(f(p), q) < \epsilon \}$

where ϵ is a constant determined by the quantization of the t_i .

Example of enumerating $\exists pq$

$$P, Q \subseteq \mathbb{R}^2$$

$$\exists: \{f_{\theta, \Delta x, \Delta y} \mid f_{\theta, \Delta x, \Delta y}(x, y) =$$

$$(x \cos \theta + y \sin \theta + \Delta x, -x \sin \theta + y \cos \theta + \Delta y)$$

Given $p \in P, q \in Q$, how do we enumerate $\exists pq$?

inefficient procedure: For each quantization

level of θ , compute all $\Delta x, \Delta y$ s.t.

$$|f_{\theta, \Delta x, \Delta y}(p) - q| < \epsilon$$

a) inefficient: For each $(\Delta x, \Delta y)$

compute all θ s.t. ...

(Ballard)

Procedure GHT1 (P, Q, \exists , H)ORIGINAL PAGE IS
OF POOR QUALITYFor each $p \in P$ For each $q \in Q$ Compute $\exists' pq$ For each $t_1, \dots, t_n \in \exists' pq$

$$H(t_1, \dots, t_n) := H(t_1, \dots, t_n) + 1$$

endf

endf

endf

endP

After GHT1

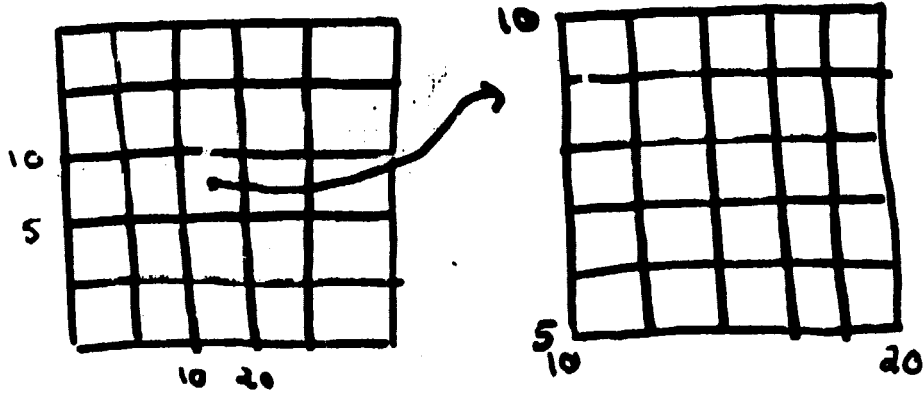
$$H(t_1, \dots, t_n) = \#(Q \cap f_{t_1, \dots, t_n}(P))$$

Therefore, the f which maximizes H , minimizes v .

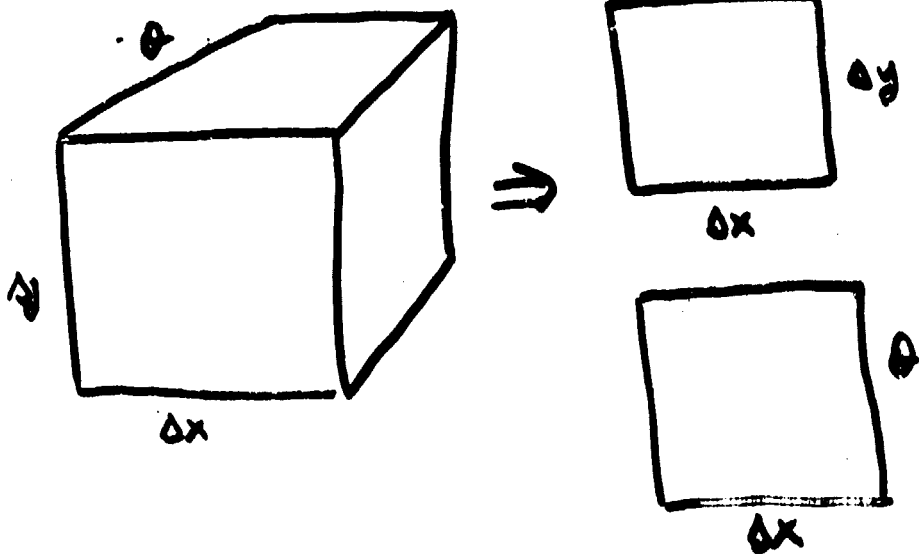
Representing high-dimensional Hough arrays

ORIGINAL PAGE IS
OF POOR QUALITY

① coarse-to-fine quantization



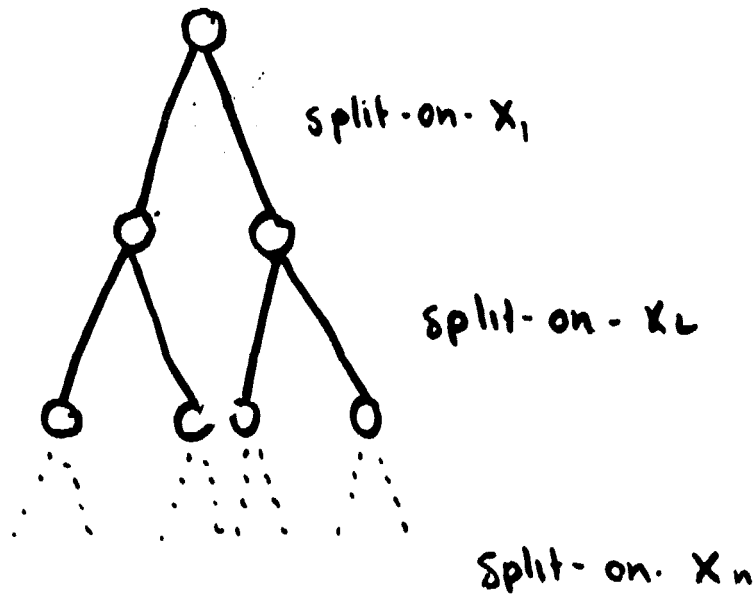
② multiple projections



② Tree-structures (k-d trees)

ORIGINAL PAGE IS
OF POOR QUALITY.

- sequence through parameters one level at a time



- nodes are split if parts within node are not "uniformly" distributed

- nodes are merged to increase uniformity

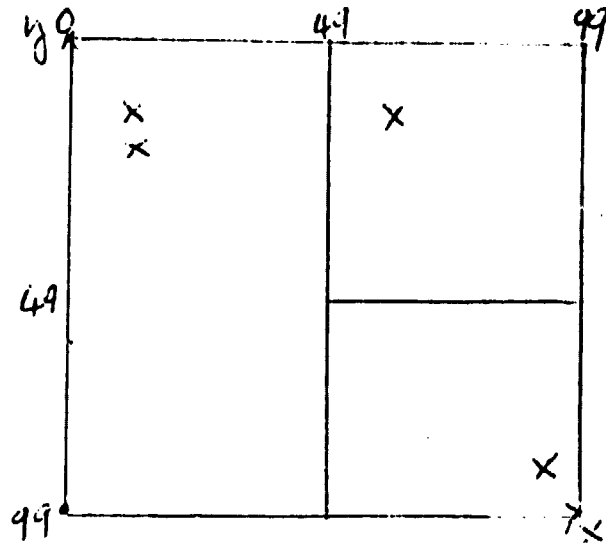


Figure 4a. 2-d quantized space

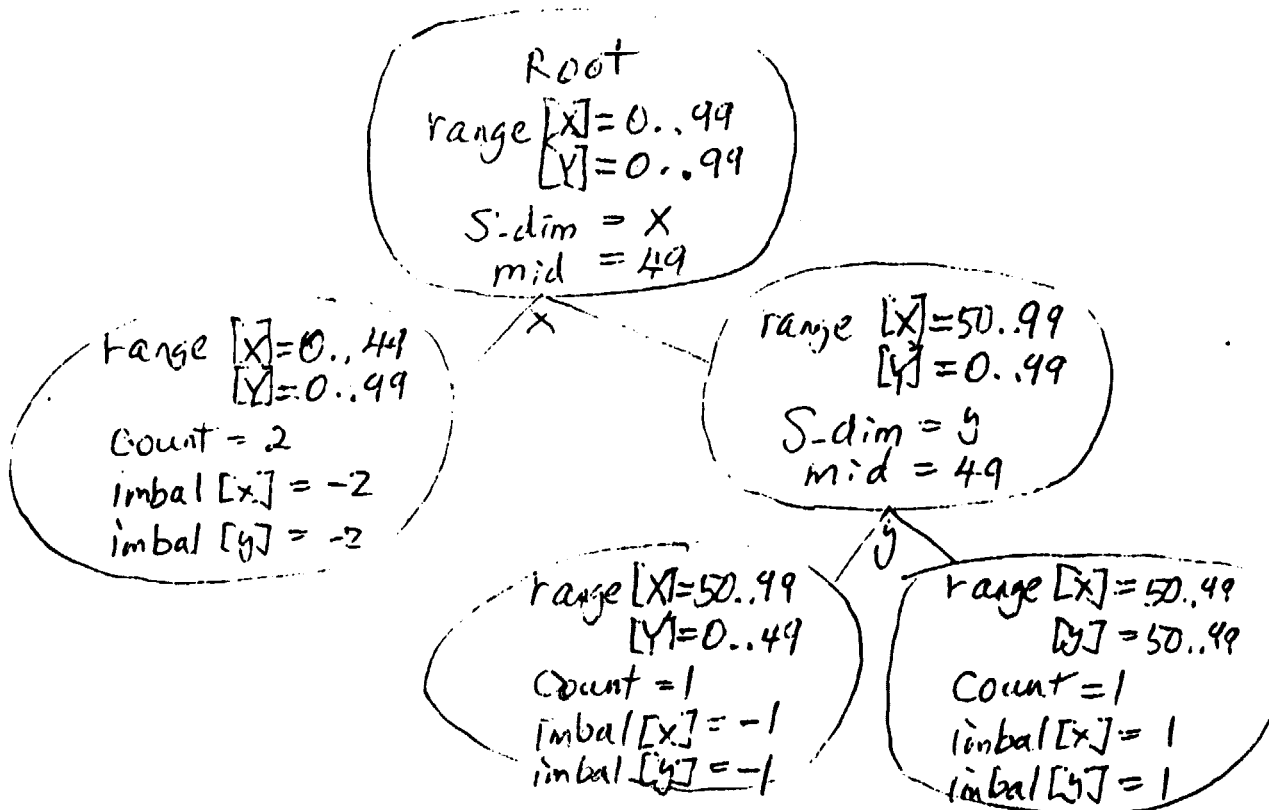
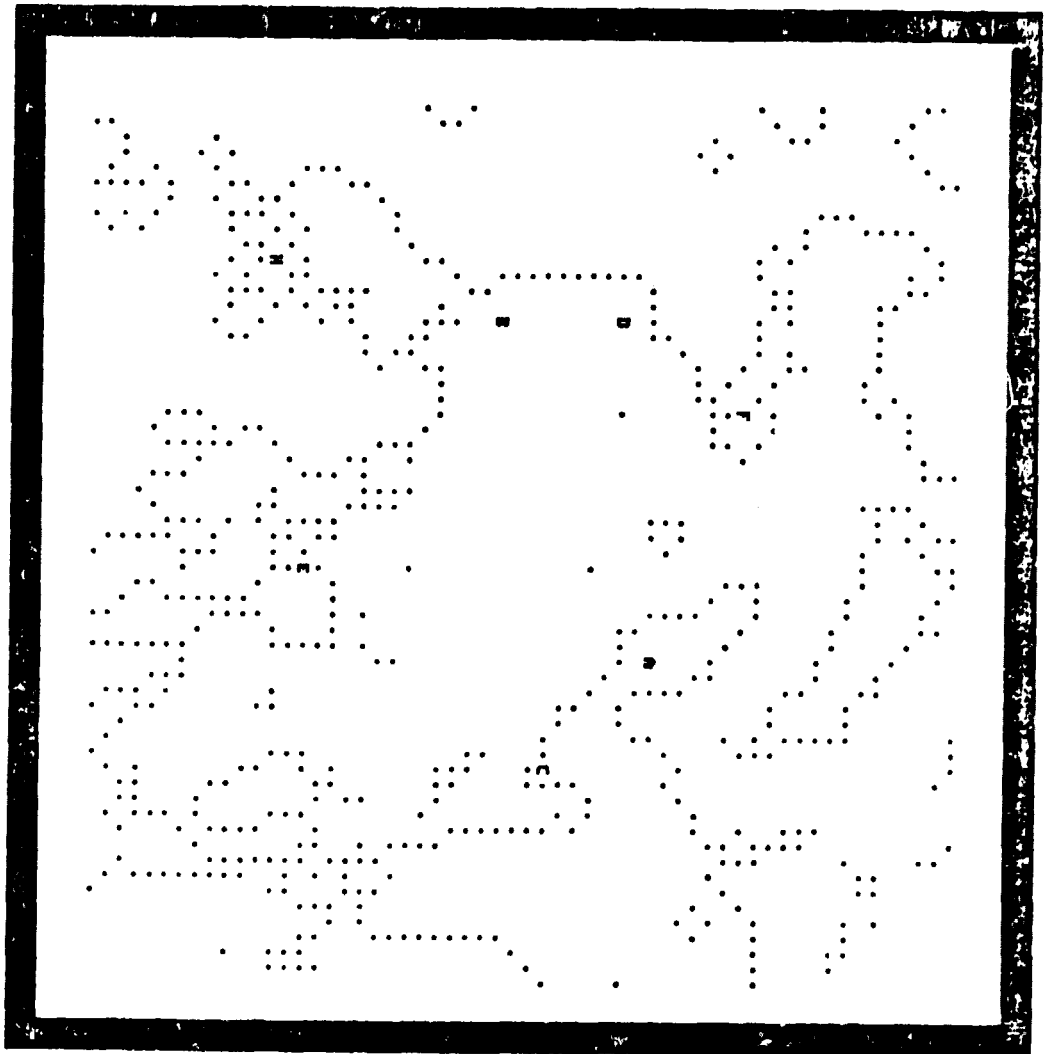


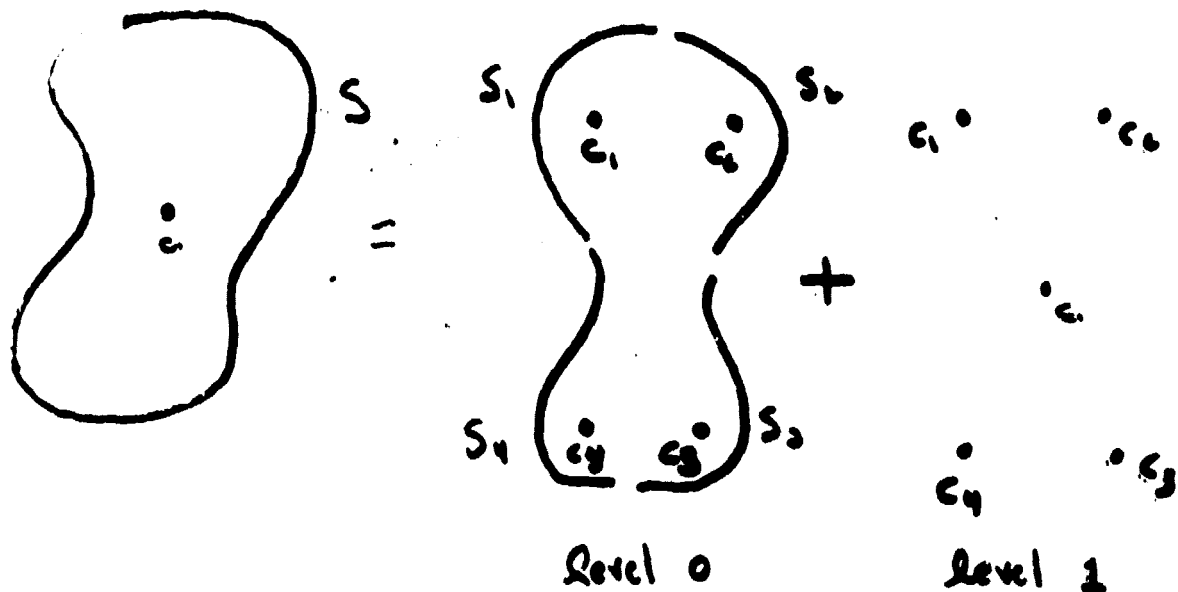
Figure 4b. 2-d tree structure

ORIGINAL PAGE IS
OF POOR QUALITY



Hierarchical Hough Transforms

ORIGINAL PAGE IS
OF POOR QUALITY



① Given a pattern of points P , compute all level 0 Hough transforms: $H_{01}, H_{02}, H_{03}, H_{04}$.

② Let M_i be the set of above-threshold peaks in H_{0i} , $i=1, \dots, 4$.

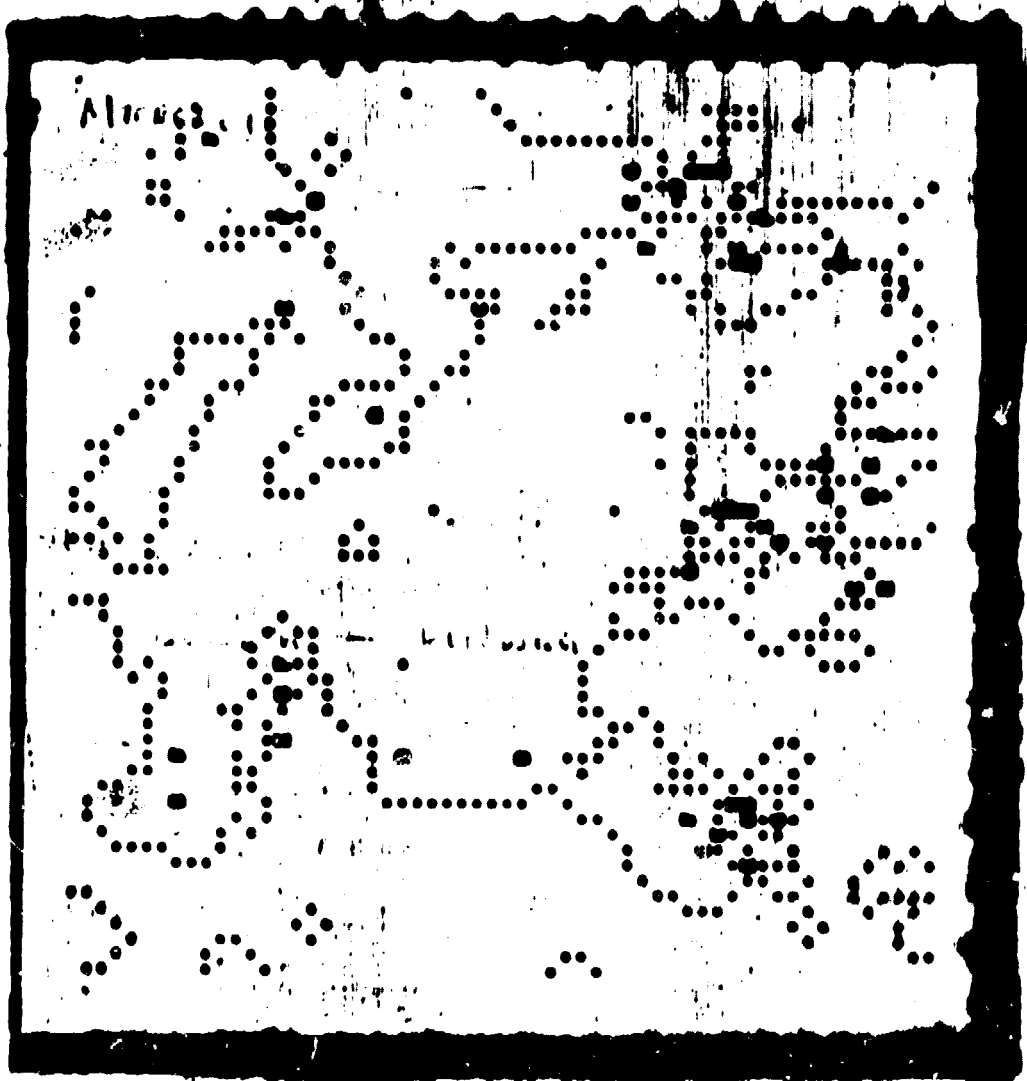
③ Compute the Hough transform of level 1 with the sets M_i

for each c_i in level 1

for each m_j in M_i

increment the appropriate subspace of HT

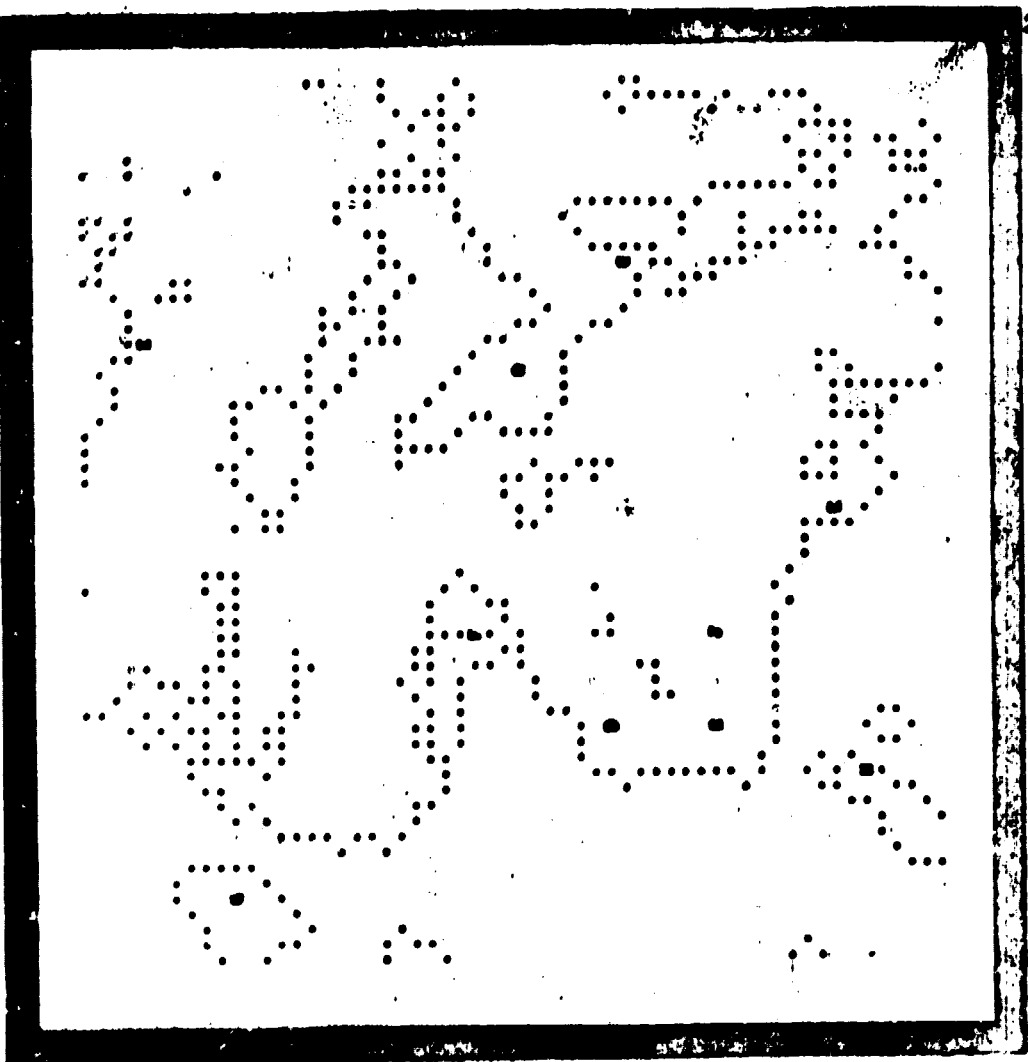
ORIGINAL PAGE IS
OF POOR QUALITY



18/4/80

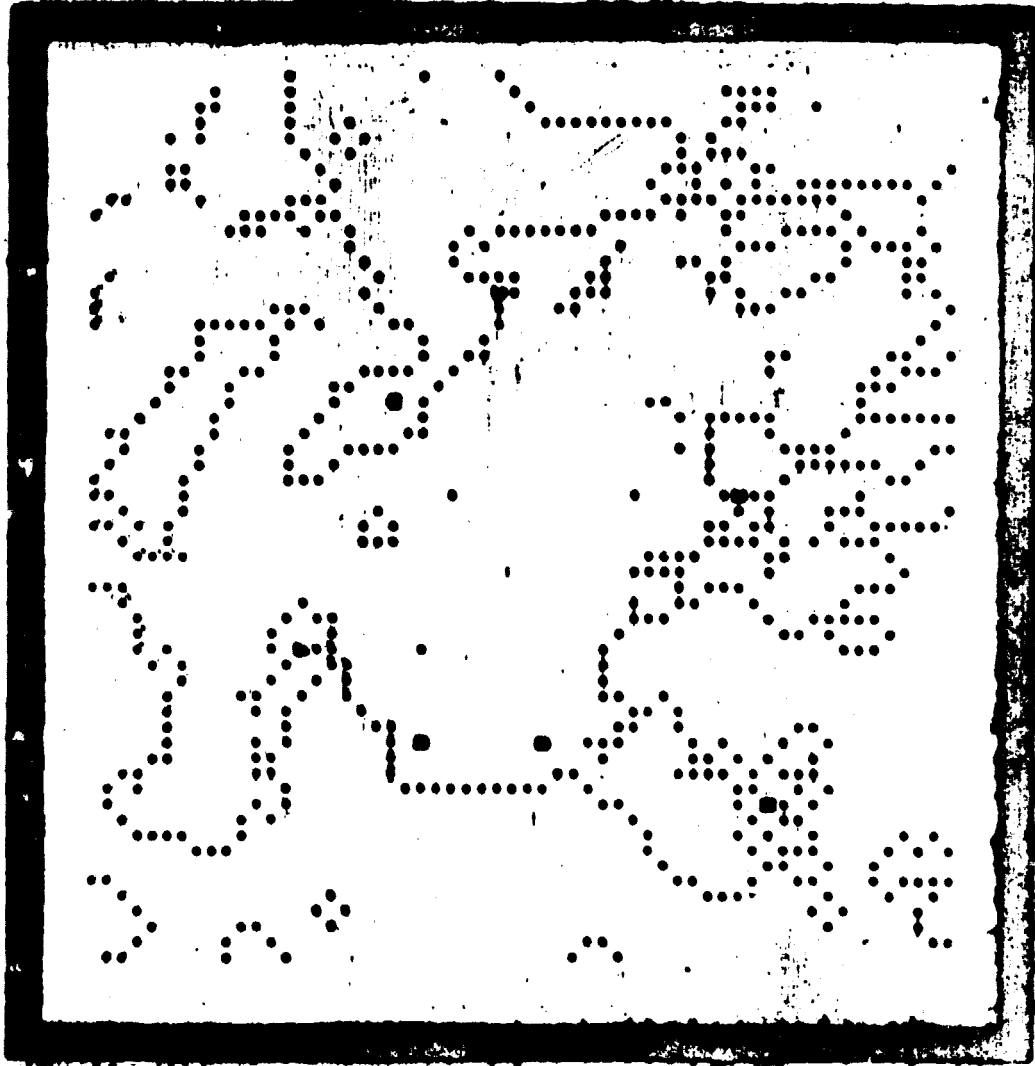
Potential matches in Frame 2

ORIGINAL PALETTE
OF POOR QUALITY



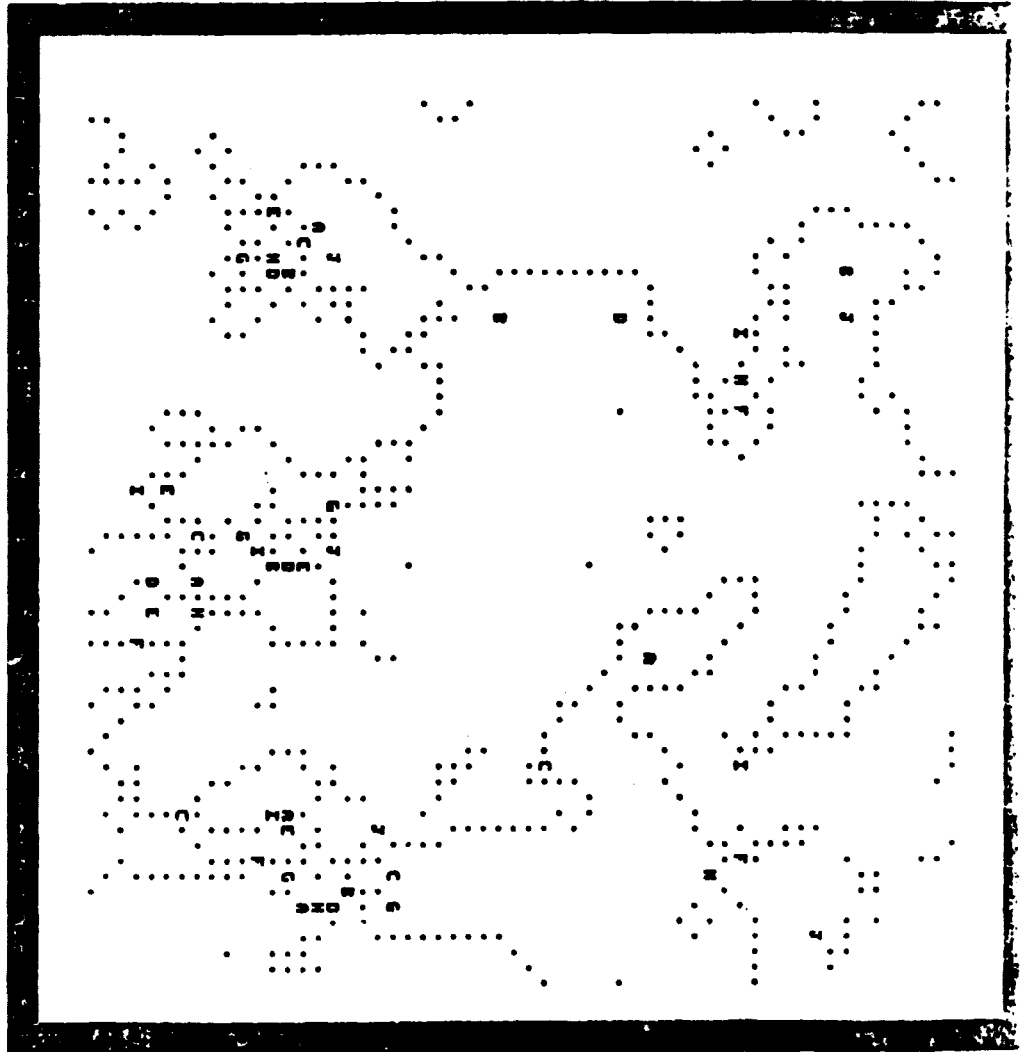
Interest Points in Frame 1

ORIGINAL PAGE IS
OF POOR QUALITY



Best match in frame 2

ORIGINAL PAGE IS
OF POOR QUALITY



Hough Transforms for linear patterns

ORIGINAL PAGE IS
OF POOR QUALITY

- $L = \{L_1, \dots, L_n\}$ - set of line segments which define the pattern
- $L' = \{L'_1, \dots, L'_m\}$ - set of observed line segments.
- Define $L_i - L_j$ as follows
 - if L_j is a subsegment of L_i , then $L_i - L_j \equiv L_j - L_i$
 - otherwise, $L_i - L_j \equiv L_i$
- Let \mathcal{F} be a set of transformations that map lines to lines.

Matching problem

Given L, L' , and \mathcal{F} , find $f \in \mathcal{F}$ s.t.

$$r(f) \equiv \sum_{L_i \in L} \sum_{L'_j \in L'} [L_i - f(L'_j)]$$

is minimal.

ORIGINAL PAGE IS
OF POOR QUALITY

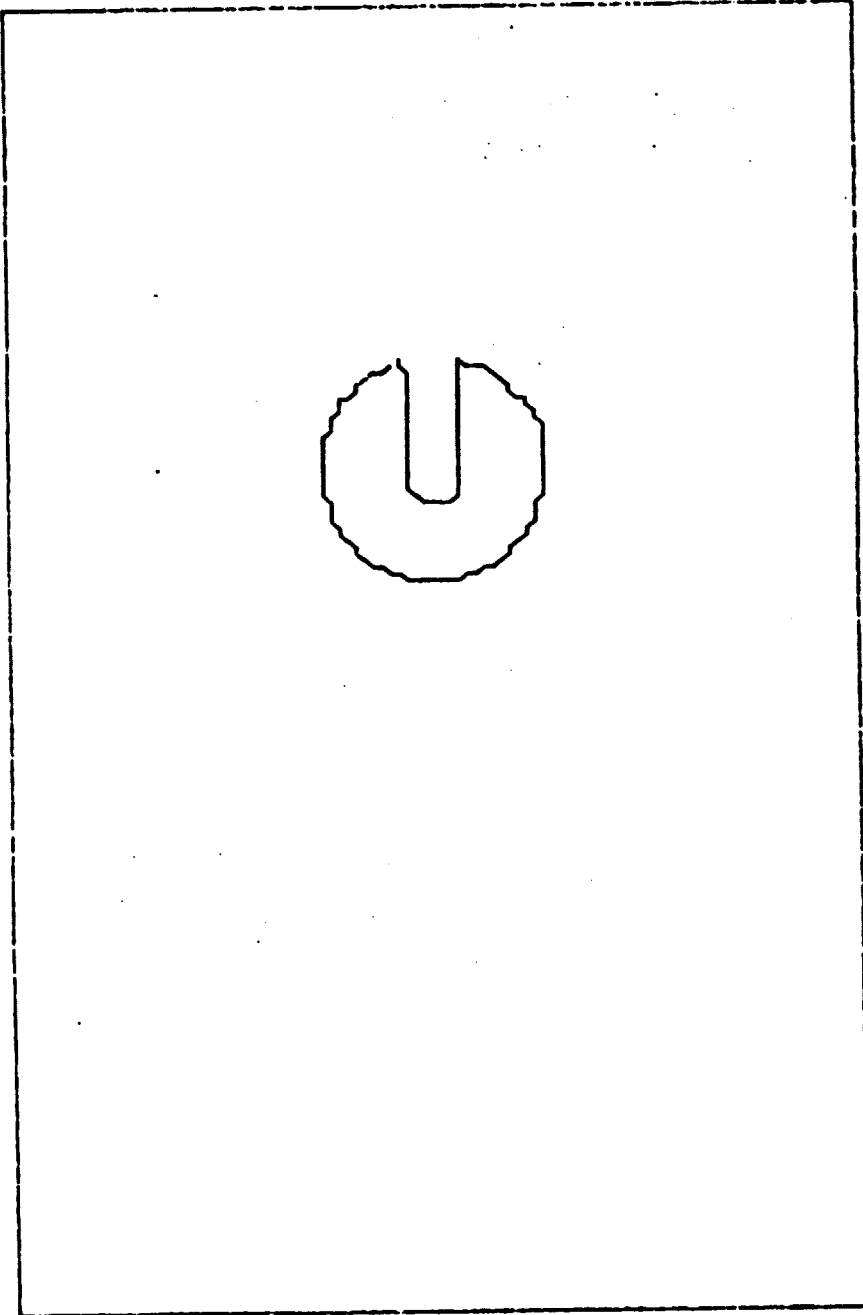


Figure 5a

ORIGINAL PAGE IS
OF POOR QUALITY

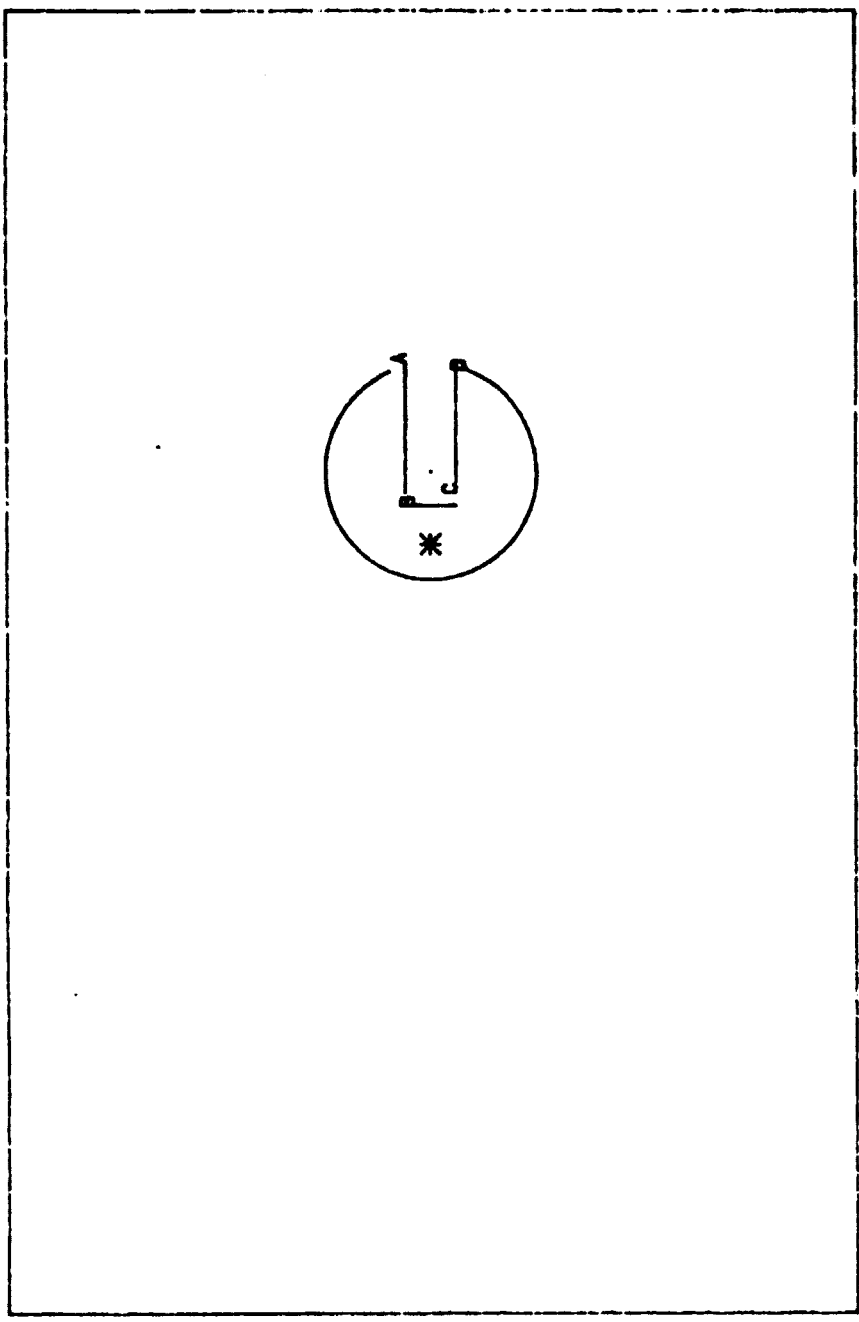


Figure 6a
Figure 7a

ORIGINAL PAGE IS
OF POOR QUALITY

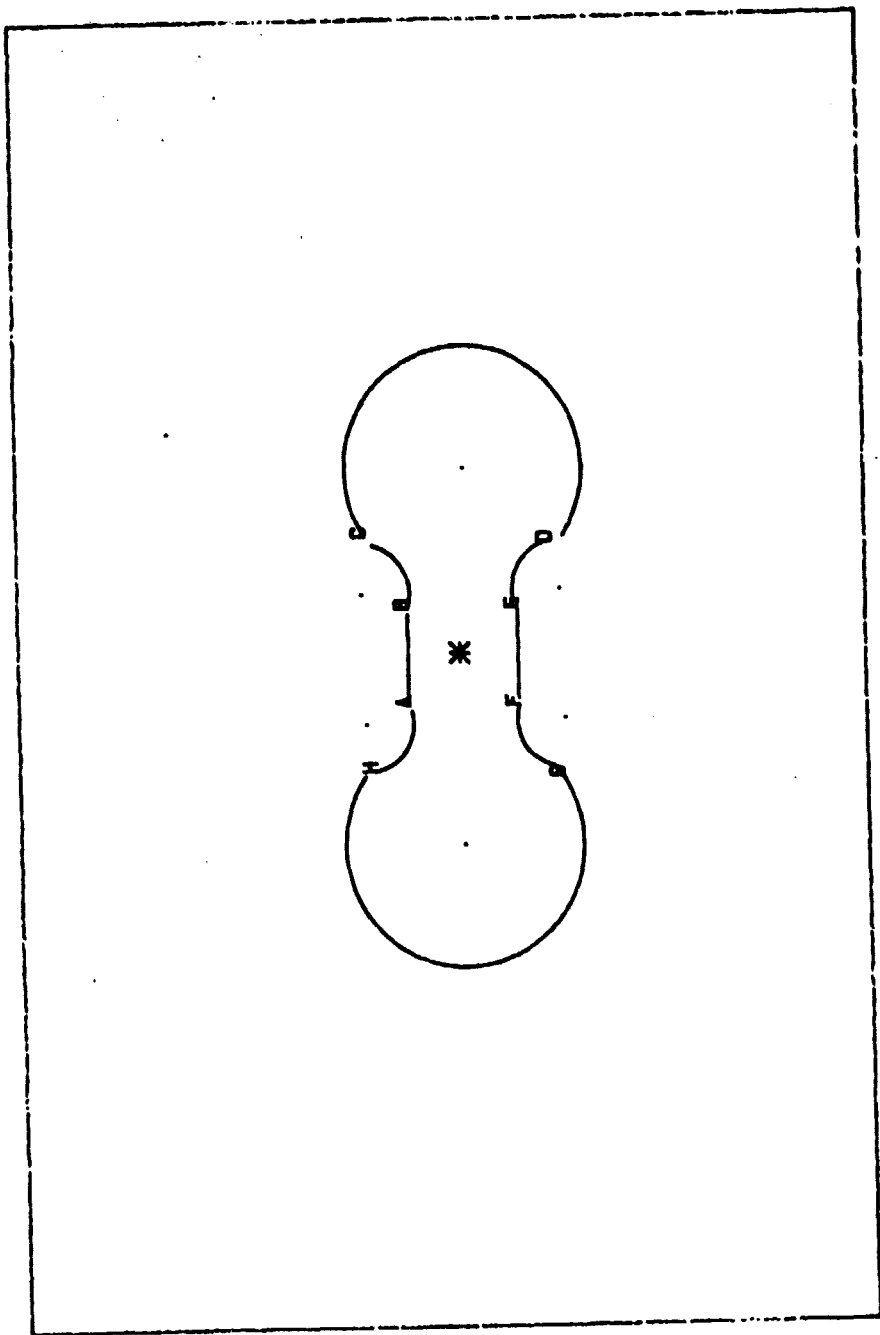


Figure 6(bii)

ORIGINAL PAGE IS
OF POOR QUALITY.

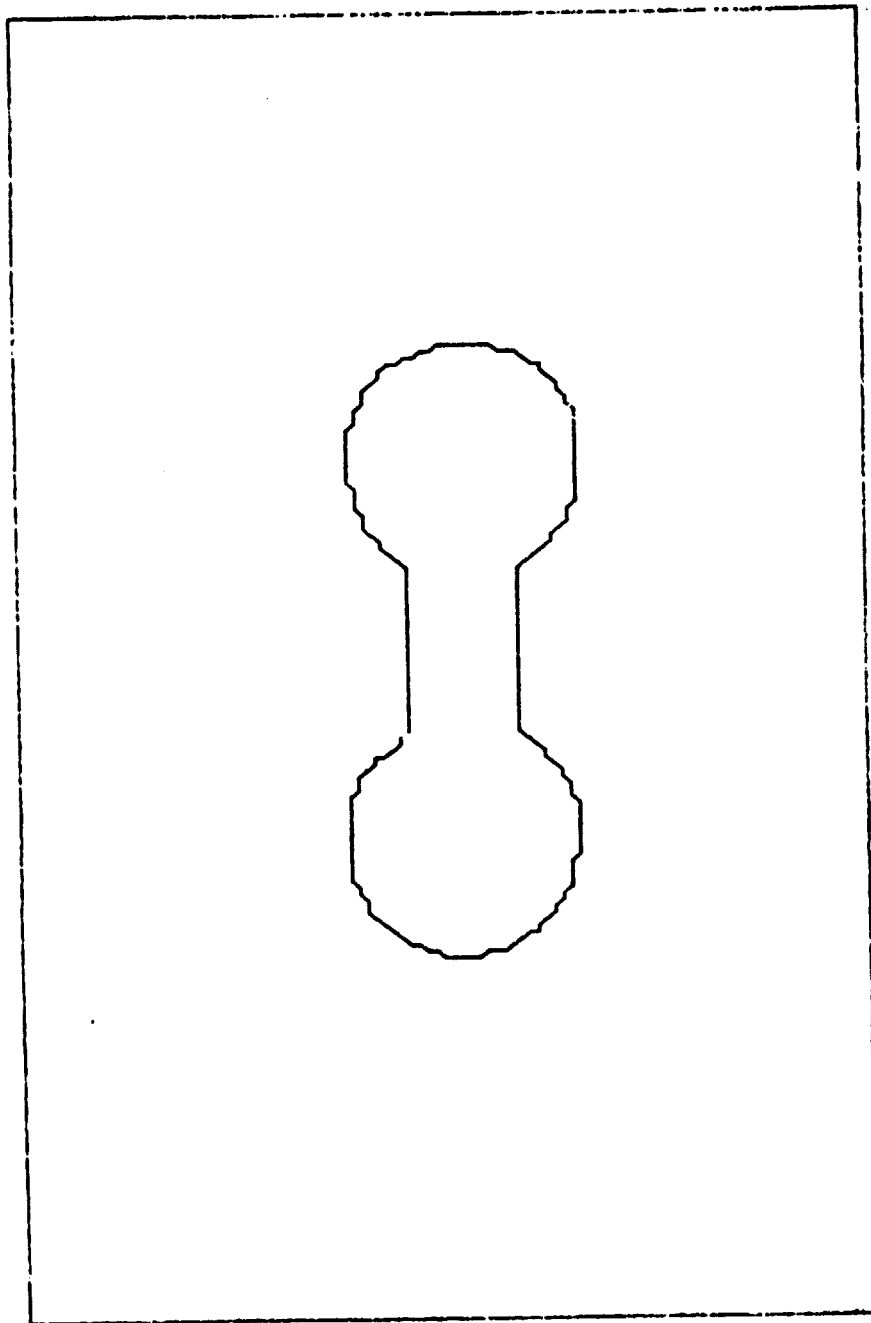


Figure 5b

ORIGINAL PAGE IS
OF POOR QUALITY

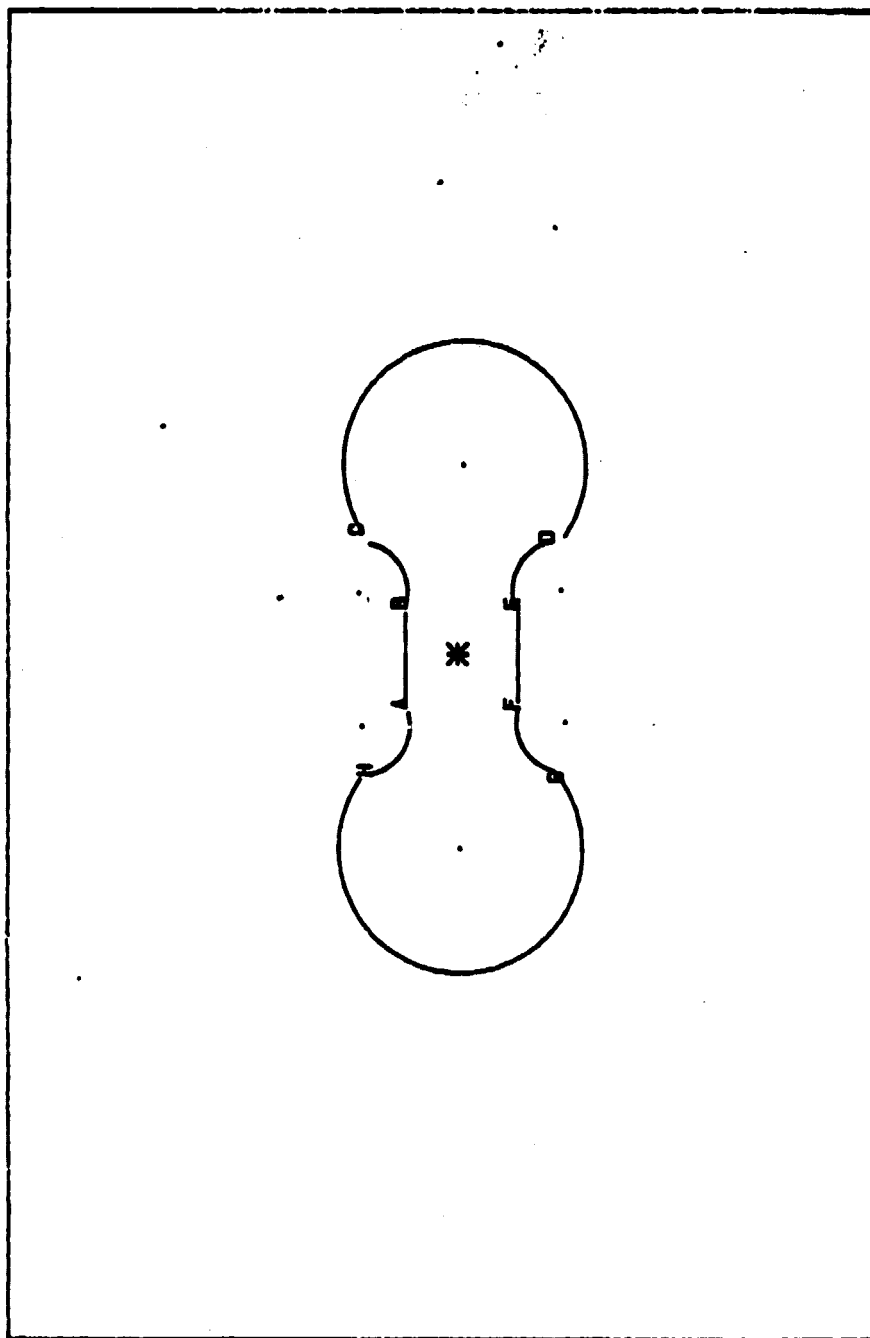


Figure 6(bii)

ORIGINAL PAGE IS
OF POOR QUALITY.

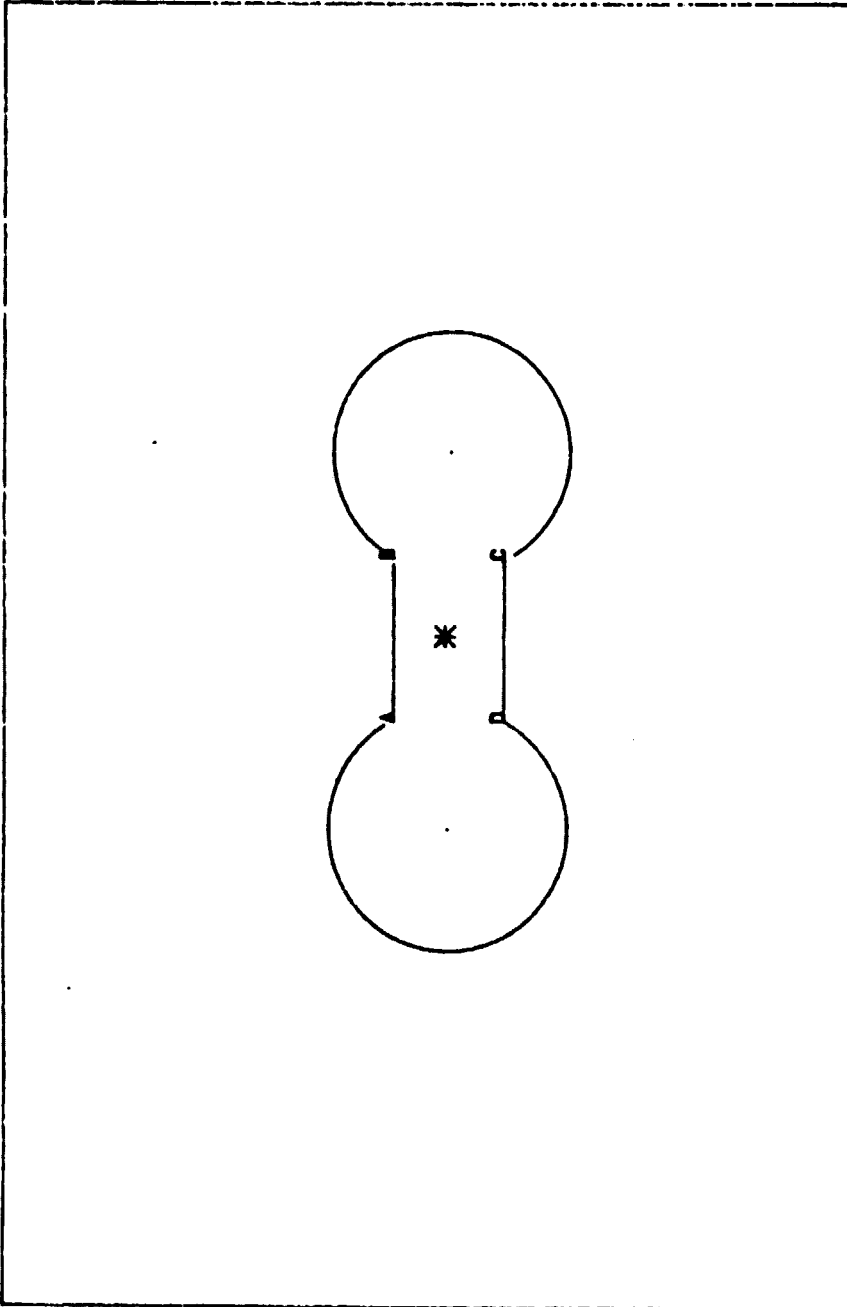
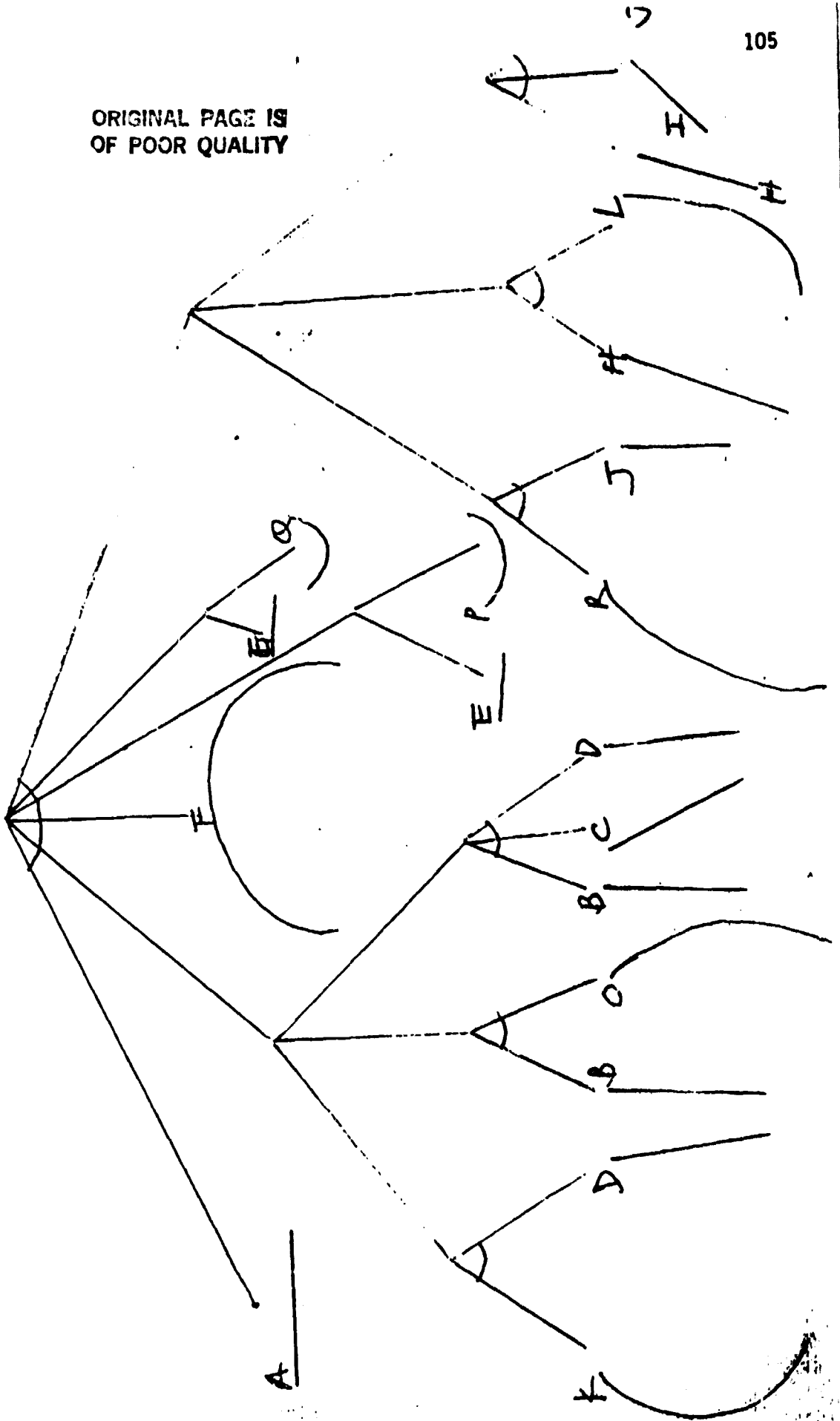


Figure 6 b(ii)

ORIGINAL PAGE IS
OF POOR QUALITY

Figure 15



ORIGINAL PAGE IS
OF POOR QUALITY

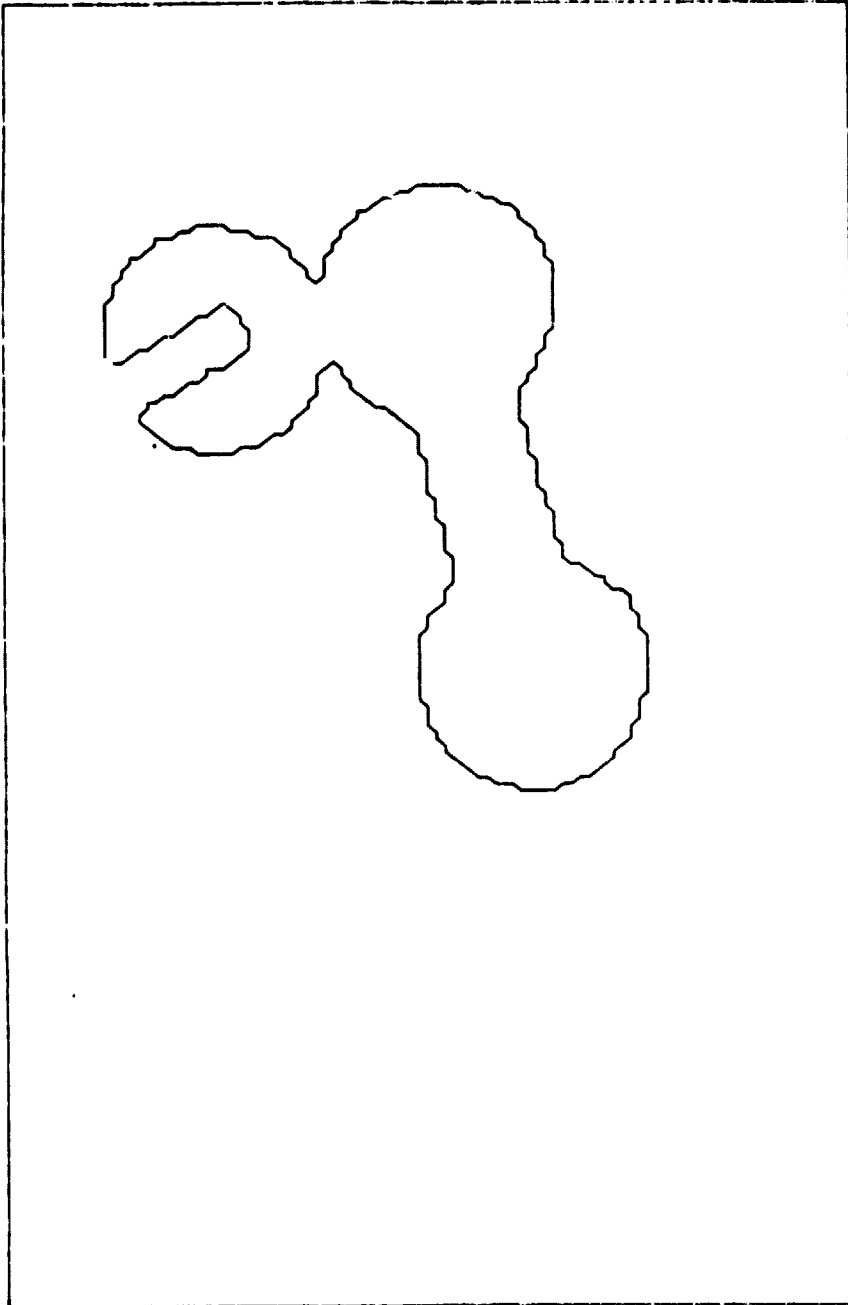


Figure 8 (1)

ORIGINAL PAGE IS
OF POOR QUALITY

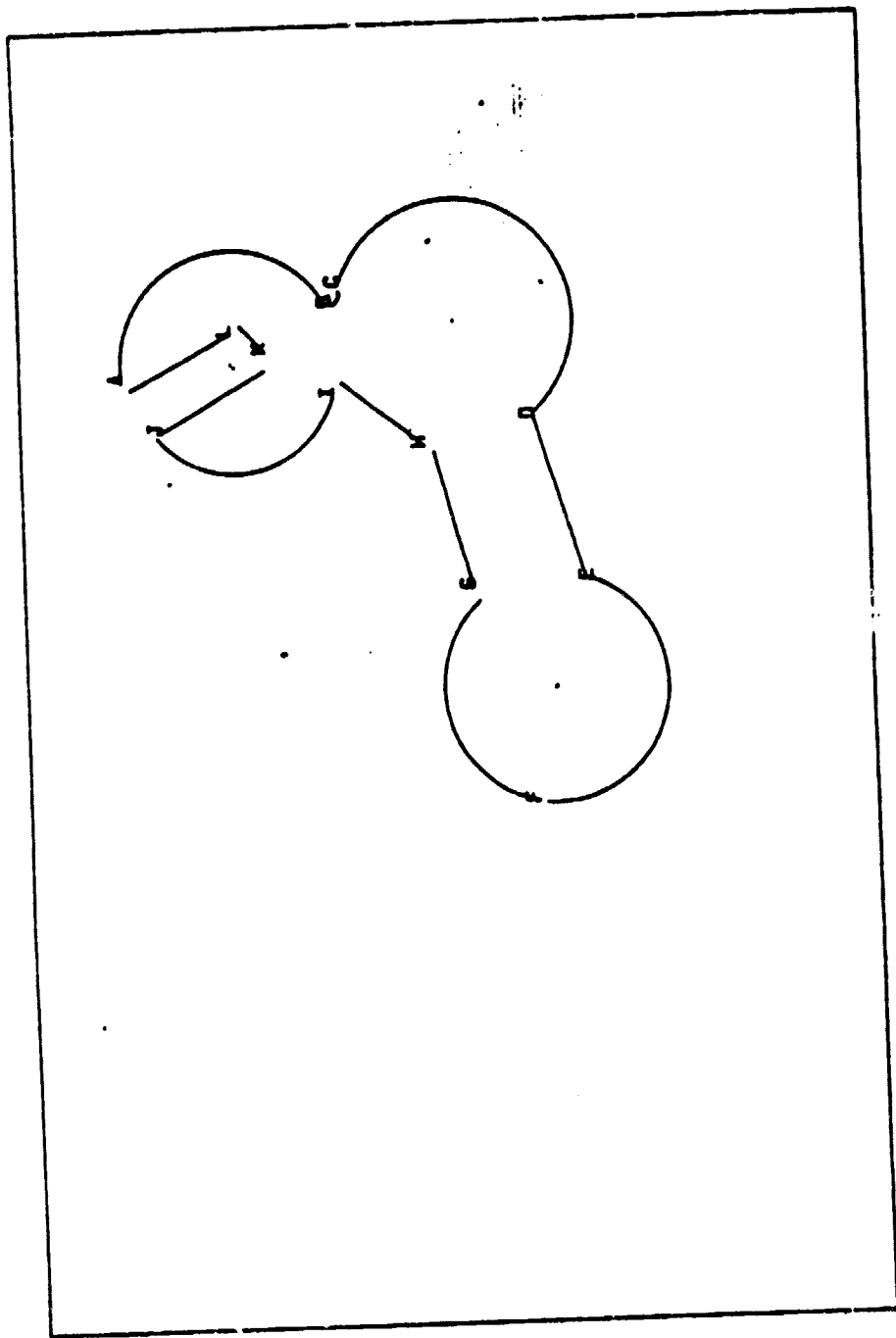


Figure 10(c)

ORIGINAL PAGE IS
OF POOR QUALITY

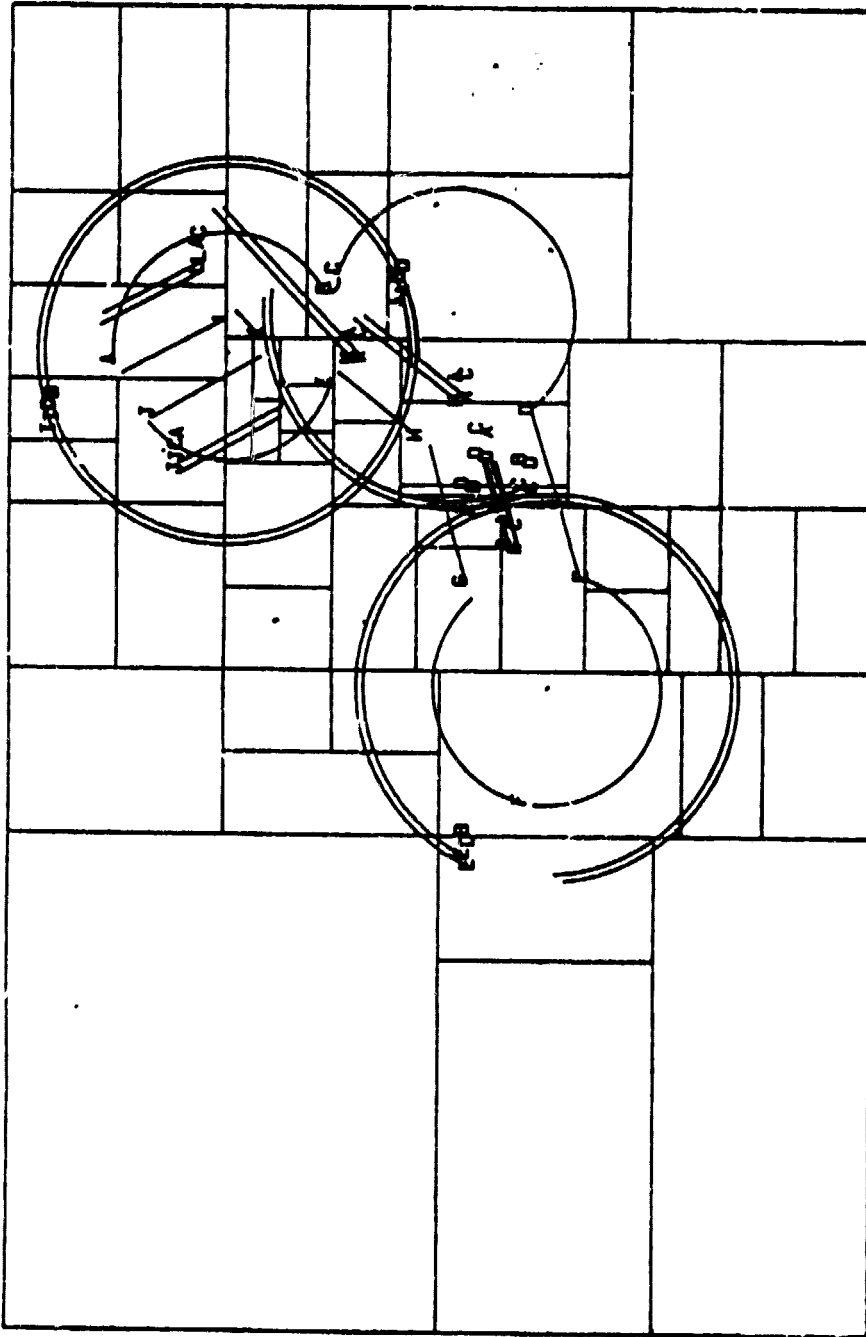


Figure 1A(1). Insize matched to model 2

D5

ORIGINAL PAGE IS
OF POOR QUALITY.

Subpixel Registration Accuracy
and Modelling

Laveen N. Kanal
LNK Corporation

INTRODUCTION

- HOW ACCURATELY CAN A LANDSAT IMAGE BE REGISTERED TO A REFERENCE IMAGE?
- HOW CAN SUBPIXEL ACCURACY BE ACHIEVED?
- WHAT FACTORS AFFECT REGISTRATION ACCURACY?
- HOW SHOULD THE REFERENCE IMAGES BE FORMED?
- HOW CAN VARIOUS ALGORITHMS BE EVALUATED?

ORIGINAL PAGE IS
OF POOR QUALITY

HIGH REGISTRATION ACCURACY

- NEEDED TO MERGE DATA FROM DIFFERENT SOURCES
 - MULTITEMPORAL DATA
 - MULTISENSOR DATA

- MISREGISTRATION RESULTS IN REDUCED CLASSIFICATION ACCURACY

ORIGINAL PAGE IS
OF POOR QUALITY

TYPICAL REGISTRATION REQUIREMENTS

- LESS THAN .5 PIXEL GEODETIC REGISTRATION ERROR
- .3 PIXEL RELATIVE (BETWEEN TWO IMAGES)

ABOVE STANDARDS MUST BE MET 90% OF THE TIME.

ORIGINAL PAGE IS
OF POOR QUALITY

CURRENT REGISTRATION APPROACH

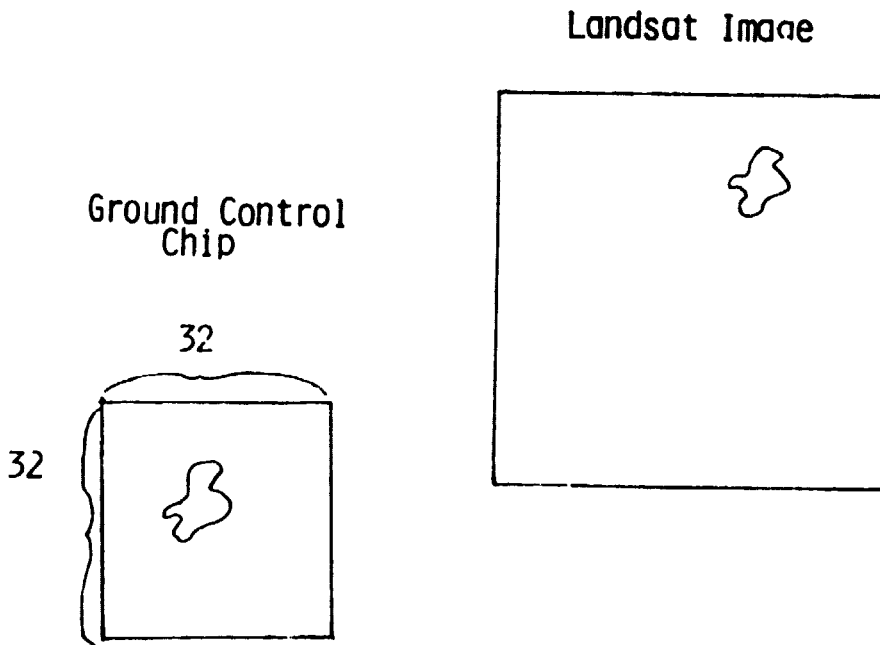
- DEVELOP CONTROL POINT CHIP LIBRARY (CPC)
 - CPC-SET OF RECOGNIZABLE POINTS

- EXTRACT CONTROL POINT NEIGHBORHOOD (CPN)
FROM SCENE TO BE REGISTERED

- FIND BEST LOCATION IN CPN MATCHING CPC

SUBPIXEL REGISTRATION ACCURACY

Basic Problem: Find a translation aligning a reference
(Ground Control Chip) and a Landsat image
to less than one pixel



SUBPIXEL ACCURACY PROBLEMS

1) WHAT IS SUBPIXEL ACCURACY?

Image distortion is nonlinear.

MEASURE OF ACCURACY? Maximum error, average error,
percentage of points lying far away?

2) HOW CAN CLAIMS FOR SUBPIXEL ACCURACY OF ALGORITHM BE ASSESSED?

- Experimental methods

- Analytical methods

- Probabilistic image models for correlation procedures

- Geometric models for feature (edge) matching

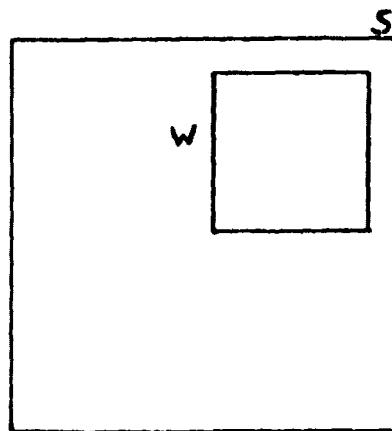
- Assume error bounds on feature detection

- Compute bounds on estimation of edge location

PROBLEMS (Cont'd.)

- 3) WHAT SCENE PROPERTIES SHOULD BE USED TO SELECT GROUND CONTROL CHIPS FOR AN IMAGE?
- 4) HOW SHOULD THE LANDSAT IMAGE BE PROCESSED TO FORM AN IMAGE SUITABLE FOR MATCHING?
- Edge enhanced image
 - Edge image
 - Isolated significant point image
 - Corners
 - Intersections
 - High curvature points

CLASSICAL CORRELATION



S = Scene

W = Window

$$R(u,v) = \frac{\sum_{j=1}^K \sum_{i=1}^J S(i,j)W(i-u,j-v)}{\left[\sum_{j=1}^K \sum_{i=1}^J S^2(i,j) \right]^{1/2} \left[\sum_{j=1}^K \sum_{i=1}^J W^2(i,j) \right]^{1/2}}$$

Can be applied to Landsat image, edge enhanced image,
binary image, etc.

One dimensional example

Image 1



Image 2

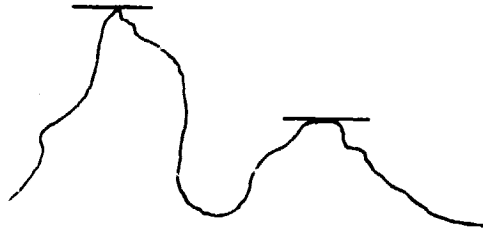


Correlation

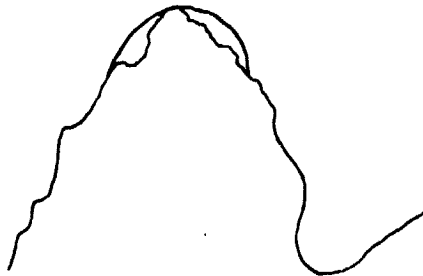


CORRELATION SURFACE QUALITY
MEASURES

- PEAK TO SIDELobe RATIO



- CURVATURE OF THE PEAK



BASIC SUBPIXEL REGISTRATION APPROACH

- FIND THE CROSS-CORRELATION BETWEEN A
CPC AND THE CORRESPONDING CPN
- INTERPOLATE THE CORRELATION FUNCTION
TO FIND THE CONTINUOUS CORRELATION SURFACE
PEAK

CPC AND CPN MAY BE PREPROCESSED TO IMPROVE
CORRELATION ACCURACY.

INTERPOLATION FOR SUBPIXEL
ACCURACY

- 1) Fit surface to correlation function in a neighborhood.
 - 5x5 neighborhood is common
 - Up to the 4th order bivariate polynomials are used
 - Successive orders can be used, use RMS residual error to select order
 - Elliptical cones have been used

PROBLEM:

Sensitivity of peak location to fitting function

ORIGINAL PAGE IS
OF POOR QUALITY.

INTERPOLATION (Cont'd.)

- 2) Use centroid of correlation function in a neighborhood
- 3) Spatial offset corresponds to non-vanishing phase in frequency domain
 - Transform phase portion of correlation back to spatial domain to locate peak

PROBLEM:

Non symmetry of cross-correlation function about peak causes error in phase

ESTIMATING CORRELATION PEAK
UNCERTAINTY

- 1) Curvature at peak
- 2) Second moment of correlation samples around peak
- 3) Rate of decline away from peak

USES OF MEASURES:

- Reject Matching
- Weight for mapping function fit.

FEATURE IMAGE MATCHING

FEATURES

EDGES

INTERSECTION

HIGH CURVATURE POINTS

- Feature matching is growing in popularity
- Robustness under spectral change
 - Crop growth
 - Water content
 - Illumination

METHODS OF FEATURE MATCHING

- Correlation of Edge Images

- Correlation of Binary Edge Images

- Lineal Correspondence (L.N.K. procedure)
 - Real lineals
 - Abstract vectors

- Point Matching
 - Relaxation

LITERATURE INTRODUCTION

- REVIEW FIVE PREVIOUS STUDIES OF LANDSAT REGISTRATION ACCURACY
- COMMON FLAW - REFERENCE IMAGE ASSUMED HIGHLY ACCURATE
- SOME SOURCES OF REFERENCE IMAGE ACCURACY
 - 1) POLYNOMIAL FITTING ON ENLARGING REFERENCE IMAGE TO MATCH MAP
 - 2) FITTING POLYNOMIAL TO DETERMINE ATTITUDE AND ALTITUDE CORRECTION
- COMBINED ERROR EFFECTS ESTIMATED ACCURACY $\frac{1}{4}$ PIXELS
 - 90% OF ALL POINTS HAD POSITIONAL ERROR WITHIN 23 METERS (NIBLACK 1981)
 - BASIS FOR ABOVE NOT ADEQUATELY DESCRIBED IN PAPER.

DEPARTURE FROM PREVIOUS EXPERIMENTS

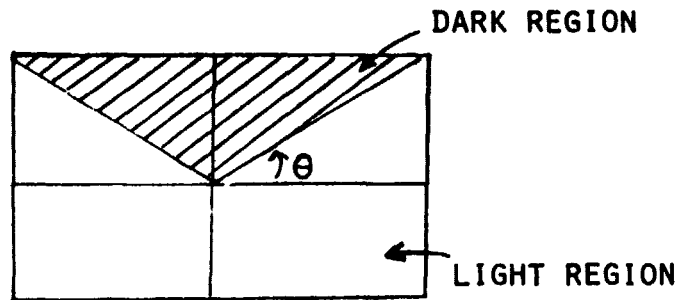
- PREVIOUS THEORETICAL AND SIMULATION STUDIES OF REGISTRATION ACCURACY MEASURE PERFORMANCE IN ONE OF TWO WAYS:
 - (1) SINGLE OFFSET PROBABILITY OF FALSE ACQUISITION TO DETERMINE ACCURACY TO NEAREST PIXEL, AND
 - (2) EITHER EXPECTED VALUE OF THE ERROR OR ROOT MEAN SQUARE OF THE ERROR, TO MEASURE SUBPIXEL ACCURACY.

- WE PROPOSE TO REPLACE THE ABOVE BY THE FOLLOWING:
 - (1) PROBABILITY OF FALSE ACQUISITION OVER THE ENTIRE IMAGE, AND
 - (2) THE PROBABILITY DISTRIBUTION OF THE ERROR.

EXPERIMENTAL REGISTRATION

PURPOSE - DETERMINE FEASIBILITY AND EXTENT OF SUBPIXEL ACCURACY OF EDGE LOCATION UNDER IDEAL CIRCUMSTANCES.

METHOD: GENERATE A REFERENCE IMAGE CONSISTING OF TWO HOMOGENEOUS REGIONS



- θ IS A PARAMETER
- THE TWO REGIONS HAVE DIFFERENT MEANS AND I.I.D. PIXELS
- SENSOR IMAGE CONSISTS OF A SUBPOINT OF THE REFERENCE IMAGE WITH NOISE ADDED
- GREY LEVEL CORRELATION USED TO MATCH IMAGES
- FOURTH-ORDER BIVARIATE POLYNOMIAL FIT TO CORRELATION IN A 5×5 NEIGHBORHOOD
- PEAK TAKEN AS MATCH POINT

NOTE: NO TRANSLATION WAS INTRODUCED. EFFECT OF NOISE ON OFFSET WAS DESIRED.

EXPERIMENTAL RESULTS

OUTCOME:

- CORRELATION FUNCTION TURNED OUT TO BE ALMOST CIRCULARLY SYMMETRIC
- ESTIMATED PEAK ALWAYS NEAR CENTER OF PIXEL
- PEAK IS ESTIMATE OF WHERE CORNER LIES WITHIN PIXEL
- TRUE CORNER WAS OFTEN NEAR PIXEL BOUNDARY
- SUBPIXEL ACCURACY WAS POOR
- WINDOW SIZE (225 PIXELS) WAS LARGE ENOUGH TO MAKE LAW OF LARGE NUMBERS APPLICABLE
- NUMERATOR AND DENOMINATOR OF CORRELATION FUNCTION CHANGE LITTLE IN NEIGHBORHOOD OF CORRECT MATCH POINT, THUS EXPLAINING SYMMETRY
- FUTURE EXPERIMENTS WILL ASSUME NOISE POINTS ARE CORRELATED AND REFERENCE POINTS ARE CORRELATED (NOT INDEPENDENT)
- THIS WILL ALLEVIATE THE ABOVE PROBLEMS AND MAKE SIMULATIONS MORE REALISTIC.

COMPARISON OF OUR SIMULATIONS WITH NOVAK'S

- NOVAK'S WORK DID BETTER THAN OURS SINCE HE ONLY CONSIDERED A SMALL STRIP AROUND THE EDGE
 - HERE A PIXEL SHIFT IN THE TEMPLATE CAUSES A LARGE DIFFERENCE IN THE STATISTIC
- COMBINATION OF NOVAK'S SIMULATION AND OURS GIVES INSIGHT INTO MATCHING PROBLEM
 - MAXIMUM LIKELIHOOD MAKES MOST EFFICIENT USE OF DATA
 - FROM THIS VIEWPOINT NOVAK METHOD POOR FOR FINDING EDGE TO NEAREST PIXEL
 - ONE SHOULD USE FULL CONTROL CHIP SINCE MAXIMUM LIKELIHOOD ESTIMATE USES ALL PIXELS.
- SUBPIXEL ACCURACY
 - MAXIMUM LIKELIHOOD FOR SUBPIXEL ACCURACY USES ONLY EDGE PIXELS
 - OTHER PIXELS ADD NO INFORMATION - ONLY CAUSE FURTHER ERROR
 - NOVAK'S METHOD SUPERIOR HERE

COMPARISON WITH NOVAK'S METHOD (CONT'D.)

● CONCLUSION (TENTATIVE)

- PERFORM CORRELATION ON WHOLE CONTROL CHIP TO GET PIXEL ACCURACY
- ONLY USE PIXELS WITH A HIGH LIKELIHOOD OF SUB-PIXEL INFORMATION (E.G., ON OR NEAR EDGES) FOR SUBPIXEL MATCHING.

MOSTAFAVI-SMITH MODEL

**ORIGINAL PAGE IS
OF POOR QUALITY**

$$i_r = p(x) + n_r(x)$$

$$i_s = p_d(x) + n_s(x)$$

$$p_d(x) = p(Ax + x_0)$$

$x = (x_1, x_2)'$ point in plane

A: 2x2 distortion matrix

p: noise free image either a deterministic
or a random signal

For p deterministic, $p(x)$, $p_d(x)$ or their Fourier
Transforms available. For p random: signal spectrum
assumed known p , n_r , n_s zero mean, 2nd order, inde-
pendent Gaussian Processes with spatially invariant
statistics.

MOSTAFAVI-SMITH MODEL FOR REGISTRATION

GOAL: Find image size and shape minimizing probability of false acquisition and maximizing local accuracy.

MEASURES OF CORRELATOR PERFORMANCE

1. Ratio of mean cross-correlation peak to standard deviation of cross-correlation in the sidelobes (called Peak-to-Sidelobe Ratio).
2. Probability that the correlation function of some point far from the correct registration exceeds some threshold. (called the single-offset probability of false acquisition.)
3. First order approximation to local registration error using the correlation function gradient and curvature.

BASIC ASSUMPTIONS: Gaussian images, additive Gaussian noise, the two images to be registered are related by an affine transformation.

- RESULTS
- 1) Derives image size to minimize probability of false acquisition under geometric distortion.
 - 2) Derives expression for minimum achievable probability of false acquisition.
 - 3) For circularly symmetric autocorrelation functions, the square window is optimal among rectangle windows.
 - 4) Derives optimal window size to maximize local accuracy.
 - 5) For a fixed geometric distortion the image size resulting in minimum local error is smaller than the size giving a minimum probability of false acquisition.

ORIGINAL PAGE IS
OF POOR QUALITY

FUNDAMENTAL ASSUMPTIONS

MOSTAFAVI-SMITH (1978)

REFERENCE IMAGE $I_R(x)$ SPATIALLY STATIONARY*
SENSED IMAGE $I_S(x)$

$$I_S(x) = I_R(\theta+x) + I_N(\theta+x) **$$

NOISE INDEPENDENT OF I_R

I_R, I_N GAUSSIAN

COMMENTS

RETAINED ONLY TRANSLATIONS,
NOT DISTORTIONS, CONSIDERED
NOW
NEED ONLY I_R, I_S JOINTLY
STATIONARY ALTHOUGH
INDEPENDENT CASE IS
SIMPLEST NOT NEEDED AT
ALL ***

* STATISTICS SPATIALLY SHIFT-INVARIANT

** ADDITIVE NOISE UNREALISTIC ESPECIALLY FOR PREPROCESSED OR
EDGE-ENHANCED OR BINARY PICTURES

*** SINCE WEAK ASSUMPTIONS ON I_R, I_S GUARANTEE THE CORRELATION
PROCESS $C(x)$ AT VARIOUS OFFSETS x IS ESSENTIALLY GAUSSIAN
FOR LARGE WINDOWS (SENSED IMAGES).

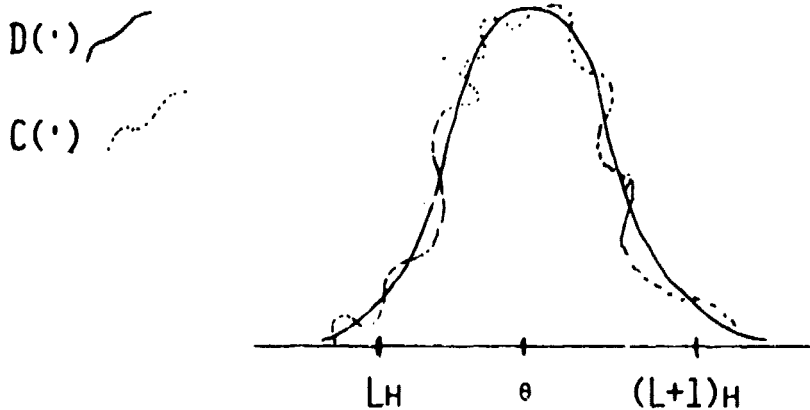
DEFINITIONSORIGINAL PAGE IS
OF POOR QUALITY

$$D(x) = E \{C(x)\}$$

PICTURE OF ONE-DIMENSIONAL CASE

D(x) "KNOWN" FOR $x = 0, \pm H, \pm 2H, \dots$

H = PIXEL WIDTH

 θ^* = ESTIMATED (FROM $C(\cdot)$) MAXIMUM LOCATIONFIGURE OF MERIT⁽⁺⁾

$$Q(T) = \text{PR} \{ |\theta^* - \theta| \geq T \}$$

(+) NOTE DISTINCTION FROM SINGLE-OFFSET COMPARISONS LIKE
 $\text{PR} \{ C(0) \geq C(x) \}$ FOR VARIOUS x , AS USED BY MOSTAFAVI-SMITH (1978)

ACCURACY BOUNDORIGINAL PAGE IS
OF POOR QUALITYIF $D(x)$ IS KNOWN AT

$$0, \pm H, \dots,$$

AND IF OBSERVED PIXEL GREY-LEVEL IS

$$X_K \equiv \frac{1}{H} \int_{KH}^{(K+1)H} I_S(T) DT$$

(OR ANY OTHER LINEARY OPERATOR OF I_S)

WITH REFERENCE-IMAGE PIXEL GREY-LEVEL

$$Y_J = \frac{1}{H} \int_{JH}^{(J+1)H} I_R(T) DT$$

THEN A RIGHT UPPER BOUND ON THE ERROR AS A FRACTION OF A
PIXEL IS

$$K = \left(\frac{H^2 D^{(IV)}(\theta)}{-12 D''(\theta)} \right)^{\frac{1}{2}}$$

QUALITATIVE MEANING AND INTERPRETATION OF K:

- (A) IF $D(x)$ IS KNOWN AT INTEGER MULTIPLES OF H , THEN TREATING $D(\cdot)$ AS QUADRATIC ON PIXEL CONTAINING θ GIVES ERROR AT MOST FRACTION K OF PIXEL.
- (B) IF I_R IS HIGHLY OSCILLATORY WITH RESPECT TO UNIT OF LENGTH H WITH CORRELATIONS OF I_R' FALLING OFF RAPIDLY THEN K IS LARGE.

EDGE SUBPIXEL ACCURACY

- Assume relatively high correlation accuracy
(within a pixel or two)

- Locate edge in image known to correspond to
straight features

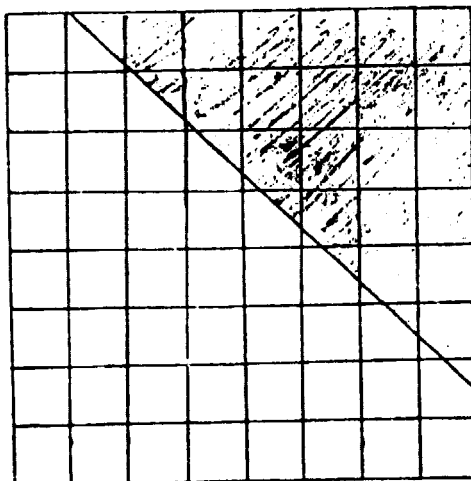
- Estimate location of line in mixed pixels

ESTIMATION PROCEDURES (Davis)ORIGINAL PAGE IS
OF POOR QUALITY

- 1) Make distributional assumptions for bordering regions.
 - Estimate mixed pixel values for each possible location of line
 - Use optimization to pick line best fitting grey level data

- 2) Find best line fitting pixels ignoring grey levels

Example: Fit line through centers



GEOMETRIC ACCURACY

BASIC QUESTIONS:

- HOW ACCURATELY CAN WE LOCATE REAL WORLD EDGES AND STRIPS GIVEN OBSERVED DIGITAL EDGES AND STRIPS?
- HOW CAN THIS ACCURACY INFORMATION BE USED TO ACHIEVE SUBPIXEL ACCURACY?
- WHAT PROPERTIES OF LINES OR STRIPS CAN BE USED TO SELECT GOOD FEATURES FOR A REFERENCE IMAGE?

TYPES OF OBSERVED EDGES

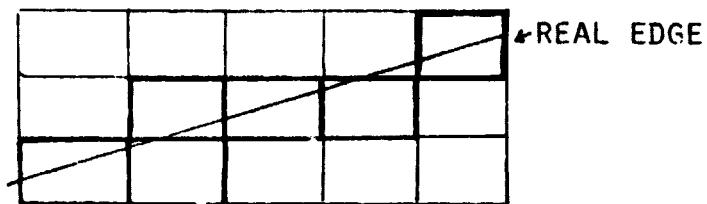
- 1) DIGITAL EDGE - THE SET OF PIXELS A REAL EDGE INTERSECTS
 - SIMPLEST MODEL BUT UNREALISTIC

- 2) DIGITAL EDGE (PIXELS MISSING) - ANY SUBSET OF A DIGITAL EDGE
 - FEASIBLE MODEL IF WE ONLY SELECT GOOD CANDIDATES FOR EDGE POINTS

- 3) DIGITAL EDGE (PIXELS MISSING, PIXELS ADDED) - A DIGITAL EDGE WITH SOME PIXELS MISSING AND SOME SPURIOUS EDGE PIXELS ADDED
 - REALISTIC MODEL

DOMAIN OF VARIABILITY

THE SET OF OBSERVED EDGE PIXELS RESULTING FROM A
REAL EDGE COULD COME FROM AN INFINITE NUMBER OF EDGES.



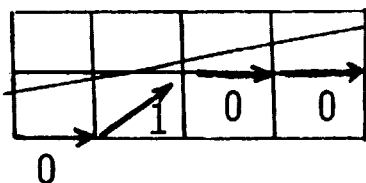
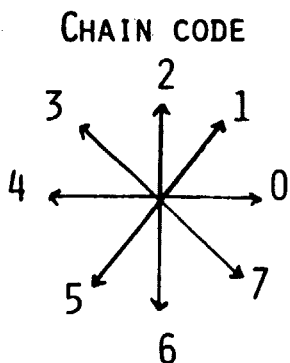
PROBLEM: HOW CAN WE PARAMETRIZE THE POSSIBLE LINES
CAUSING THESE EDGE PIXELS TO BE OBSERVED?

DIGITAL LINE DESCRIPTION (DORSE AND SMEULDERS)

ORIGINAL PAGE IS
OF POOR QUALITY

DIGITAL LINES WILL BE CHARACTERIZED BY FOUR PARAMETERS

EIGHT CONNECTED LINES ARE USED



CHAINCODE 0100

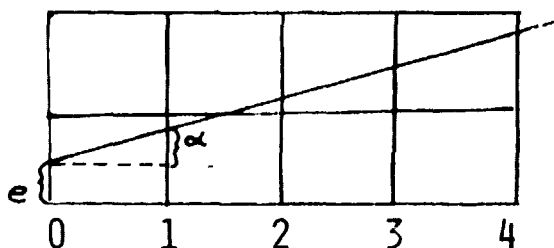
FOUR PARAMETERS:

- N - LENGTH OF CHAIN CODE
 - Q - SMALLEST PERIODICITY PRESENT IN STRING
 - R - NUMBER OF CODES PER PERIOD
 - S - STARTING POINT OF SEGMENT WITH STANDARD PERIOD
- SLOPE {

FEASIBLE PARAMETER REGION
DIGITAL EDGE

ORIGINAL PAGE IS
OF POOR QUALITY

PARAMETRIZATION OF REAL LINES



- GIVEN A DIGITAL EDGE, THE SET OF ALL LINES WHICH
COULD GIVE RISE TO THE EDGE CAN BE PARAMETRIZED
IN TERMS OF (e, α)
- FEASIBLE REGION IS A QUADRILATERAL
- VERTICES CAN BE EXPRESSED IN CLOSED FORM IN TERMS
OF (N, Q, P, S)

FEASIBLE PARAMETER REGION
DIGITAL EDGE FORMULA

DORST AND SMEULDERS (1982)

If one defines functions F and L by:

$$F(s) = s - \left\lfloor \frac{s}{q} \right\rfloor q$$

and

$$L(s) = s + \left\lfloor \frac{N-s}{q} \right\rfloor q$$

and an integer ℓ by the implicit definition

$$1 + \left\lfloor \frac{\ell^2}{q} \right\rfloor - \frac{\ell^2}{q} = \frac{1}{q} \text{ and } 0 < \ell < q$$

THEN THE CORNERS A, B, C AND D OF A DOMAIN IN (e, ω) -COORDINATES
ARE GIVEN BY:

$$A = \left(\left\lfloor \frac{F(s) p_+}{q} \right\rfloor - \frac{F(s) p_+}{q}, \frac{p_+}{q} \right)$$

$$B = \left(\left\lfloor \frac{F(s) p_-}{q} \right\rfloor - \frac{F(s) p_-}{q}, \frac{p_-}{q} \right)$$

$$C = \left(1 + \left\lfloor \frac{F(s+\ell) p_+}{q} \right\rfloor - \frac{F(s+\ell) p_+}{q}, \frac{p_+}{q} \right)$$

$$D = \left(1 + \left\lfloor \frac{F(s+\ell) p_-}{q} \right\rfloor - \frac{F(s+\ell) p_-}{q}, \frac{p_-}{q} \right)$$

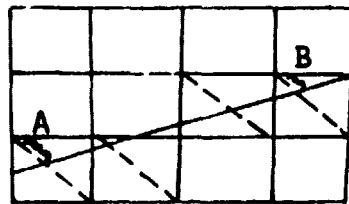
where

$$q_+ = L(s+\ell) - F(s), \quad p_+ = (pq_+ + 1)/q$$

$$q_- = L(s) - F(s+\ell), \quad p_- = (pq_- - 1)/q$$

FEASIBLE PARAMETER
REGION
DIGITAL EDGE - PIXELS MISSING

FOR SIMPLICITY ASSUME $0 \leq \text{slope} < 1$



- o EACH FEASIBLE LINE INTERSECTIONS DIAGONAL LINE WITH SLOPE -1 THROUGH SELECTED PIXELS
- o SELECT DISTANCES ALONG DIAGONAL IN LEFTMOST AND RIGHTMOST PIXELS AS PARAMETERS OF LINE
- o EACH INTERMEDIARY DIAGONAL GIVES RISE TO AT MOST TWO LINEAR INEQUALITIES RESTRICTING THE FEASIBLE REGION
- o FEASIBLE REGION IS A POLYGON IN THE (A,B) PLANE

FEASIBLE PARAMETER REGION

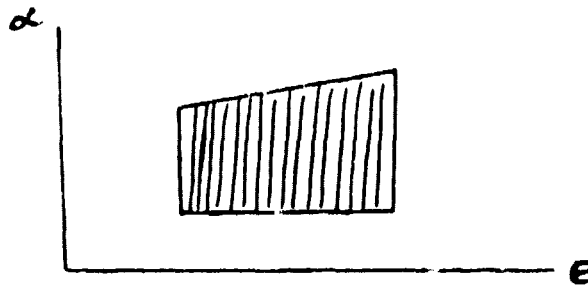
DIGITAL EDGE - PIXELS MISSING, PIXELS ADDED

- EACH SUBSET OF PIXELS THROUGH WHICH A LINE CAN PASS GIVES RISE TO A CONVEX POLYGON
- FEASIBLE REGION IS UNION OF THESE POLYGONS
- COMBINATORIAL PROBLEMS MAKE ONE OF THE FOLLOWING RESTRICTIONS DESIRABLE
 - 1) FEW WRONG PIXELS ADDED
 - OR 2) FEW PIXELS TOTAL
 - OR 3) APPROXIMATION OF FEASIBLE REGIONS
- CAREFUL THRESHOLDING AND EDGE CHECKING MAY HELP ACHIEVE THE FIRST TWO RESTRICTIONS
- APPROXIMATION OF FEASIBLE REGION
 - FIT LEAST SQUARE LINE THROUGH EDGE POINTS
 - DISCARD PIXELS NOT ON FITTED LINE
 - APPLY ANALYSIS OF CASE WHERE NO PIXELS ARE ADDED
 - IF NECESSARY PERTURB THE LINE AND REPEAT THE PROCESS
- WEIGHT POLYGONS BY THE NUMBER OF CORRESPONDING EDGE POINTS

FEASIBLE PARAMETER REGIONORIGINAL PAGE IS
OF POOR QUALITY

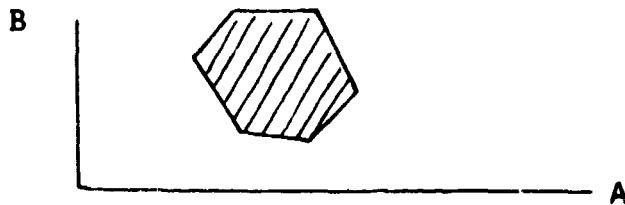
DIGITAL EDGE

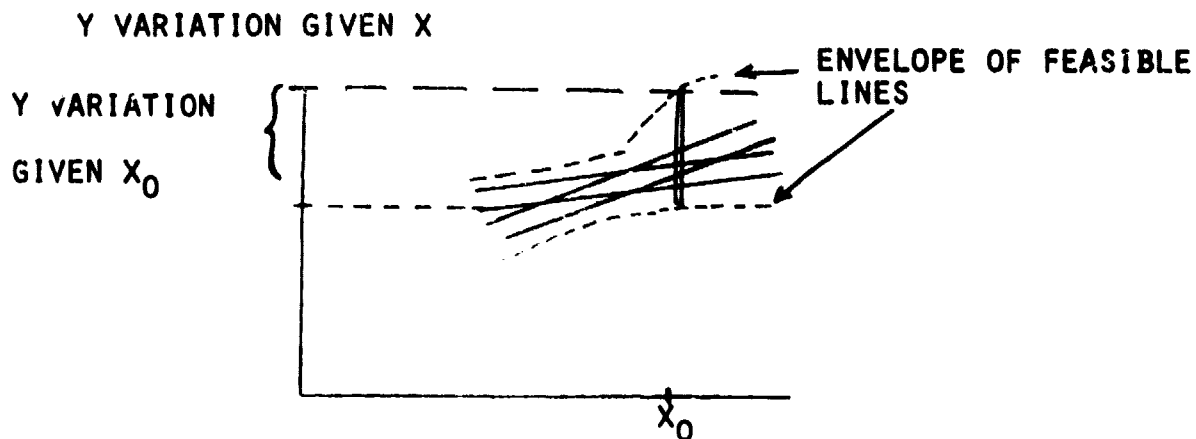
FEASIBLE REGION-QUADRILATERAL



DIGITAL EDGE (PIXELS MISSING)

- ASSUME N PIXELS GIVEN
- FEASIBLE REGION CONVEX POLYGON WITH AT MOST $2N$ SIDES



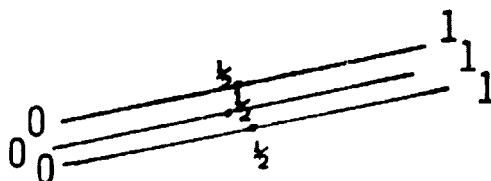
VARIATION MEASURESORIGINAL PAGE IS
OF POOR QUALITY

X VARIATION GIVEN Y IS DEFINED SIMILARLY

VARIATION MEASURES (CONT'D)

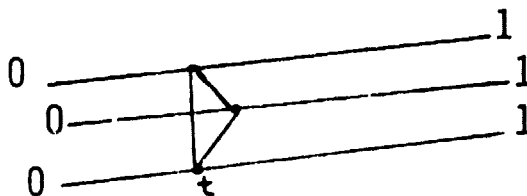
ORIGINAL PAGE IS
OF POOR QUALITY

PARAMETRIZE EACH FEASIBLE LINE SEGMENT TO HAVE
UNIT LENGTH



DEFINE VARIATION FUNCTION $V: [0,1] \rightarrow \mathbb{R}^+$

BY $V(t) =$ MAXIMUM DISTANCE BETWEEN FEASIBLE
LINES, MEASURED t UNITS DOWN EACH
LINE.



VARIATION MEASURES (CONT'D.)

VARIANCE OF Y GIVEN X

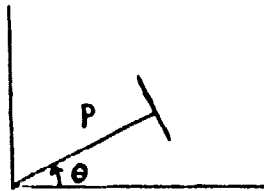
VARIANCE OF X GIVEN Y

VARIANCE OF POINT T UNITS DOWN EACH LINE

DISTRIBUTIONS ON LINES

- MANY DISTRIBUTIONS ON LINES ARE FEASIBLE
- UNIFORM DISTRIBUTION DEPENDS UPON THE PARAMETRIZATION
- INVARIANCE UNDER ROTATION AND TRANSLATION SINGLES OUT A DISTRIBUTION:

UNIFORM DISTRIBUTION IN (p, θ)



WHERE THE DISTRIBUTION IS OVER ALL LINES
PASSING THROUGH A GIVEN BOUNDED FIGURE

STATISTICS OF Y-VARIATION

- LET x_0 BE FIXED
- FIND THE MEAN AND VARIANCE OF THE Y VALUES OF THE FEASIBLE LINES AT x_0
- FIND A CONFIDENCE INTERVAL FOR THE Y-COORDINATE BEING WITHIN A SPECIFIED DISTANCE FROM THE MEAN
- MEAN AND VARIANCE CAN BE CALCULATED EASILY NUMERICALLY
- WE ARE WORKING ON CONFIDENCE INTERVALS

VARIATION GOALS

- 1) DERIVE BOUNDS FOR EACH VARIATION MEASURE
AS A FUNCTION OF DIGITAL EDGE PARAMETERS

- 2) COMPUTE THE MEAN AND VARIATION OF EACH VARIATION
MEASURE

- 3) FIND THE X,Y OR F VALUE WHICH MINIMIZES THE
CORRESPONDING VARIATION MEASURE

- 4) FIND GOOD DIGITAL EDGE CHARACTERISTICS, E.G.,
SLOPE WHICH CAN BE USED TO MINIMIZE VARIATION
MEASURES

ANGLES

ASSUME WE HAVE TWO REAL LINE SEGMENTS SHARING AN
END POINT

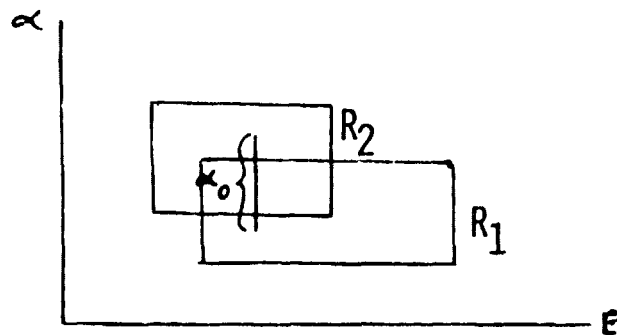


- HOW CAN WE USE THIS KNOWLEDGE TO REFINE OUR ESTIMATION OF POSITIONS?
- WHAT ANGLES ARE BEST FOR ESTIMATION?
- WHAT CAN BE DONE IF THE LINE SEGMENTS DON'T INTERSECT?

ANGLE CONSTRAINTS

ASSUME WE OBSERVE THE DIGITAL EDGES RESULTING FROM A REAL ANGLE.

WE GET A FEASIBLE REGION FOR EACH REAL LINE SEGMENT:



- A FEASIBLE ANGLE IS A PAIR OF POINTS ONE IN EACH FEASIBLE REGION
- COMMON VERTEX IMPLIES BOTH POINT LIE ON SAME VERTICAL LINE
- FIXED ANGLE IMPLIES DISTANCE BETWEEN TWO POINTS IS CONSTANT
- LET α_0 DENOTE THIS DISTANCE
- FEASIBLE REGION = $\{(e, \alpha) \in R_1 : \text{THERE EXISTS A POINT } (e, \beta) \in R_2 \text{ WITH } \beta - \alpha = \alpha_0\}$

ERROR BOUNDS ON POINT MATCHING

- EACH EDGE GIVES RISE TO A POINT TO BE MATCHED WITH A POINT IN THE REFERENCE IMAGE

- WHAT CAN BE SAID ABOUT THE ACCURACY OF THE ESTIMATED TRANSFORMATION GIVEN THE BOUNDS OR STATISTICS OF THE INDIVIDUAL POINT LOCATION ACCURACIES?

- WORK ON THIS PROBLEM WILL BE PERFORMED WHEN WE HAVE FINISHED OUR ESTIMATES FOR THE POINT ACCURACY WITH DIGITAL EDGES (PIXELS MISSING)

- FINAL RESULT:
 ERROR BOUNDS ON TRANSFORMATION ACCURACY GIVEN OBSERVED EDGES

EXPERIMENTAL CORRELATION STUDIES:

- SIMULATION RESULTS INDICATE THAT CORRELATION AND SURFACE FITTING TO ATTAIN SUBPIXEL ACCURACY SHOULD BE BASED ON PIXELS LIKELY TO CARRY SUBSTANTIAL SUBPIXEL INFORMATION (NEAR EDGES).
- FUTURE SIMULATIONS WILL BE MORE REALISTIC AND WILL STUDY THE ABOVE PHENOMENON IN MORE DETAIL.

ANALYTIC STUDY OF PROBABILISTIC SUBPIXEL ACCURACY:

- TWO MODELS WERE DEVELOPED
 - 1) ERROR EFFECT DUE TO QUANTIZATION WHEN REFERENCE IMAGE IS RANDOM
 - 2) ERROR EFFECT WITH DETERMINISTIC IMAGE (KNOWN SHAPE) DUE TO FITTING ERROR

GEOMETRIC ERROR ANALYSIS:

- FEASIBLE PARAMETER REGIONS FOR LINES PASSING THROUGH SETS OF PIXELS HAVE BEEN OBTAINED
- EXPRESSIONS FOR MAXIMUM X,Y VARIATION AND MEANS AND VARIANCES HAVE BEEN DEVELOPED.

PROGRESS AND FUTURE WORK (CONT'D.

GEOMETRIC ERROR ANALYSIS (CONT'D.

- CONSTRAINTS ON FEASIBLE REGIONS IMPOSED BY ANGLES HAVE BEEN DERIVED
- EVALUATION OF THE ABOVE ESTIMATES TO DERIVE OPTIMAL FEATURES AND QUALITY MEASURES OF FEATURES ARE UNDERWAY
- WE ARE CURRENTLY ATTEMPTING TO DERIVE A FORMULA FOR THE FEASIBLE REGION IN A DIGITAL EDGE WITH PIXELS MISSED
- THE EFFECTS OF THE ABOVE ESTIMATES OF POINT LOCATION ACCURACY ON REGISTRATION TRANSFORMATION ACCURACY WILL BE STUDIED
- EFFECTS OF GEOMETRIC DISTORTION ON THE ABOVE ANALYSIS WILL BE STUDIED.

ORIGINAL PAGE IS
OF POOR QUALITY

Improving Spatial Modelling
in Remote Sensing

Hunter College:

A. H. Strahler

C. E. Woodcock

U. C. Santa Barbara:

J. R. Tobler

Assisted by R. Irish

PRECEDING PAGE BLANK NOT FILMED

~~158~~ INTENTIONALLY BLANK

Remote Sensing Models: A General Framework

ORIGINAL PAGE IS
OF POOR QUALITY

Definitions

Sensor: Device that measures intensity of EMR

IFOV (Instantaneous Field of View): Field of view over which the EMR is integrated by the sensor.

MTF (Modulation Transfer Function): Describes way in which EMR in IFOV is integrated to produce a measurement.

Measurement: Output of a sensor in response to this integration. Usually digital, in our case.

Scene: Spatial & temporal distribution of matter and energy fluxes from which the sensor draws measurements.

Image: Collection of measurements produced by a sensor that are arrayed in a systematic fashion derived from the spatial or temporal position from which they were collected.

Resolution Cell: Average rectangular area of a scene that is associated with each measurement.

Structure of Model

- Real scenes are not chaotic, but possess order, at least to some extent.
 - Only certain combinations of energy and matter occur.
- Energy flux incident upon & emitted from scene passes through atmosphere.
 - Back scattering, multiple scattering, etc.
- Sensor will measure EMR flux imperfectly.
 - Calibration; nonlinearities, etc.

Leads to concept of three components to RS model

Three Components of

Remote Sensing Model

- ① Scene Model: Specifies form & nature of energy & matter within the scene & their spatial & temporal order.
- ② Atmospheric Model: Describes the interaction between atmosphere & energy incident on/exiting from the ground scene.
- ③ Sensor Model: Describes behavior of the sensor in response to energy fluxes incident upon it & in producing the measurements that constitute the image.

FUNDAMENTAL REMOTE SENSING PROBLEM:

Inferring the order in the properties and distributions of energy and matter in the scene from the set of measurements that comprise the image.

- Scene inference always implies the application of a remote sensing model
 - Assumptions always made concerning ground scene, atmosphere, & sensor
- Scene inference is thus a problem of model inversion in which the order in the real scene is reconstructed from the image & the remote sensing model.
- This research focuses on the scene model
 - Transparent atmosphere

Scene Model

ORIGINAL PAGE IS
OF POOR QUALITY

Components:

Element: Abstraction of class of real objects having uniform properties or parameters.

- Properties may be fundamental and invariant -- (e.g., heat capacity, conductivity, emissivity, etc.)
- Or stochastic & characterized by distribution parameters (e.g., size, shape, color, etc.)
- Examples:
 - Leaf, branch, plant, row, tree, field, stand
 - Lawn, car, street, house, pool
 - Airplane, runway, truck, tank
- Typically, a scene will contain several elements

Background: Is spatially continuous w/ uniform properties & parameters & is obscured by elements

- Examples: soil, snow, rock, understory

ORIGINAL PAGE IS
OF POOR QUALITY

Energy Fluxes Into Scene : Characterized by wave length, intensity, polarization; distributed hemispherically.

- Passive systems : Typically assume incoming flux characteristics are spatially & temporally stationary
- Active systems : Flux characteristics a function of source-sensor relationship

Types of Scene Models

H-Resolution: Resolution cell smaller than elements.

L-Resolution: Resolution cell larger than elements.

Deterministic: Utilizes basic physical laws concerning interaction of matter & EMR.

- Includes emissivity, scattering, etc., of elements as properties or parameters.
- Utilizes principles of conservation of energy & matter (e.g., radiative transfer equation) and/or laws of thermodynamics.
- Often L-Resolution.

Empirical: Associates observed sensor measurements with scene elements

- Typically statistical.
- Typically H-Resolution.

Actually, D. & E. are endpoints of a continuum.

Invertibility

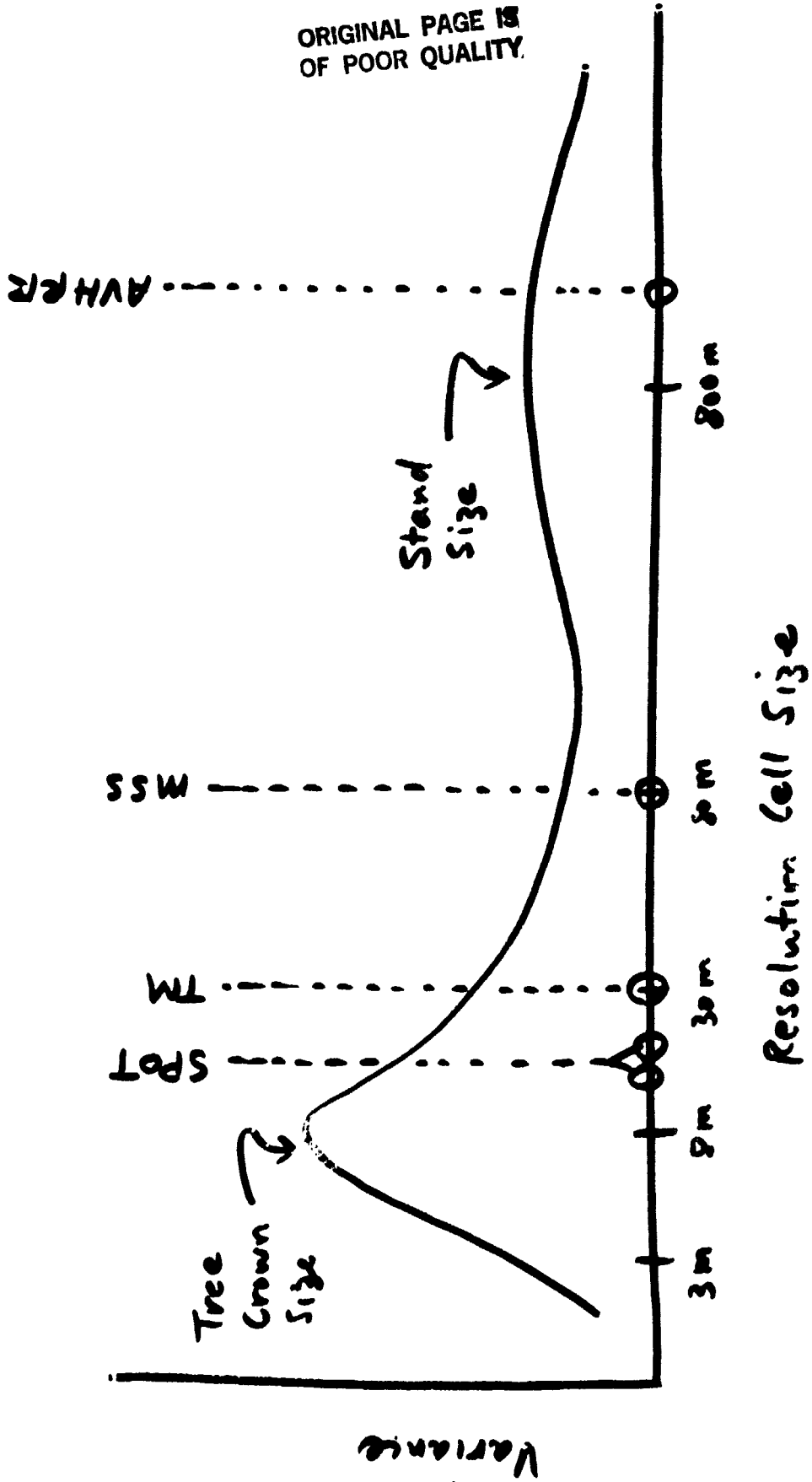
Remote sensing models are usually invertible because they are constructed for scene inference.

- Manual Photointerpretation: Inversion of a model in the mind of the photointerpreter.
- Automatic: Explicitly invertible by virtue of side constraints.
 - E.g., maximum likelihood.

ORIGINAL PAGE IS OF POOR QUALITY.

Variance vs. Resolution Cell Size

Example: Conifer Forest



Model: I: Objects are trees
S: Objects are stands
F: Objects are foliage
Elements

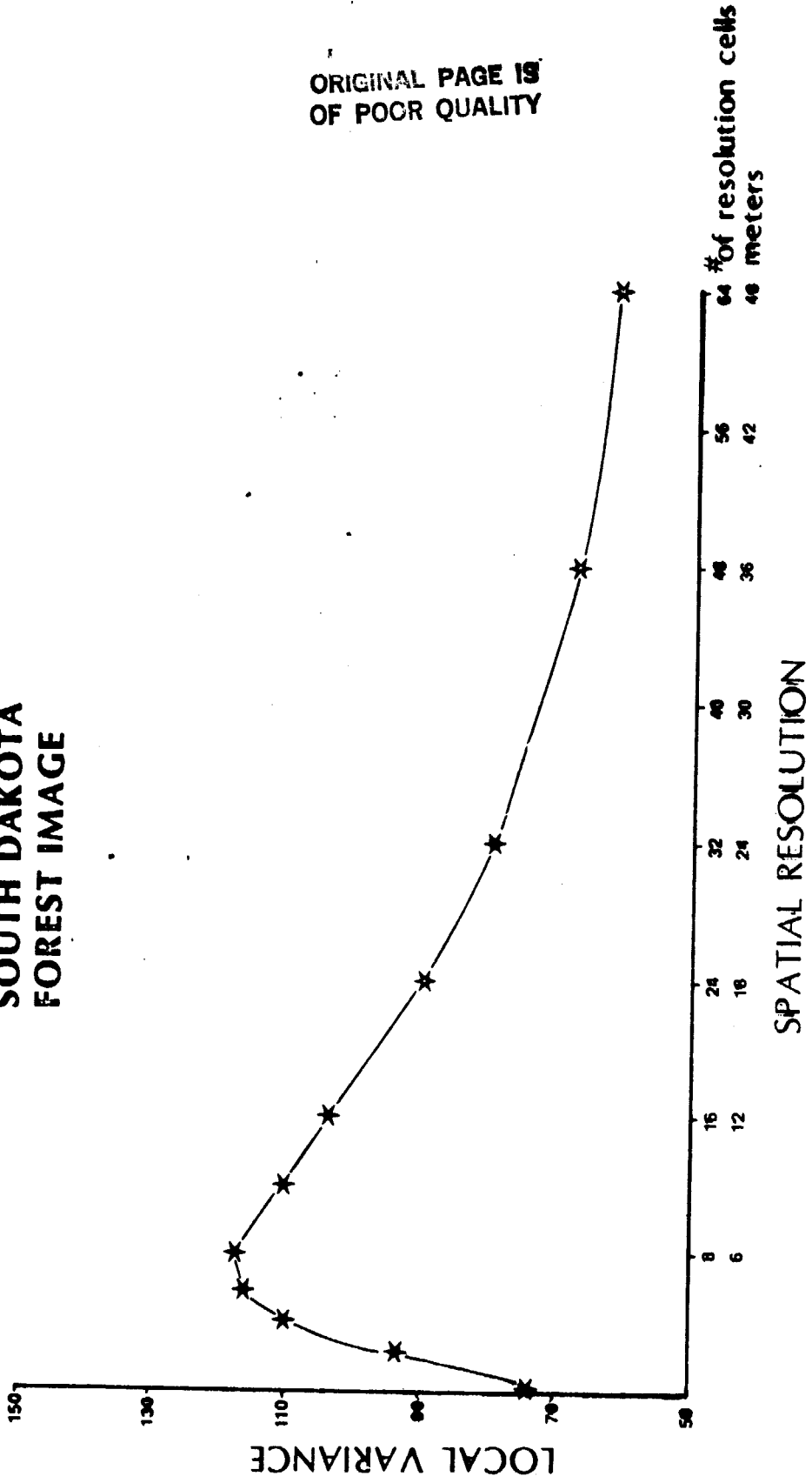
Model/Approach	Type	H, E	T: H	S: H	L, D	T: L	Modified
Conventional Supervised & Unsupervised Classification		H, E	T: H	S: H			
Spatial/Spectral Classification BLOB, ECHO, AMORSA, FACET		H, E	T: H	S: H			
Invertible Coniferous Forest Canopy Reflectance Model		L, D				T: L	?
Proportion Estimation/ Mixture Modeling		L, E				T: L	S: L
Smith/Kinos Monte Carlo Conf. Canopy Model		L, D	F: L				



H: H-Resolution D: Deterministic
L: L-Resolution E: Empirical

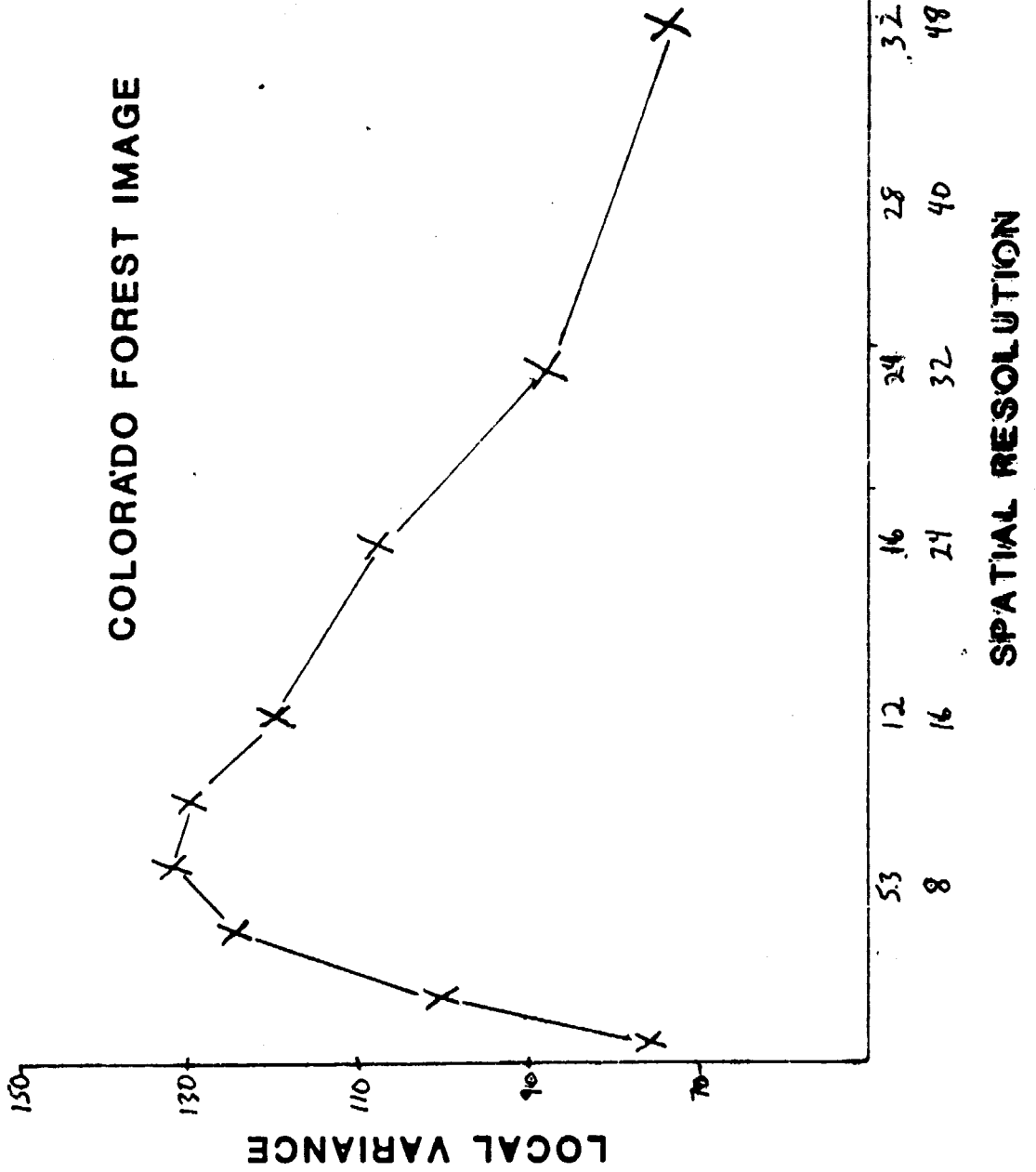
ORIGINAL PAGE IS
OF POOR QUALITY

**SOUTH DAKOTA
FOREST IMAGE**



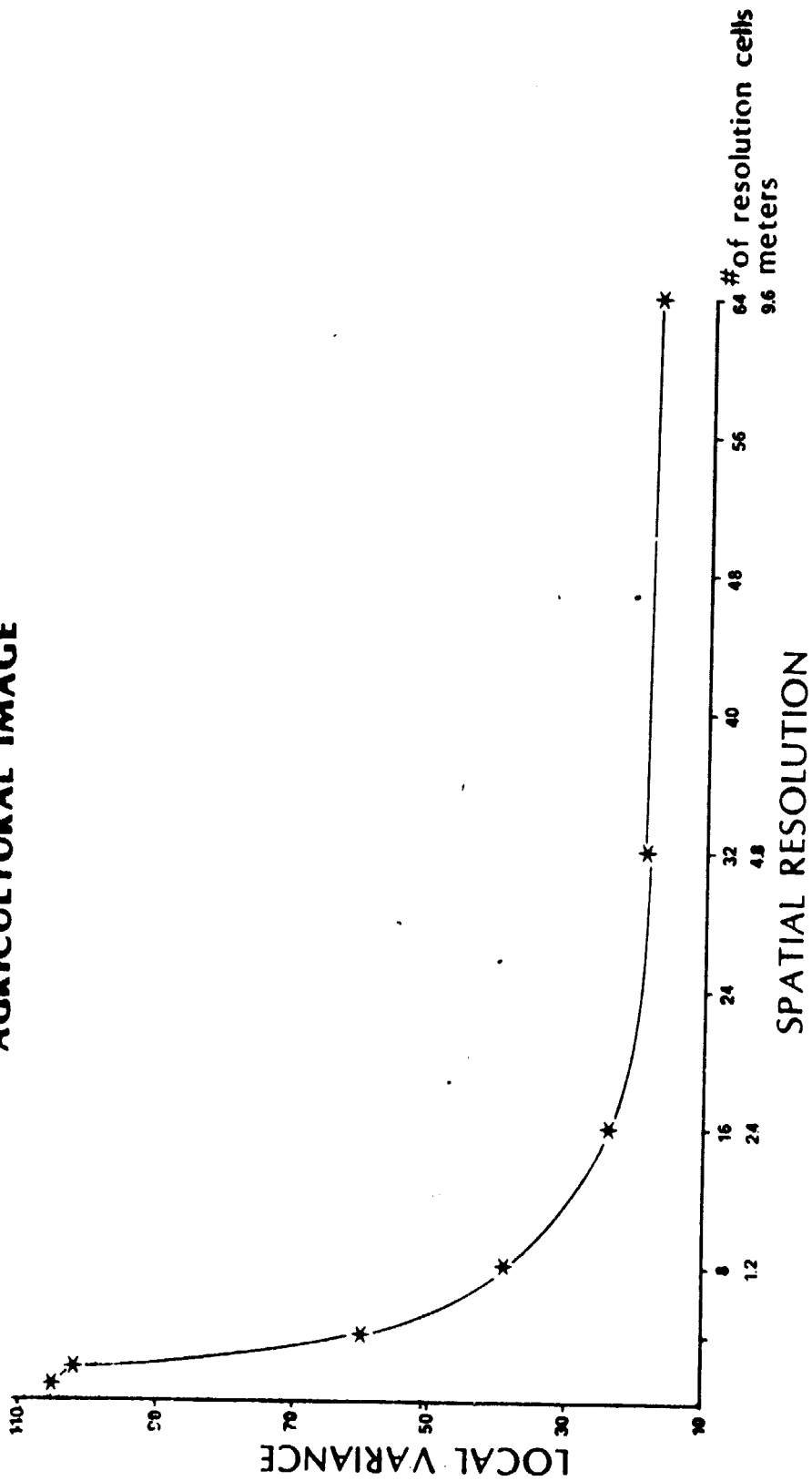
of resolution cells
64
48
36
24
18
12
8
6

SPATIAL RESOLUTION



ORIGINAL PAGE IS
OF POOR QUALITY

AGRICULTURAL IMAGE



row 2 6 res. cells

Slides

South Dakota Set - coarsening resolution

Digitized @ true scale of $\approx 3/4$ m.

Used red filter on CIR Air Photo

<u>Cell Size</u>	<u>Res'n</u>
1	.75 m.
4	3 m
8	6 m
12	9 m
16	12 m
24	18 m
32	24 m

Colorado Scene - digitized @ true scale of ≈ 1.5 m.

Az. Image - digitized @ true scale of 15 cm

Theory of Regionalized Variables (TRV)

- Looked to Spatial Statistics to build bridge between scene model and image variance/resolution concept.

ORIGINAL PAGE IS
OF POOR QUALITY

- Regionalized Variable: Random variable with an associated position in time or space.
 - Considerable theoretical work done in past twenty yrs, esp. in Geology.
 - Simple, basic approach.

Theoretical Framework

- $Y(\underline{x}_i)$ is R.V. associated with spatial position \underline{x}_i .
- E.g. - digital image, where \underline{x}_i , $i=1, \dots, n$, correspond to resolution cells
- If $Y(\underline{x}_i)$ are independent, then image will consist of random noise.
- If $Y(\underline{x}_i)$ are somehow related, then there will be spatial structure in the scene.

History of TRV

Developed independently in at least three fields

- Geology: Krige, Matheron - classic work
- Meteorology: Gandin, Matern - "objective analysis"
- Geophysics: Graterend, Morawitz - "collocation theory"

Geologic applications -- especially in mining industry, as concentrations of minerals in ores.

- Provide minimum variance estimators of concentration at arbitrary location (Kriging).
- Locate position of add'l samples that will most effectively reduce estimate variances.
- estimate weighted average or mean value within a region with minimum variance.
- estimate a drift or linear trend.

Simplest Assumption: Intrinsic Hypothesis

- Deal with difference in two values as a function of spatial increment h :

$$Y(\underline{x+h}) - Y(\underline{x})$$

- Assume first moment is constant or only slowly varying w/ \underline{x} . I.e.,

$$E[Y(\underline{x+h}) - Y(\underline{x})] \approx \text{constant}$$

- Then second moment is:

$$2\gamma(h) = E[(Y(\underline{x+h}) - Y(\underline{x}))^2]$$

$2\gamma(h)$ is termed variogram;

$\gamma(h)$ is termed semivariogram

Spatial Autocorrelation in TRV

- Assume $E[Y(\underline{x})]$ is stationary in \underline{x} .

$$m = E[Y(\underline{x}_i)] = E[Y(\underline{x}_j)]$$

for two locations \underline{x}_i & \underline{x}_j .

- Assume covariance between $Y(\underline{x}_i)$ & $Y(\underline{x}_j)$ is a function only of distance d between \underline{x}_i & \underline{x}_j .

$$d^2 = (\underline{x}_i - \underline{x}_j)'(\underline{x}_i - \underline{x}_j)$$

$$\text{Covariance} = C(d) = E[Y(\underline{x}_i)Y(\underline{x}_j)] - m^2$$

- Correlogram - ρ as a function of distance

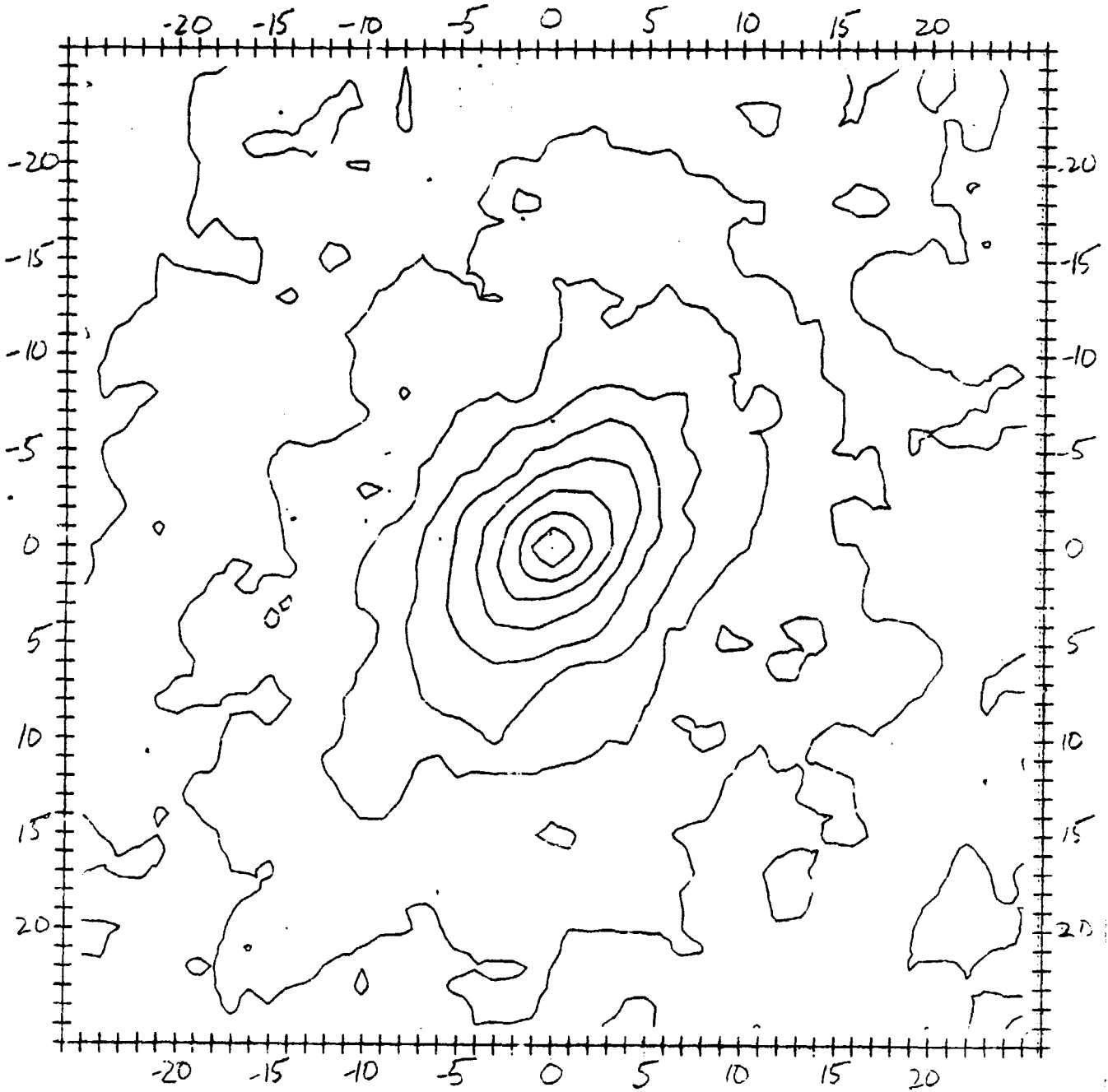
$$\rho(d) = \frac{C(d)}{C(0)},$$

where $C(0)$ is just variance of $Y(\underline{x})$

Thus, spatial autocorrelation is easily related to TRV.

Also, power spectral density function is Fourier transform of spatial autocorrelation function \rightarrow Fourier domain.

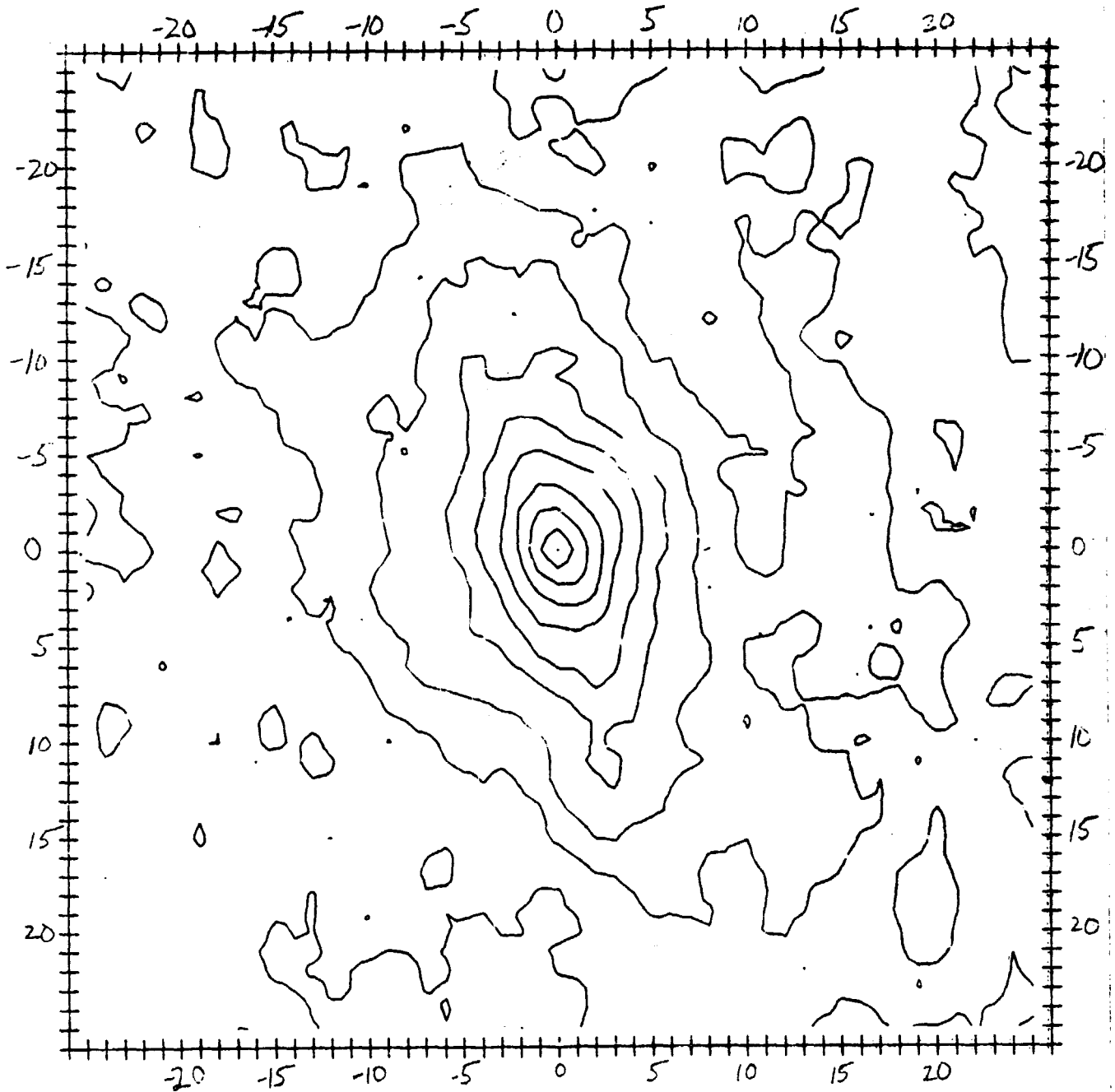
ORIGINAL PAGE IS
OF POOR QUALITY



VARIOGRAM OF SOUTH DAKOTA FOREST SCENE

one pixel = 0.75m

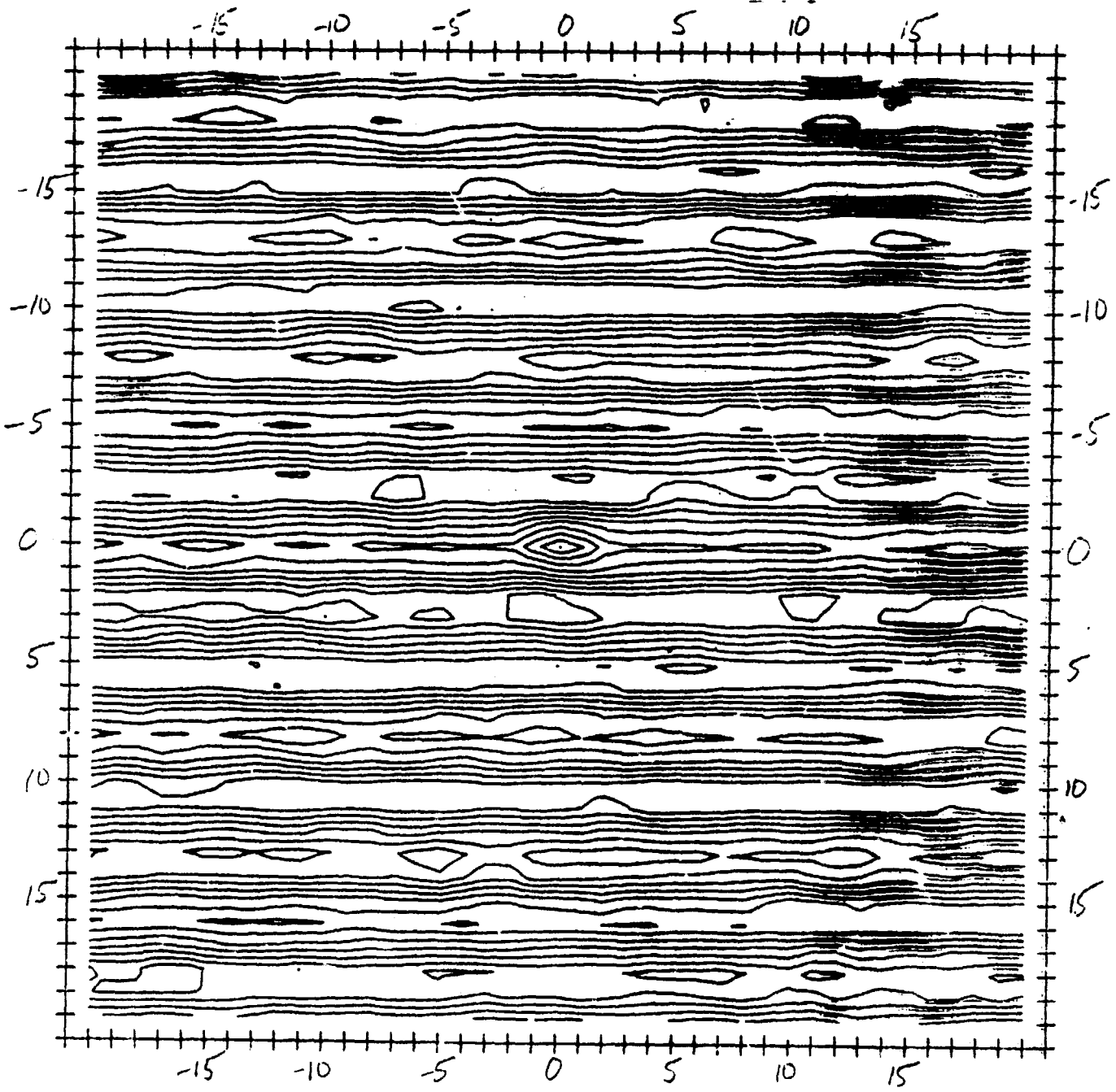
ORIGINAL PAGE IS
OF POOR QUALITY



VARIOGRAM OF COLORADO FOREST SCENE

one pixel = 1.5 m

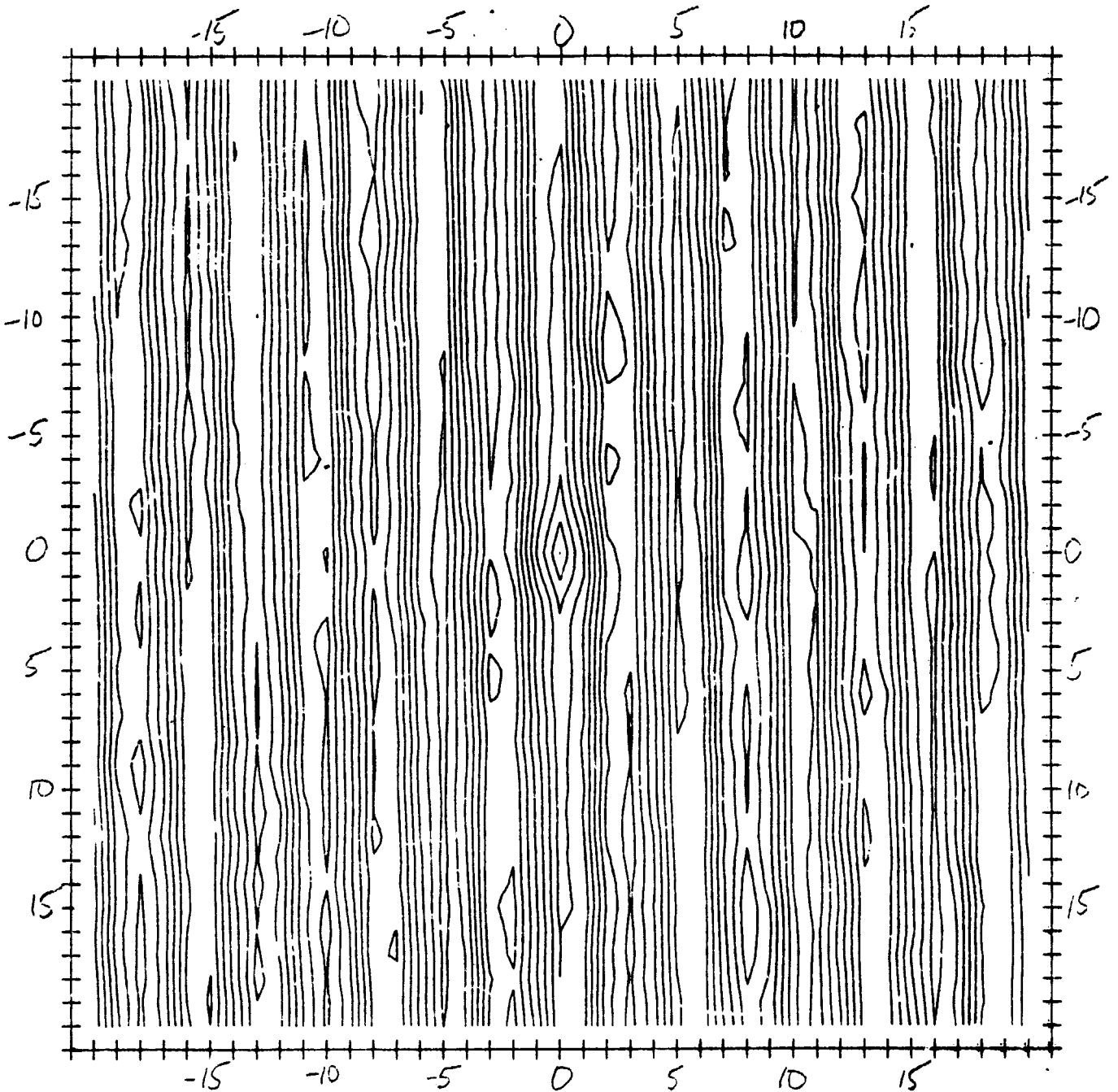
ORIGINAL PAGE 19
OF POOR QUALITY



VARIOGRAM OF AGRICULTURE SCENE, UPPER LEFT

one pixel = 0.15m

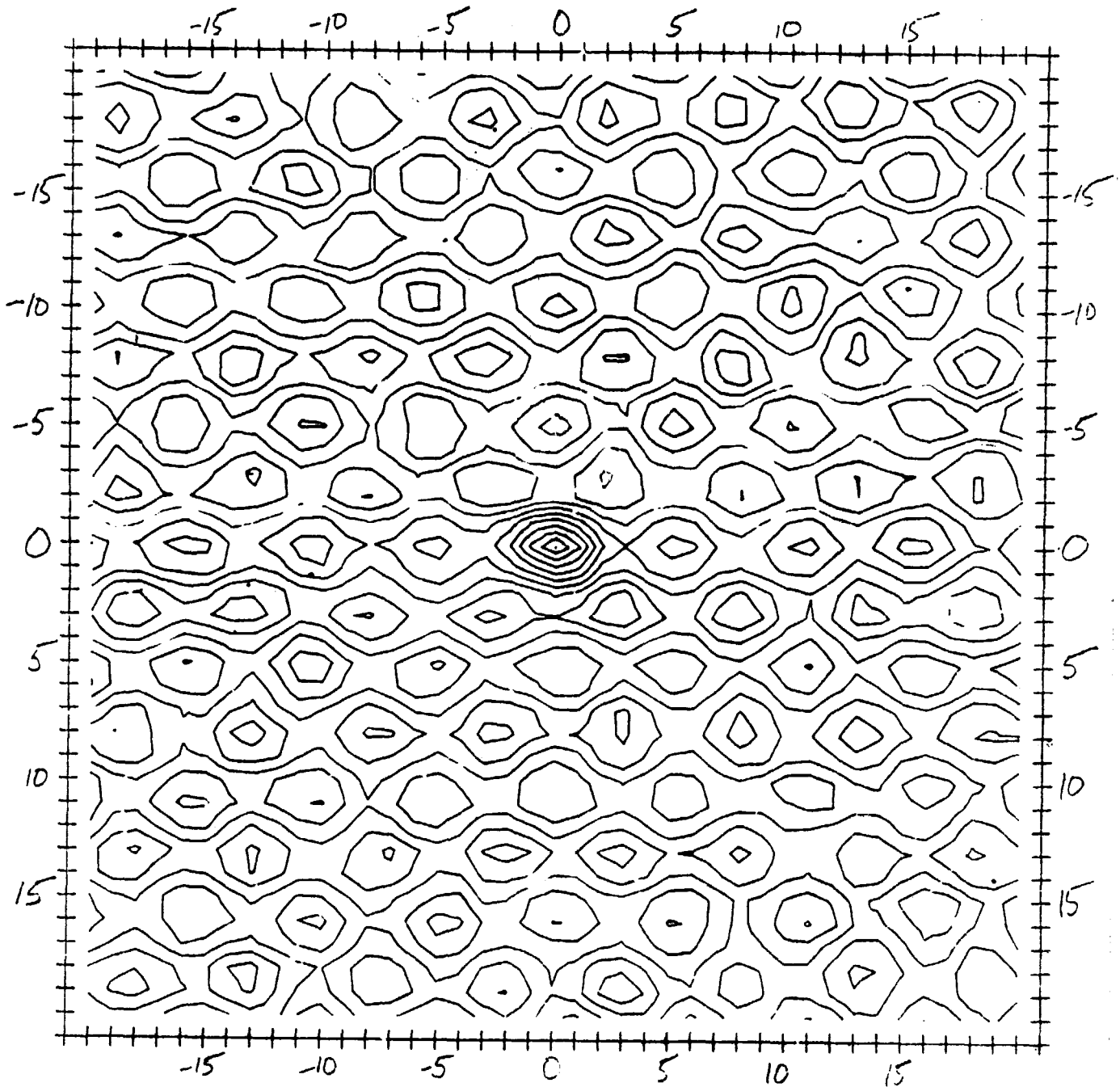
ORIGINAL PAGE IS
OF POOR QUALITY



VARIOGRAM OF AGRICULTURE SCENE, LOWER LEFT

one pixel = 0.15m

ORIGINAL PAGE IS
OF POOR QUALITY



VARIOGRAM OF AGRICULTURE SCENE

one pixel = 0.15 m

Main Thrust of Work

Apply TRV to development & utilization of remote sensing models.

- Formalize relationship between variogram, correlogram, resolution, local variance, image texture for various scene models
- Investigate invertibility -- deriving parameters of elements & their distributions from the variograms
- Consider multiple spatial structures -
e.g., plant \rightarrow row \rightarrow field \rightarrow agricultural region

Primary Tasks, Yr 1

ORIGINAL PAGE IS
OF POOR QUALITY

① Application of TRV to RS scores (Strahler, Woodcock: Hunter)

- Examine RS scores, determine variograms empirically.
 - Forests; agricultural scores; housing developments; urban areas, etc.
- Explore effects of resolution & influence on image texture.
 - Scan photos; TM & MSS imagery
- Construct simple scene models & generate variograms for them.

② Formalize relation between variogram, image texture & Scene model (Tobler: UCSB)

- Examine math. relationship between variogram & image texture measures.
- Explore conventional texture measures in context of TRV & scene model.

③ Other possible topics

- Generalize theory of regionalized variables to multidimensional case for application to remote sensing (UCSB).
- Use of point process models for locating objects in scenes & the variograms that such point processes imply (Hunter).
- Possible use of alternate geographic models -- diffusion, gravity (Hunter).
- Use of TRV to interpolate missing measurements due to clouds, scanner or transmission-related problems (UCSB).

① Application of TRU to RS Scenes.

Phase I: Empirical Characterization of Spatial Patterns in RS data

186
Graph of local Variance/Resolution

	<u>Resolution</u>	<u>Scanning</u>	<u>Variogram(s)</u>	<u>Graph of local Variance/Resolution</u>
1. Forest scene - S. D.	3/4 m	Done	Done	Done
2. Forest scene - Colorado	1 1/2 m	Done	Done	Done
3. Ag. Image	15 cm	Done	Done	Needs work
4. Housing Development	2-4 m			

5. Forest Scene - TM NA
6. Ag. Scene - TM NA
7. Housing Dev. - TM NA

Phase II: Monte Carlo modeling of Spatial Patterns

	<u>Res'n</u>	<u>Objects</u>	<u>Spatial Pattern</u>	<u>Inventability</u>
Forest scene	Fine	Trees	Point process	Yes
	Coarse	Stands	?	?
Ag. Scene	Fine	Crop fields	Regular	?
	Coarse	Fields	Regular	?
Housing Development	Fine	Houses, lanes, driveways	?	?
	Coarse	Tracts	?	?

N83 23080 D7

187



APPROACHES TO IMAGE REGISTRATION AND SEGMENTATION

Grahame Smith

Image-to-Image Correspondence

different viewing conditions

different resolutions, spectral responses

temporal changes

Approach

- **Detect easily recognized / physically meaningful structures**
- **Label structures**
- **Build description of structure**
- **Match descriptions - rough camera model**
- **Select feature points**
- **Predict how the feature points appear in image**
- **Match feature points - precise transform**

Image Segmentation

recover scene entities

- single land cover class
- no internal boundaries

- Recover surface shape
- Initial classification
- Edge / Linear structure detection
- 'Convergence of Evidence' decision making

Detection of Linear Structures

two-fold purpose: image registration and class boundary detection

Algorithm

Peak and trough method

Finds ridge lines (skeleton)

Uses local and global nature of intensity peak

Initial Segmentation

- based on the reflectance
- little human intervention
- use catalog of reflectance versus land cover
- delineate single land cover area rather than identify class

Atmospheric Model $I = R + S$

Film Model $D = a \times \ln(I) + d$

Isotropic Scattering $R = EAN$

$$D = a \times \ln(A + b) + c$$

Surface Shape Recovery

slant of ground plane
surface shape

ORIGINAL PAGE IS
OF POOR QUALITY

$$I(x, y) = R(l, m)$$

- type of scattering
- position and strength of light source
- surface albedo
- boundary conditions

$$\frac{1 - m^2}{lm} = \frac{I_{xx}}{I_{yy}}$$

$$\frac{1 - l^2}{lm} = \frac{I_{yy}}{I_{xx}}$$

Physical Models needed to interpret image

**ORIGINAL PAGE IS
OF POOR QUALITY**

- **Linear feature finder**
- **Image classification**
- **Shape recovery**

Physical models not all encompassing

- **Evidential Reasoning**

Primary Areas of Focus

**ORIGINAL PAGE IS
OF POOR QUALITY**

- **Image-to-Image Correspondence**
 - registration of multiple data sources
- **Image Segmentation - context:land-use**
 - scene entities
- **'Convergence of Evidence' Decision Making**
 - multi-source integration

Approach

- **Physical Modeling**
- **Generic Techniques based on Stable Properties**
- **Discover Stable Attributes**

OMIT TO
P207
197

**ORIGINAL PAGE IS
OF POOR QUALITY**

Reduction and Utilization of
Speckle Noise in SAR Imagery

Daniel Held
Jet Propulsion Lab

PRECEDING PAGE BLANK NOT FILMED

SPECKLE REDUCTION



rel s1k err

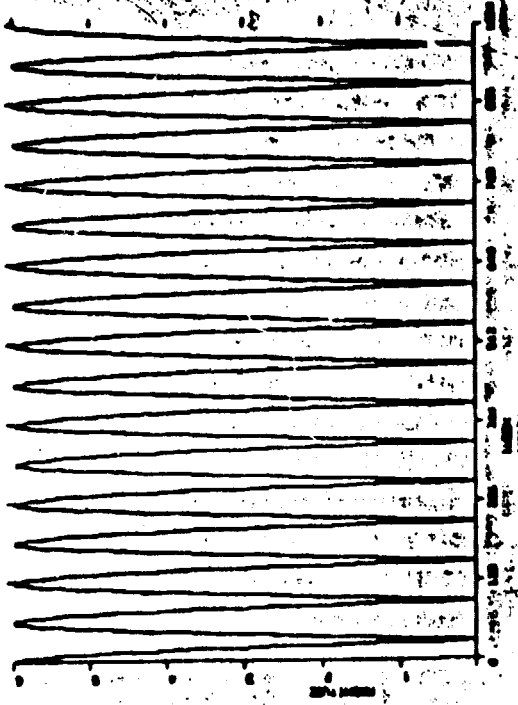


Figure 2c: dc + sinusoid scene magnitude.

rel s1k err



Figure 2d: Sum

rel s1k err

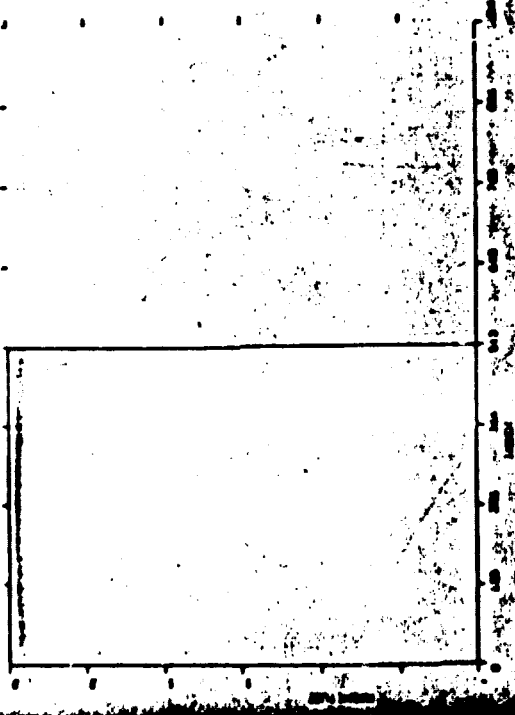


Figure 2a: Step scene magnitude.

rel s1k err

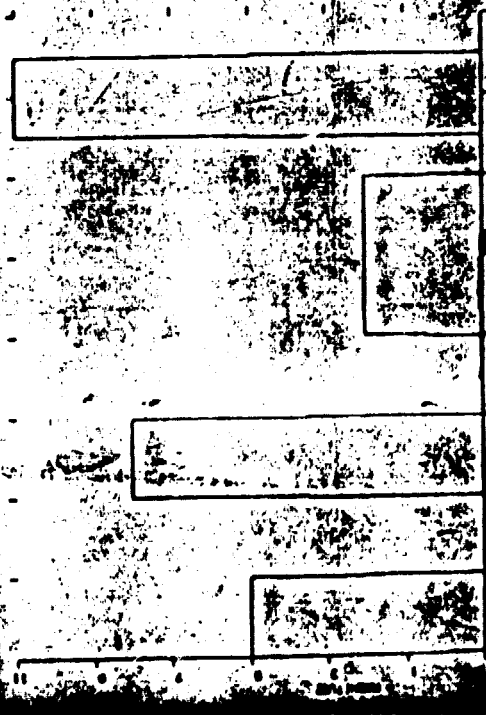


Figure 2b: Rectangular scene magnitude.

$$H(\omega) =$$

$$\frac{S(\omega)}{S(\omega) + N(\omega)}$$

$$\int S(\omega) d\omega \approx \int N(\omega) d\omega$$

WFS: WFS

Filter

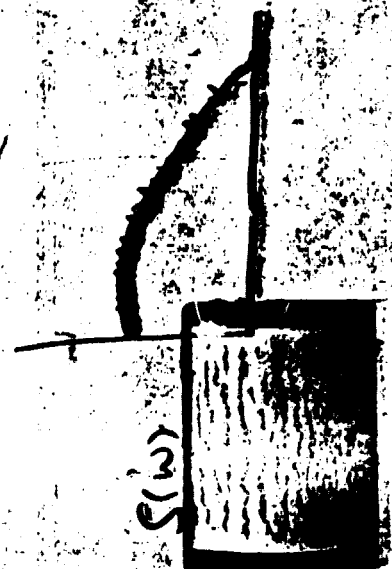
$$S(\omega) = |FFT(I)|^2 = \frac{1}{2} |FFT(I)|^2$$

$$S(\omega) + N(\omega) = |FFT(I)|^2$$

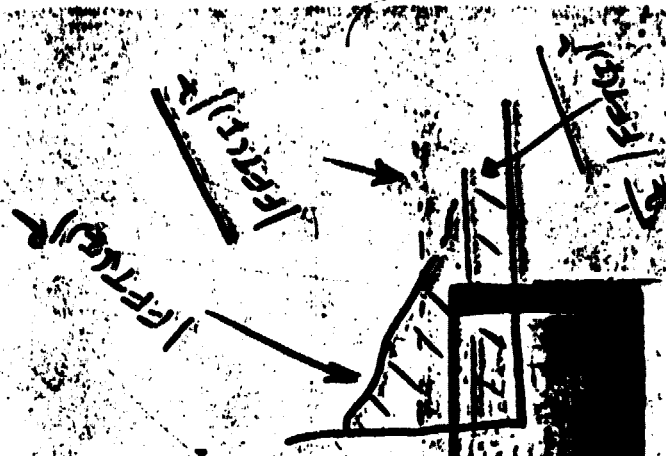
Constant

ORIGINAL PAGE IS OF POOR QUALITY

Intensity Image



$$(S(\omega) + N(\omega)) S$$



original hat

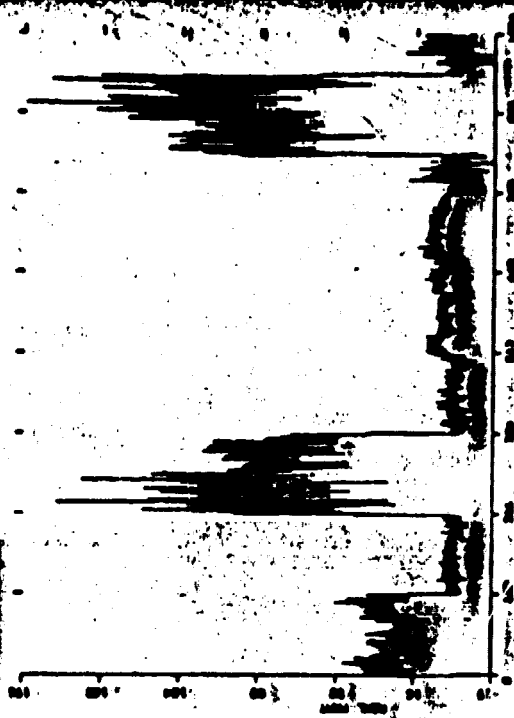
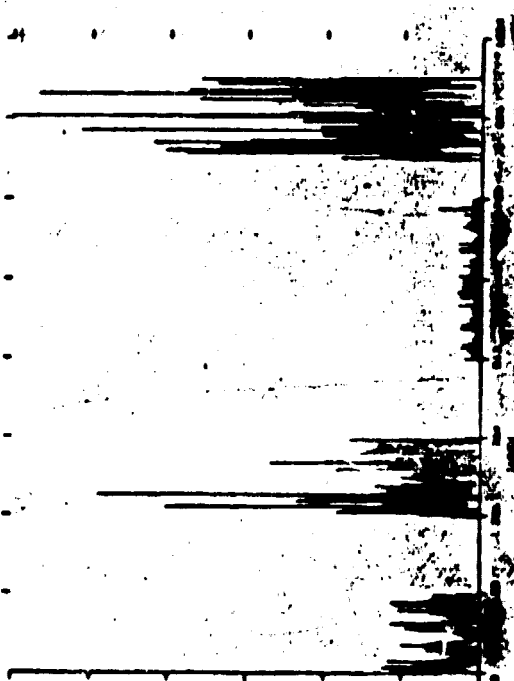


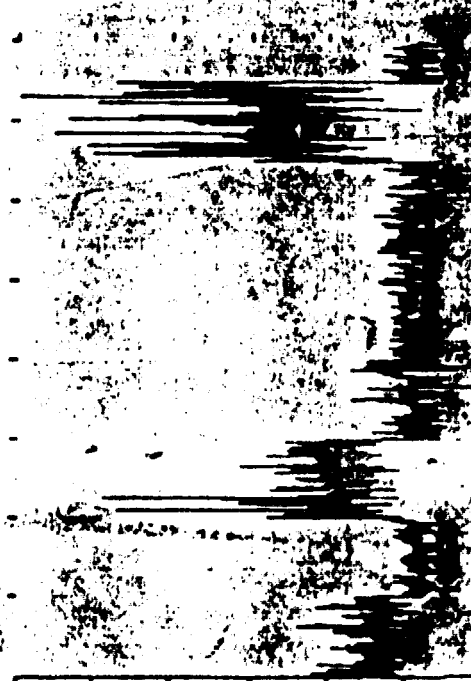
Figure 10c. Wiener filtered with smoothed Walsh transform estimate.

original hat



10a. Speckled rectangular intensity image.

original hat



original hat



Walsh transform

Walsh transform

ORIGINAL PAGE IS OF POOR QUALITY



Figure 3a. Speckled scene intensity.

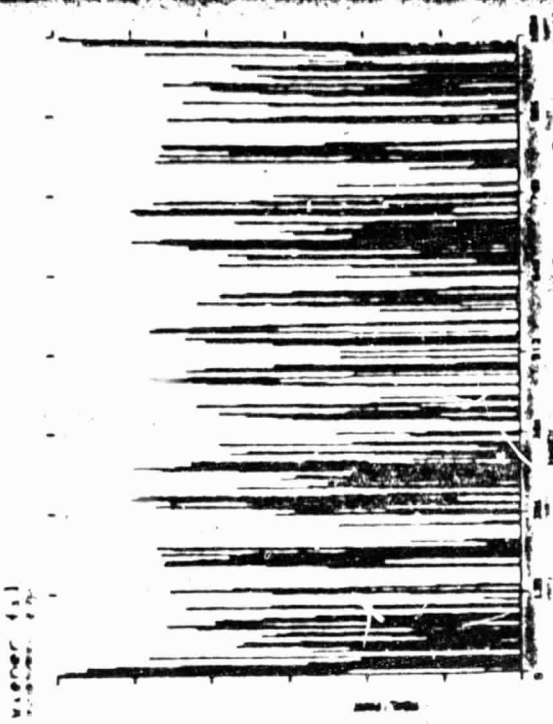


Figure 3c. Wigner filter $(|FFT|^2 - \frac{1}{2} |FFT|^2) / |FFT|^2$

ORIGINAL PAGE IS OF POOR QUALITY

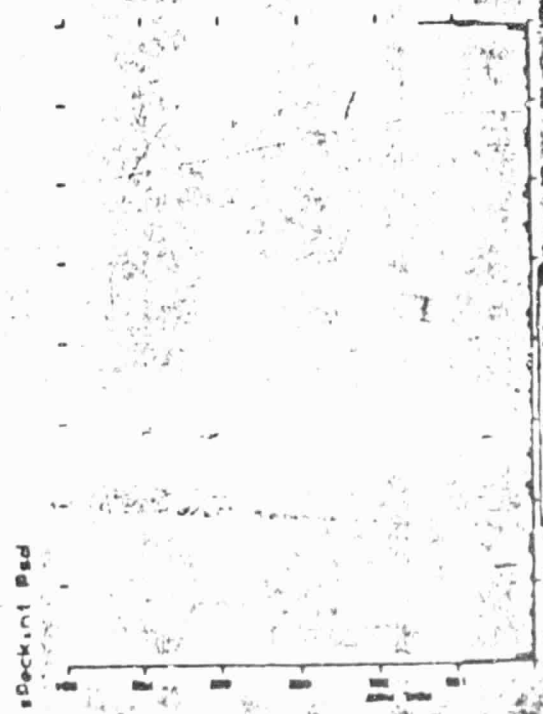


Figure 3b. Intensity image.

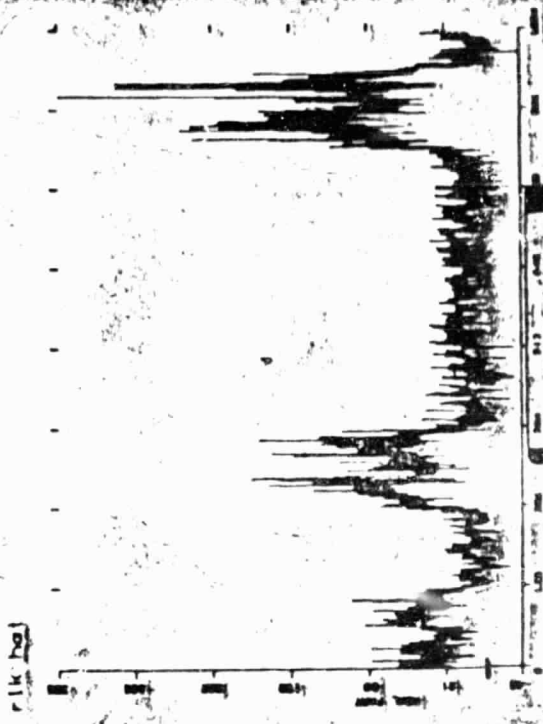


Figure 3d. Filtered image.

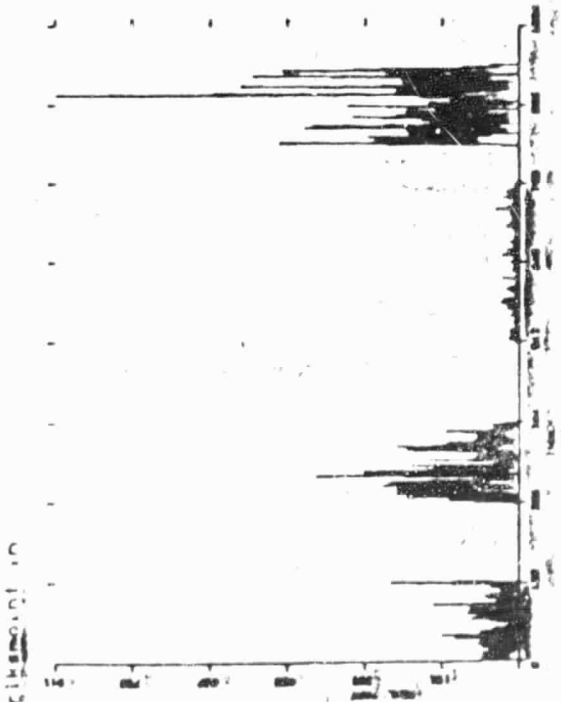


Figure 3e. Speckled scene intensity.

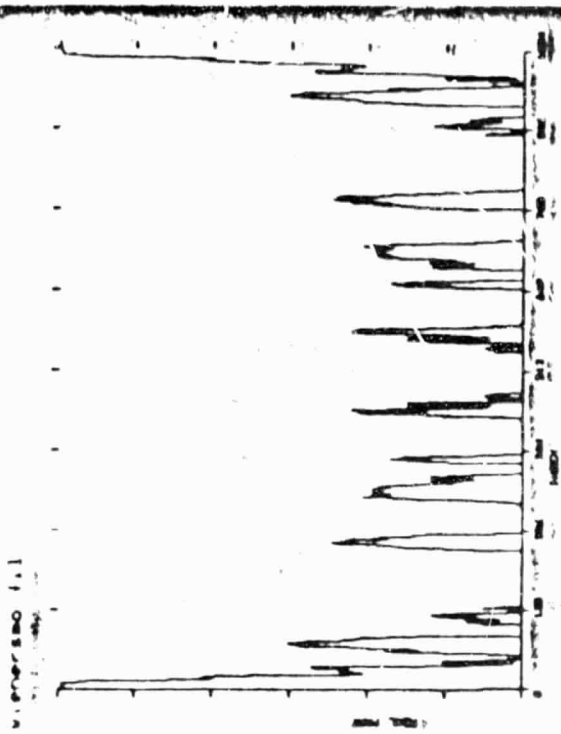


Figure 3g. Wiener filter using smoothed spectrum.



Figure 3f. Smoothed version of $|FFT|^2$.



Figure 3h. Filtered image.

ORIGINAL PAGE IS
OF POOR QUALITY

SPECKLE UTILIZATION



SPECKLE STATISTICS



ORIGINAL PAGE IS
OF POOR QUALITY

CHANGE DETECTION



N83 23081 28

207

ORIGINAL PAGE IS
OF POOR QUALITY

Progress in the Scene-to-Map Registration Task

David D. Dow
National Space Technology Labs

RTOP: SCENE-TO-MAP REGISTRATION COMPARISON FOR LANDSAT MSS AND
THEMATIC MAPPER DATA

PRINCIPAL INVESTIGATOR: DAVID D. DOW

PROJECT DURATION: FY1981 - FY1984

FUNDAMENTAL RESEARCH AREA: MATHEMATICAL PATTERN RECOGNITION-
GEOMETRIC PREPROCESSING

ORIGINAL PAGE IS
OF POOR QUALITY

TECHNIQUE DEVELOPMENT GROUP

SPECIAL STUDIES

SCENE-TO-MAP REGISTRATION

OBJECTIVE: ASSESSMENT OF GEOMETRIC ACCURACY OF SCENE-TO-MAP REGISTRATION
OF LANDSAT MSS AND TM SENSOR PRODUCTS. DEVELOPMENT OF
IMPROVED PROCEDURES FOR THE REGISTRATION AND RECTIFICATION
OF LANDSAT DATA.

TEST LOCATIONS: SOUTHEASTERN LOUISIANA AND EASTERN KANSAS

POTENTIAL APPLICATIONS:

- (1) COMPONENT OF MULTISOURCE DATA BASE
- (2) DEVELOPMENT OF A CHANGE DETECTION PRODUCT
- (3) INPUT TO HABITAT CLASSIFICATION

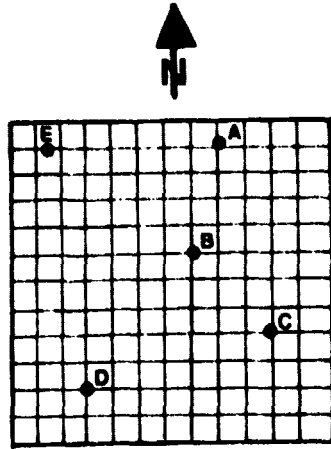
ORIGINAL PAGE IS
OF POOR QUALITY

TECHNICAL QUESTIONS ADDRESSED:

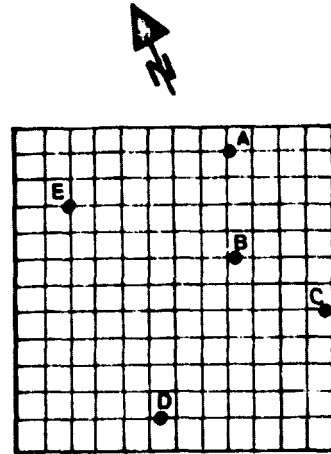
1. GEOMETRIC FIDELITY OF P-FORMAT LANDSAT MSS AND LANDSAT D TM DATA.
2. INFLUENCE OF PRODUCT SCALE ON THE GEOMETRIC ACCURACY OBTAINABLE WITH CURRENT REMAPPING TECHNIQUES AND RESAMPLING FUNCTIONS.
3. ROLE OF GROUND CONTROL POINT SELECTION PROCEDURES ON DIMINISHING SPATIAL DISTORTIONS IN A-FORMAT LANDSAT MSS DATA.
4. GEOMETRIC ERRORS INTRODUCED BY CONVERSION BETWEEN BASE MAP PROJECTIONS (UTM, HOM, AND SOM).

ORIGINAL PAGE IS
OF POOR QUALITY

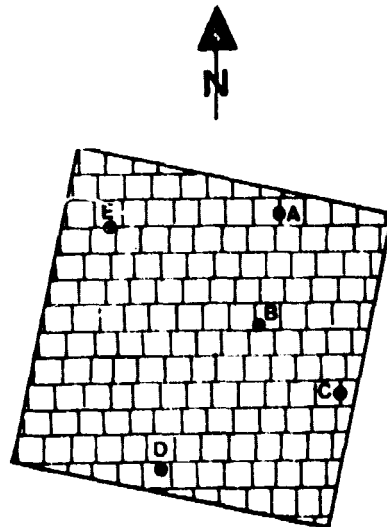
ORIGINAL PAGE IS
OF POOR QUALITY



(A) HYPOTHETICAL GROUND
CONTROL POINTS ON A
UTM GRID

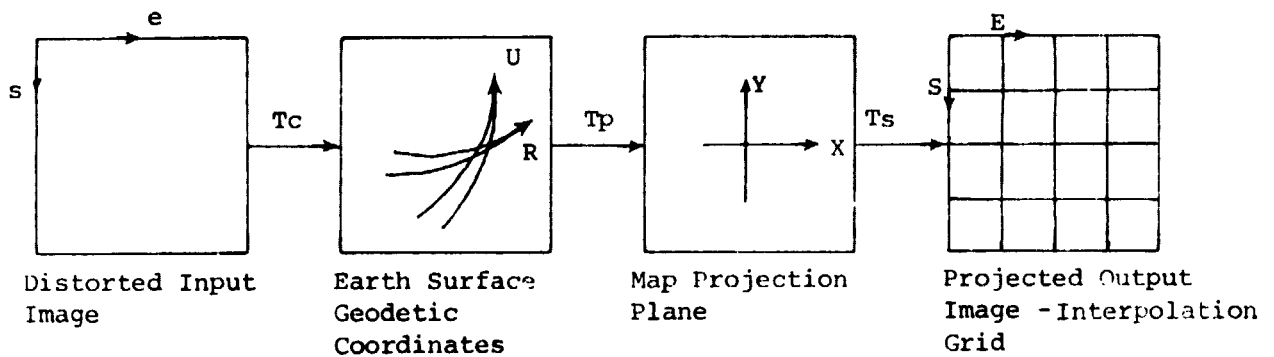


(B) SAME POINTS ON UNCORRECTED
LANDSAT DATA (NOTE THE
DIFFERENT ORIENTATION)



(C) SAME POINTS ON GEO-REFERENCED
LANDSAT DATA (ORIENTATION HAS
BEEN ROTATED)

ORIGINAL PAGE 19
OF POOR QUALITY



Where mapping function relates

$$(E, S) = T_s T_p T_c (e, s) = T(e, s)$$

and T_s , T_p and T_c are vector functions

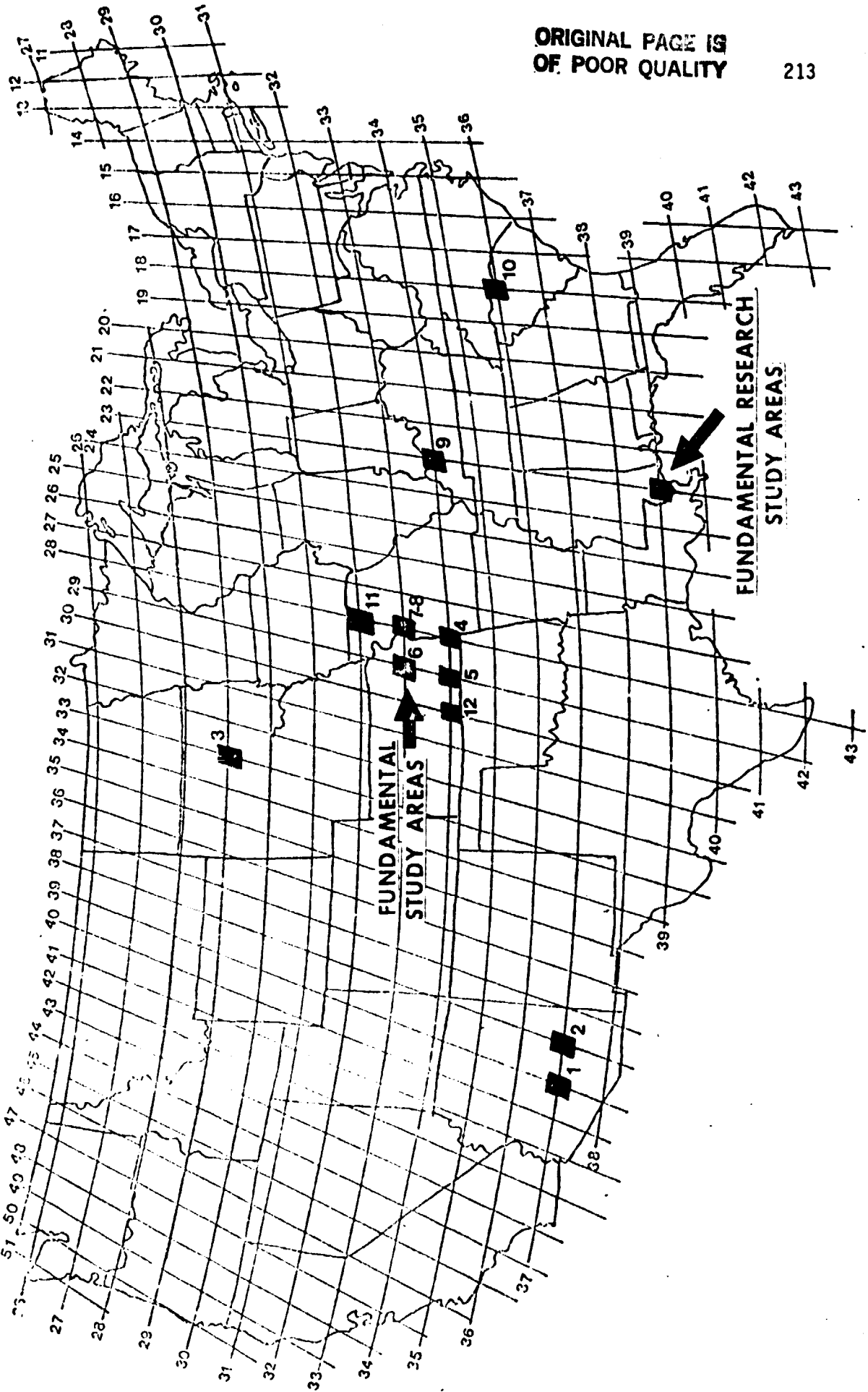


Figure 1. DISTRIBUTION OF 12 LANDSAT SCENES ACCORDING TO PATH AND ROW NUMBERS

SCENE - TO - MAP REGISTRATION

ASSESSMENT OF GEOMETRIC

ACCURACY OF SCENE - TO - MAP

REGISTRATION OF LANDSAT P -

FORMAT MSS DATA

P - FORMAT DATA - CONTAINS RADIOMETRIC AND GEOMETRIC CORRECTIONS

ORIGINAL PAGE IS
OF POOR QUALITY

ORIGINAL PAGE 19
OF POOR QUALITY

$$\text{RBIAS} = \frac{\sum_{i=1}^{\text{NP}} (\text{ROW1}_i - \text{ROW2}_i)}{\text{NP}}$$

$$\text{RSD} = \sqrt{\frac{\sum_{i=1}^{\text{NP}} (\text{ROW1}_i - \text{ROW2}_i - \text{RBIAS})^2}{\text{NP} - 1}}$$

ORIGINAL PAGE IS
OF POOR QUALITY

INDEPENDENTLY CHOSEN CONTROL POINTS (LATITUDE, LONGITUDE, ROW2, COL2) COMPARED WITH
LANDSAT COORDINATES (ROW1, COL1) DETERMINED FROM P-FORMAT REGISTRATION FOR DATA SET 1

	LATITUDE	LONGITUDE	ROW1	ROW2	ROW1-ROW2	COL1	COL2	COL1-COL2	
1	33.68224	-112.3938	543.7	544.5	-0.8	397.4	398.9	-1.5	
2	33.21674	-112.4265	1444.3	1442.3	2.3	508.8	509.5	-0.7	
3	33.43587	-112.3752	1009.7	1010.7	-1.0	514.0	515.5	-1.5	
4	33.07320	-112.0311	1600.7	1600.4	0.3	1196.3	1198.8	-2.5	
5	32.92781	-112.1340	1909.8	1908.9	0.9	1082.5	1083.1	-0.6	
6	32.63733	-112.2030	2486.2	2487.0	-0.8	1074.5	1075.4	-0.9	
7	32.51114	-112.8239	2912.0	2913.5	-1.5	112.6	113.5	-0.9	
8	33.65125	-111.8900	452.7	451.4	1.3	1214.5	1214.4	0.1	
9	33.66678	-111.4733	295.7	296.8	-1.1	1875.0	1875.7	-0.7	
10	33.67168	-111.1606	189.2	190.5	-1.3	2372.8	2372.5	0.3	
11	33.44971	-110.8339	509.5	507.0	2.5	2978.9	2974.8	4.1	
12	33.45116	-111.5628	735.3	735.2	0.1	1811.2	1811.6	-0.4	
13	33.30510	-111.9797	1141.7	1140.9	0.8	1195.6	1195.8	-0.2	
14	33.03835	-111.3611	1461.4	1460.3	1.1	2287.5	2287.2	0.3	
15	32.97791	-110.7789	1392.1	1390.5	1.6	3246.8	3248.5	-1.7	
16	32.96735	-111.7237	1709.4	1708.5	0.9	1729.7	1730.4	-0.7	
17	32.76299	-111.7739	2115.4	2114.4	1.0	1723.1	1723.3	-0.2	
18	32.71953	-111.4468	2097.1	2097.2	-0.1	2267.3	2267.8	-0.5	
19	32.66283	-111.0500	2080.2	2078.0	2.2	2929.2	2930.0	-0.8	
20	32.49704	-111.4986	2538.3	2537.9	0.4	2265.6	2265.8	-0.2	
21	32.46094	-111.8658	2721.0	2720.3	0.7	1683.9	1684.4	-0.5	
22	32.38077	-111.1692	2656.5	2656.2	0.3	2842.2	2842.0	0.2	
23	32.76772	-111.9629	2164.2	2163.4	0.8	1416.1	1416.1	-0.0	
24	32.57899	-111.6722	2435.7	2434.4	1.3	1954.5	1954.4	0.1	
25	32.46857	-112.2679	2828.6	2828.8	-0.2	1029.3	1026.8	2.5	
				RBIAS=	0.5			CBIAS=	-0.3
				RSD=	1.1			CSD=	1.3

DATA SET	LANDSAT MISSION NO	ASSESSMENT NUMBER	DATE GEN BY MDP	RBIAS	RSD	CBIAS	CSD
1	2	5	7/23/79	0.5	1.1	-0.3	1.3
2	2	4	7/29/79	0.9	2.4	0.1	1.1
3	2	2	8/30/79	0.2	1.3	-0.2	1.0
4	3	2	4/23/80	15.8	3.9	0.6	1.7
5	2	1	5/18/80	-414.8	5.3	9.2	0.9
KS	2	0	5/18/80	-407.4	4.2	9.5	1.0
7	2	3	5/12/79	0.7	1.1	1.4	1.0
8	3	2	6/4/79	1.3	1.1	-0.8	1.2
9	3	2	9/15/80	0.3	1.1	-0.8	1.2
10	3	3	2/15/80	-3.6	1.7	3.2	1.6
11	2	2	8/5/79	2.1	1.5	0.2	2.5
12	2	4	5/28/80	10.5	2.3	9.0	1.3
LA/MS	2	3	11/21/81	-219.4	220.8	-95.6	48.8
KS	2	2	11/9/81	251.8	226.7	100.3	40.9

DEVELOPMENT OF IMPROVED

PROCEDURES FOR THE REGISTRATION

OF A-FORMAT LANDSAT

MSS DATA

A-FORMAT DATA - RADIOMETRIC CORRECTIONS ONLY

ORIGINAL PAGE IS
OF POOR QUALITY

LOUISIANA "A" FORMAT DATA GEOREGISTRATION

<u>GROUND CONTROL POINTS</u>	<u>RMS (M)</u>	<u>GROUND REFERENCE POINTS</u>	<u>RBIAS</u>	<u>RSD</u>	<u>CBIAS</u>	<u>CSD</u>
40	173	216	-0.14	0.10	-0.13	0.06
38	66	216	0.29	0.10	0.08	0.05
20	71	236	-0.23	0.11	0.05	0.07
19	58	236	-0.16	0.11	-0.05	0.07
10	55	246	0.25	0.11	0.31	0.06

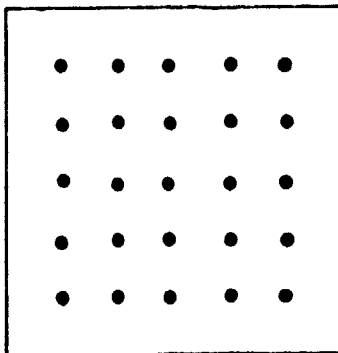
ORIGINAL PAGE IS
OF POOR QUALITY

KANSAS "A" FORMAT DATA GEOREGISTRATION

<u>GROUND CONTROL POINTS</u>	<u>RMS (M)</u>	<u>GROUND REFERENCE POINTS</u>	<u>RBIAS</u>	<u>RSD</u>	<u>CBIAS</u>	<u>CSD</u>
31	54	235	-0.08	0.06	0.01	0.05
16	30	250	0.19	0.05	-0.01	0.05
8	50	258	-0.22	0.05	0.17	0.05

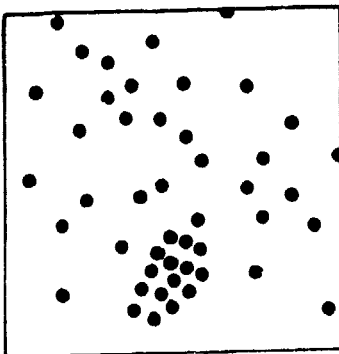
ORIGINAL PAGE IS
OF POOR QUALITY

A. REGULAR DISTRIBUTION OF POINTS

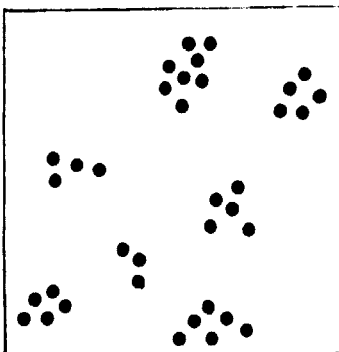


ORIGINAL PAGE IS
OF POOR QUALITY

B. RANDOM DISTRIBUTION OF POINTS



C. CLUSTERED DISTRIBUTION OF POINTS



GEOREF TEST AREA: 20% LANDSAT SCENE

<u>NO.</u> <u>PTS.</u>	<u>DIST.</u> <u>PTS.</u>	<u>BIAS</u>	<u>SCAN</u>	<u>S.D.</u>	<u>BIAS</u>	<u>ELEMENT</u>	<u>S.D.</u>	<u>RMS (M)</u>
8	CLUST.	0.01		0.44	-1.35		1.34	36
8	RAND.	-0.09		0.46	0.06		0.82	44
15	CLUST.	0.20		0.43	-0.67		0.68	44
15	RAND.	-0.07		0.48	0.42		0.63	43
31	ALL	0.01		0.42	0.03		0.67	44

ORIGINAL PAGE IS
OF POOR QUALITY

ORIGINAL PAGE IS
OF POOR QUALITY

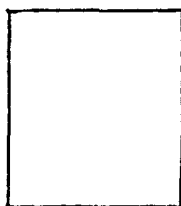
APPENDIX

D9

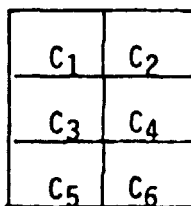
FUNDAMENTAL RESEARCH DATA BASE

At the request of Dr. R. P. Heydorn, a fundamental research data base has been created on a single 9-track 1600 BPI tape containing ground truth, image, and Badhwar profile feature data for 17 North Dakota, South Dakota, and Minnesota agricultural sites. Each site is 5x6 nm in area. Image data has been provided for a minimum of four acquisition dates for each site. All four images have been registered to one another. A list of the order of the files on tape and the dates of acquisition is provided in attachment 1.

Attachment 2 provides information on the format of the ground truth tape and a table for each year to use in interpreting the information on the ground truth tape. Ground truth codes vary depending on the year. Like the Landsat image files, ground truth files cover an image 196 pixels wide by 117 lines long, but the actual size of the ground truth image is 392 pixels by 234 lines. The reason for this difference is that there are six ground truth subpixels for each Landsat pixel, as illustrated.



Landsat Pixel



Ground Truth Pixel

The symbols C_1 , C_2 , C_3 , C_4 , C_5 and C_6 represent the ground truth crop code for the various sub-parts of the Landsat pixel. We typically use a plurality rule to decide on a single label for a Landsat pixel.

All files are stored on tape in universal format. Image files and Badhwar profile feature files contain four channels of data, but since three Badhwar profile features are provided in the feature files (t_p , σ , and G_{max}) the fourth channel is always zero. The format for image and profile files is the same and is provided in attachment 3.

PRECEDING PAGE BLANK NOT FILMED

ORIGINAL PAGE IS
OF POOR QUALITY

File	Type	Segment	Year	State	Positions (Julian Date)						
1-5	Image	1380	78	MN	115	169	196	204	222		
6-10		1394	78	ND	120	174	211	220	238		
11-15		1531	77	MT	112	129	147	184	220		
16-20		1537	78		122	141	159	194	221		
21-27		1544	78	MT	104	122	140	158	176	221	230
28-32		1553	78	MT	122	194	203	211	220		
33-37		1566	78	MN	115	133	169	196	232		
38-43		1619	77	ND	122	140	158	175	176	230	
44-48		1636	78	ND	135	154	190	207	226		
49-53		1650	78	ND	156	191	209	218	236		
54-58		1653	78		136	154	155	191	208		
59-63		1663	77	ND	121	138	156	174	211		
64-68		1676	79	SD	120	165	184	211	237		
69-73		1755	79	SD	120	147	166	184	220		
74-78		1784	78	SD	133	169	196	223	241		
79-83		1825	78	MN	133	196	206	223	224		
84-88		1899	77	ND	122	140	157	175	193		
89-94	Image	1920	78	ND	101	136	199	209	217	236	

File	Type	Segment	File	Type	Segment
95	GT	1380	113	Profile	1380
96		1394	114		1394
97		1531	115		1531
98		1537	116		1537
99		1544	117		1544
100		1553	118		1553
101		1566	119		1566
102		1619	120		1619
103		1636	121		1636
104		1650	122		1650
105		1653	123		1653
106		1663	124		1663
107		1676	125		1676
108		1755	126		1755
109		1784	127		1784
110		1825	128		1825
111		1899	129		1899
112		1920	130		1920

Two end-of-files

ATTACHMENT 2

ORIGINAL PAGE IS
OF POOR QUALITY

3.2.1 HEADER RECORD

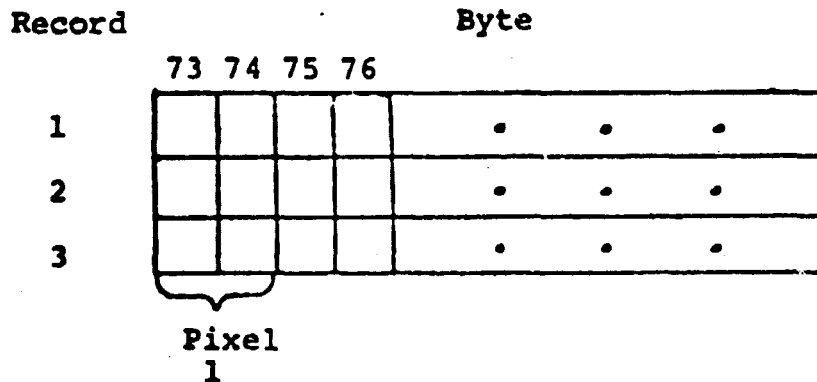
The Header Record is the first record on the tape and contains 3060 bytes (8 bits per byte). The record is zero filled except for those bytes listed in the following table. The values contained in the listed bytes are all constant except for bytes 61 through 63. The attached tape format contains identification and descriptions for each byte. The description and format of the Header Record is contained in attachment 3.

<u>Byte</u>	<u>Value</u>	<u>Byte</u>	<u>Value</u>	<u>Byte</u>	<u>Value</u>
61	Day	96	1	111	120
62	Month	97	-120	1778	1
63	Year	100	2	1786	1
81	-128	101	28	1787	1
89	1	104	1	1788	-120
90	1	106	70		
91	8	109	1		
93	1	110	1		

Each video scan line is 504 bytes long; a 2-byte record counter, a 70-byte ancillary block, and 392 bytes of ground truth (two of the six subpixels for a 196 pixel scan line). It takes three video scan lines to complete one scan line of ground truth. See the following page for diagram.

Each video block will be the same number of bytes in length. If this tape contains raw data the FCM sync words associated with the video data, if any, will be included, with the video data on this tape. If this tape contains processed data, no sync words will be present.

The arrangement of data for each pixel is shown in the following diagram. Data for subpixels 1 and 2 for pixel 1 is found in bytes 73 and 74 of the first data record. Data record 2 and 3 contain data for subpixel 3 through 6 in the same format as record 1.



ORIGINAL PAGE IS
OF POOR QUALITY

APPROVED SYMBOL LIST

C S. W. L. E. N.

1976 8 1977

229

SYMBOL	DESCRIPTION	GREY SCALE LEVEL	HARVESTED	ABANDONED	STRIP FALLOW	STRIP FALLOW ABANDONED	STRIP FALLOW HARVESTED
A	ALFALFA	90	115	140	165	190	215
(B)	BARLEY	101	126	151	176	201	226
BN	BEANS	91	116	141	166	191	216
C	CORN	92	117	142	167	192	217
CN	COTTON	111	136	161	186	211	236
(FX)	FLAX	103	128	153	178	203	228
G	GRASS	105	130	155	180	205	230
H	HAY	106	131	156	181	206	231
I/CC	IDLE COVER CROP	252	-	-	-	-	-
I/CS	IDLE CROPLAND STUBBLE	251	-	-	-	-	-
I/F	IDLE CROPLAND FALLOW	254	-	-	-	-	-
I/RE	IDLE CROPLAND RESIDUE	253	-	-	-	-	-
M	MILLET	112	137	162	187	212	237
MT	MOUNTAINS	241	-	-	-	-	-
NA	NON-AG	242	-	-	-	-	-
(O)	OATS	104	129	154	179	204	229
P	PASTURE	107	132	157	183	207	232
PF	PROBLEM FIELD	80	-	-	-	-	-
(R)	RYE	102	127	152	177	202	227
SB	SUGAR BEETS	98	123	148	173	198	223
SF	SAFFLOWER	93	118	143	168	193	218
SG	SUDAN GRASS	95	120	145	170	195	220
SR	SORGHUM	96	121	146	170	196	221
SU	SUNFLOWER	94	119	144	169	194	219
(SW)	SPRING WHEAT	100	125	150	175	200	225
SY	SOYBEANS	97	122	147	172	197	222
T	TREES	108	133	158	183	208	233
TR	TRÉTRICALE	109	134	159	184	209	234
VN	VOLUNTARY WHEAT	110	135	160	185	210	235
(W)	WINTER WHEAT	99	124	149	174	199	224
*	WATER	240	-	-	-	-	-
X	HOMESTEAD	250	-	-	-	-	-

Changes from 1977-1978 Codes

1-30)

HARVESTED

ABANDONED

STRIP FALLOW

STRIP FALLOW
ABANDONED

STRIP FALLOW
HARVESTED

20	Proble- Fie. (PF)						
90	Alfalfa (A)	115	140	165	190	215	
91	Beans (BN)	116	141	166	191	216	
92	Corn (C)	117	142	167	192	217	ORIGINAL PAGE IS OF POOR QUALITY.
93	Safflower (SF)	118	143	168	193	218	
94	Sunflower (SU)	119	144	169	194	219	
95	Durum Wheat (DW)	120	145	170	195	220	
96	Sorghum (SR)	121	146	171	196	221	
97	Soybeans (SY)	122	147	172	197	222	
98	Sugar Beets (SB)	123	148	173	198	223	
99	Winter Wheat (WW)	124	149	174	199	224	
100	Spring Wheat (SW)	125	150	175	200	225	
101	Spring Barley (BS)	126	151	176	201	226	
102	Rye (R)	127	152	177	202	227	
103	Flax (FX)	128	153	178	203	228	
104	Spring Oats (SO)	129	154	179	204	229	
105	Fall Oats (FO)	130	155	180	205	230	
106	Fall Barley (FB)	131	156	181	206	231	
107	Cotton (CN)	132	157	182	207	232	
108	*Peanuts (PN)	133	158	183	208	233	
109	*	134	159	184	209	234	
110	*	135	160	185	210	235	
111	Grass (G)						
112	(H) (SG) (ML) Hay, Sudan Grass, Millet						*Open - to be assigned as needed
113	Pasture (P)						
114	Trees (T)		136	Pasture * Mix (PH)	188	* C (over) 80	243
			137	WW to * SH Grain	189	*	244
240	Water (*)		138	WW to Annual	211	*	245

Attachment 2 to Ref: 642-7665
1979 Crop Year Keys and Delineation Codes

Crop Type	Crop Key	Crop Harvested	Crop Abandoned	Crop Harvested for Silage
Alfalfa	AH	101	151	201
Buckwheat	BW	102	152	202
Barley	BR	103	153	203
Clover	CL	104	154	204
Corn	CR	105	155	205
Cotton	CT	106	156	206
Dry Bean	DB	107	157	207
Durum Wheat	DW	108	158	208
Flax	FX	109	159	209
Millet	ML	110	160	210
Oats	OA	111	161	211
Peanuts	PE	112	162	212
Potatoes	PO	113	163	213
Rice	RI	114	164	214
Rye	RY	115	165	215
Sugar Beets	SB	116	166	216
Sugar Cane	SC	117	167	217
Safflower	SF	118	168	218
Soybeans	SO	119	169	219
Sorghum	SR	120	170	220
Sunflower	SU	121	171	221
Spring Wheat	SW	122	172	222
Tobacco	TB	123	173	223
Vegetables	VE	124	174	224
Winter Wheat	WW	125	175	225
Small Grains/Strip Fields	--	126	176	226
*		127	177	227
*		128	178	228
Grasses	GS	131		
Other Hay	OH	132		
Orchard/Vineyards	OR	133		
Pasture	PA	134		
Trees	TR	135		
Water > 5 acres	WA	136		
Non-Agriculture	XX	140		
Idle Land/Fallow	IL	231		
Previous Year				
Residue/Stubble	R	232		
Mixed Crop in Field	M	233		
Problem Field		99		
Non-Inventoried Land		255		

*Open--to be assigned as needed (through code 130). Other open codes include 137 through 139, 141 through 150, 161 through 200, 234 through 254.

ATTACHMENT 3

232

UNIVERSAL FORMAT TAPE HEADER RECORD FORMAT (3060 Bytes)

<u>BYTE</u>	<u>CONTENTS</u>	<u>DESCRIPTION</u>	ORIGINAL PAGE IS OF POOR QUALITY
1-32	LACIE V&DPF&...&	Computing system id-EBCDIC	
*33-38	XXXXXX	6-digit unload tape number	
*39-52	PYYDDDI...R&SSTH	RUNID (EBCDIC)	
53-60	ERTS&ISS&...&	Sensor id-EBCDIC	
61-63		Date of this tape generation	
61		Day of month - Binary	
62		Month number - Binary	
63		Year - last 2 digits - Binary	
64	S	Daily tape serial number - Binary	
65-66		ERTS mission number - Binary 1 = ERTS A 2 = ERTS B	
67-68		Site - Binary (sample segment number) Range 1-5000	
69	00000000	Line - Binary	
70	00000000	Run - Binary	
71-72		Orbit number of new data - Binary	
73-80		Time of first scan in this job (for LACIE this is the time of the center scan of the ERTS scene containing the sample segment to the last ten seconds)	
73-74		Tenths of seconds x 1000 - Binary	
75		Seconds - Binary	
76		Minutes - Binary	
77		Hours - Binary	
78		Day of month - Binary	
79		Month number - Binary	
80		Year - last 2 digits - Binary	
81-88		Bands active in this job, 1 bit per band left to right (MSB to LSB). Video data always appears in the order indicated here. 1 = active.	
81	11110000	Bands 1, 2, 3, 4 active	
82-88	0	Bands 5-64 not applicable to LACIE	
89	0	Processing flag - raw data - Binary	
90	4	Number of bands in this job - Binary	

<u>BYTE</u>	<u>CONTENTS</u>	<u>DESCRIPTION</u>
91	8	Number of bits in a picture element - Bin
92-93	1	Address of start of video data gives loca of start of video within scan - Binary
94-95	0	Address of start of first calibration area within the scan - Binary
96-97	196	Number of video elements per scan within a single band - Binary
98-99	0	Number of calibration elements in the first calibration area within the scan in a single band - Binary
100-101	900	Physical record size in bytes - Binary
102	0	Number of bands per physical record of data set starting with the second record of the data set - Binary
103	0	Number of physical records per scan per band - Binary. Zero unless the elements per band is greater than 3K.
104	1	Number of records to make a complete data set - Binary.
105-106	70	Length of ancillary block in bytes - Binary
107	0	Data order indicator - Binary 0 = video ordered by band
108-109	1	Start pixel number number of the first pixel per scan on this tape referenced to the start of the scan - Binary
110-111	196	Stop pixel number number of the last pixel per scan on this tape referenced to the start of the scan - Binary
112-623		Coefficients and exponents-of-ten to linearly translate parameter values from up to 64 bands to engineering units. Two bytes per coefficient or exponent with each pair of bytes expressed in signed binary. (MSB a sign bit: 0=+, 1=-. (Remaining 15 bits straight binary).
112-119	0	A0 coefficients for bands 1-4
120-239	0	Bands 5-64 not applicable to LACIP
240-247	0	E0 exponents of ten for bands 1-4
248-367	0	Bands 5-64 not applicable to LACIE
368-369	1	A1 coefficient for band 1
370-371	1	A1 coefficient for band 2

<u>BYTE</u>	<u>CONTENTS</u>	<u>DESCRIPTION</u>	<u>ORIGINAL PAGE IS OF POOR QUALITY</u>
371-373	1	A1 coefficient for band 3	
374-375	1	A1 coefficient for band 4	
376-495	0	Bands 5-64 not applicable to LACIE	
496-503	0	E1 exponents of ten for bands 1-4	
504-629	0	Bands 5-64 not applicable to LACIE where for each band Y = Engineering Units, C = Parameter Value: $Y = A * 10^{**E} + C * A * 10^{**E}$	
624-687	To be supplied by JSC	Color code information - one byte per band in same order as "channel active on this tape" indicator - Binary. 0 = no color assignment	
688-751	0	Scale factor - one byte per band in same order as "channel active on this tape" indicator - Binary 0 = not active	
752	0	Offset constant - Binary	
753	16	Word size of generating computer. This is the smallest quantity in bits that the computer can write on tape.	
754-1777		Shortest and longest wave-length of each band - EBCDIC. Eight bytes per limit, 16 bytes per band - mili microns	
754-769	0000050000000600	Band 1 - EBCDIC	
770-785	0000060000000700	Band 2 - EBCDIC	
786-801	0000070000000800	Band 3 - EBCDIC	
802-817	00000800000001100	Band 4 - EBCDIC	
818-1777	0	Bands 5-64 not applicable to LACIP - EBCDIC	
1778	1	Number of data sets per physical record - Binary	
1779-1780	0	Address of start of second calibration within a scan - Binary	
1781-1782	0	Number of calibration elements in the second calibration area within the scan in a single band - Binary	
1783	0	Calibration source indicator - Binary	
1784	0	Fill zero.	
1785-1786	4	Number of bands in the first record of the data set - Binary	
1787-1788	196	Total number of elements per scan per band - Binary	

<u>BYTE</u>	<u>CONTENTS</u>	<u>DESCRIPTION</u>	ORIGINAL PAGE IS OF POOR QUALITY
1789-1790	1	Pixel skip factor - the quantity to be added to the number of the last pixel processed yield the number of the next pixel to be processed - Binary 1 = Process every pixel	235
1791-1791	1	Scan skip factor - the quantity to be added to the number of the last scan processed yield the number of the next scan to be processed - Binary. 1 = Process every scan	
1793-2940		General information. Information in EBCDIC generated to satisfy user requirements. Contents will be unique for each user and depend not only on the sensor, but also on specifications of the user for whom the tape is generated. Bytes for which user specific requirements will contain fill zeros.	
1793-2086		Fill zeros	
2087-2184		General annotation byte assignment for ERTS LACIE	
2087-2094	+X.XXXXX	Peak sharpness - EBCDIC	
2095-2102	+X.XXXXX	Normalized peak to background ratio - EBCDIC	
2103		Manual registration flag 0 = Automatic 1 = Manually assisted	
2104		Zero fill flag - Binary 0 = The sample segment contains no zero fill data 1 = Part of the sample segment contains zero fill data	
2105-2106		Orbit number of reference data set - Binary (not used = 0)	
2107-2109		Zero fill	
2110		Cloud cover - Binary - percent of 10X11 KM search area covered by clouds	
2111		Zero fill	
2112-2120		ERTS scene/frame id number for reference data set - EBCDIC - ADDDNHNS (see bytes 2123-2131 for content)	
2121		Zero fill	
2122		Flag indicating whether a reference scene has been used for registration - Binary 0 = hasn't been used 1 = has been used	
2123-2131		ERTS scene-frame id number for new data-EBCDIC-ADDDNHNS	

BYTECONTENTSDESCRIPTION

2123

A = ERTS mission number

2124-2126

DDD = Day number relative to launch at time of observation

2127-2128

HH = hour at time of observation

2123-2130

MM = minute at time of observation

2131

S = tens of seconds at time of observation

2132

Zero fill

2133

Data quality classification

0 = acceptable

1 = marginal

2134-2145

Center of sample segment - EBCDIC right justified and padded with zeros

2134-2139

Latitude

2134

"N" = North "S" = South

2135-2137

Degrees - integral

2138-2139

Minutes - integral

2140-2145

Longitude

2140

"E" = East; "W" = West

2141-2143

Degrees - integral

2144-2145

Minutes - integral

2146-2149

Band sync status - Binary - the number of lines for which sync could not be maintained during pre-processing by band

2146

Band 1

2147

Band 2

2148

Band 3

2149

Band 4

2150-2156

Zero fill

2157-2170

Sun angle - EBCDIC

2157-2162

SUN EL

"SUN EL" - EBCDIC

2163-2164

Sun elevation - integral degrees EBCDIC

2165-2167

AZ

"AZ" - EBCDIC

2168-2170

Sun azimuth - integral degrees - EBCDIC

2171-2178

Time and date of last update to controlling information - EBCDIC - YDDDMH221

2179-2184

Zero fill

ORIGINAL PAGE IS
OF POOR QUALITY

<u>BYTE</u>	<u>CONTENTS</u>	<u>DESCRIPTION</u>
*		Sun angles are 2 byte binary
*2201-2202		Sun angle for RSEG channels 1-4
*2203-2204		Sun angle for RSEG channels 5-8
*2205-2206		Sun angle for RSEG channels 9-12
*2207-2208		Sun angle for RSEG channels 13-16
*2249	YDDD	1st acquisition date (characters)
*2254	X	Average soil greenness for 1st acquisition (binary number)
*2257	YDDD	2nd acquisition date or blanks
*2262	X	Average soil greenness for 2nd acquisition
*2265	YDDD	3rd acquisition date or blanks
*2270	X	Average soil greenness for 3rd acquisition
*2273	YDDD	4th acquisition date or blanks
*2278	X	Average soil greenness for 4th acquisition
2551-2642	0	General annotation byte assignments for the cyber at JSC
2643-2940		General annotation byte assignments for the production film converter
2643-2658		Bias factors and scaling factors - signed Binary. Four bytes per channel, where first two bytes = bias factor; second two bytes = scaling factor. Each factor has an implied decimal point to the left of the least significant decimal digit. If MSB = 1 the factor is negative; if the MSB = 0 the factor is positive.
*2643-2646		Channel 1
*2643-2644		Bias factor
*2645-2646		Scaling factor
*2647-2650		Channel 2
*2647-2648		Bias factor
*2649-2650		Scaling factor
*2651-2654		Channel 3
*2651-2652		Bias factor
*2653-2654		Scaling factor
*2655-2658		Channel 4
*2655-2656		Bias factor
*2657-2658		Scaling factor

<u>BYTE</u>	<u>CONTENTS</u>	<u>DESCRIPTION</u>
*2659-2606		Bias factor and scaling factors for channels 5-16 in the same format as above.
2758		
2759	1	N thousand scan lines per frame - Binary
*2760-2783		User ID
*2784-2789		Blanks
2790-2792	0	Altitude in meters - Binary
2793-2794	0	Ground speed in MET/SEC - Binary
2795	1	Scan Type - Binary 00000000 = Raw data 00000001 = Smoothed data
2796	0	Angle of ABC in degrees - Binary
2797	1	Camera - Binary 00000000 = 70 MM 00000001 = 5 inch
2798	0	Input device - Binary 00000000 = 9-track 00000001 = high density tape
2799	2	Truncation 0 = 2 low order bits 1 = 2 high order bits 2 = no truncations
2800-2807		Channels requested. 1 bit per channel - Binary
2800-2801	11110000 00000000 (1 acq) 11111111 00000000 (2 acq) 11111111 11110000 (3 acq) 11111111 11111111 (4 acq)	Channels 1, 2, 3, 4 requested
2802-2807	0	Channels 16-64 not applicable for Unload
2808	0	Processing mode - Binary 00000000 = serially 00000001 = concurrently
2809-2824	0	Density for eight saturated colors - two bytes per saturated color - Binary where first byte = low intensity level of the range; second byte = high the range of the intensity level is 0 to 255
2809-2810		Red density range
2811-2812		Blue density range
2813-2814		Green density range
2815-2816		Magenta density range
2817-2818		Cyan density range
2819-2820		Yellow density range

<u>BYTE</u>	<u>CONTENTS</u>	<u>DESCRIPTION</u>
2821-2822		White density range
2823-2824		Black density range
2825	To be supplied by JSC	Film processing flag 0 = Process this file 1 = Skip this file
2826-2873	0	Fill zero
2874	0	Color select* - Binary 0 = No color 1 = Assigned color 2 = False color 3 = Saturated color
2875	0	Image format* - Binary 0 = Single image 1 = Enhanced images 2 = Abut images 3 = Offset images
2876	6	Repeat of pixels per scan - Binary 0 = None 1 = 1 repeat 2 = 2 repeats n = n repeats
2877	8	Repeat of scan - Binary 0 = none 1 = 1 repeat 2 = 2 repeats n = n repeats
2878-2881		Partial scan - Binary
2878-2879	0	Start pixel number
2880-2881	0	Stop pixel number (If bytes 2787-2881 contain all zeros, full scan is expected - not partial)
2882-2883	0	Sensor scan rate in scans/second - Binary
2884	0	Pixel size - Binary
2885-2886	0	Angle of drift - Binary
2885		+ integer degrees
2886		Fraction
2887-2940	0	Fill zeros
2941-3000	LACIE&NDFF6...8	Title - user designated identification
3001-3060	0	Fill zeros, makes the record an integral number of computer words. These bytes must <u>never</u> contain data.

3.2.2 DATA SETS

The data follows the Header Record and is arranged in data sets. A data set is defined as the ancillary data and all of the video data for one scan line for all active channels. Data sets are recorded in variable length physical records containing a maximum of 3000 bytes of information per record. Since 3000 bytes is not compatible with the word length of all computers, the record includes a sufficient number of fill zero to make the record divisible by 32, 36, 48, and 60 bits. However, the maximum length of the record may not exceed 3060 bytes. If two or more records are needed for the data set, the data set will be divided. Under no condition will the data for a video channel begin in one record and continue into another record.

The first two bytes of each record will contain the number of the physical record within the video data set. This is for use in data sets that contain more than 3000 bytes and therefore require more than one physical record for recording. The ancillary block is the first block of a data set and follows the record counter. The length of the ancillary block is variable, with the number of bytes given in the header record.

Bytes 73 through N will be dependent on whether this job contains raw processed data (Byte 89 of the header record). The value of N will be given in bytes 105 and 106 of the header record and will always be greater than or equal to 70.

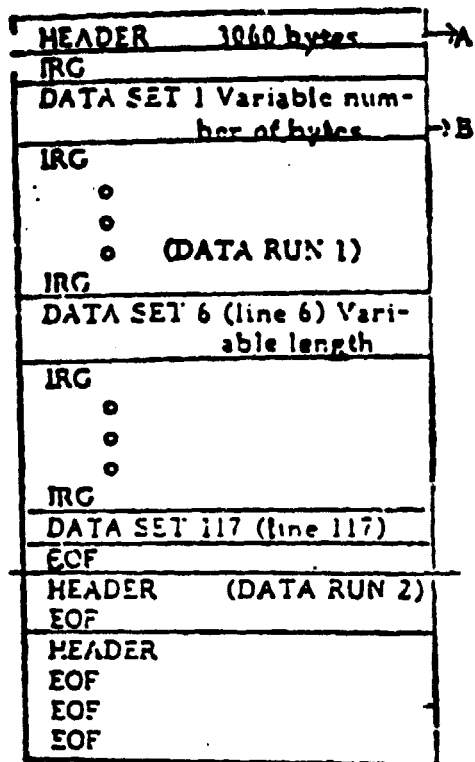
If this job contains raw data bytes 73 through N will contain the housekeeping data channel from the sensor, if one is available.

Following the ancillary data in each data set will be the video data for the one channel for one scan. The video data for the channel for one scan will comprise a video block.

UNIVERSAL FORMAT TAPE ANCILLARY BLOCK FORMAT

<u>BYTE</u>	<u>CONTENTS</u>	<u>DESCRIPTION</u>
1-68	0	Zero fill
69-70		Relative scan line number

ORIGINAL PAGE IS
OF POOR QUALITY



Note: The number of bytes for each data set will be the same in each data run.

ONE SAMPLE SEGMENT

A and B are retrieved from the image data base.

A = LSIMAGHD, master header
B = LSIMVHDR, LSIMCHAN, LSIMLAHD, Imagery data

(B₁)

RECORD COUNTER	2 bytes
ANCILLARY BLOCK	70 bytes
LINE 1, BAND 1	195 bytes
BAND 2	196 bytes
BAND 3	196 bytes
BAND 4	196 bytes
ZERO FILL	44 bytes

DATA SET FOR 1 ACQUISITION,
4 CHANNELS

900 BYTES/RECORD

Figure 3-15. ITC Unload Tape (sheet 1 of 2)

(B₃)

RECORD COUNTER	2 bytes
ANCILLARY BLOCK	70 bytes
LINE 1, BAND 1	196 bytes
BAND 2	196 bytes
BAND 3	196 bytes
BAND 4	196 bytes
BAND 5	196 bytes
BAND 6	196 bytes
BAND 7	196 bytes
BAND 8	196 bytes
BAND 9	196 bytes
BAND 10	196 bytes
BAND 11	196 bytes
BAND 12	196 bytes
ZERO FILL	96 bytes

DATA SET FOR THREE ACQUISITION,
12 CHANNELS

2520 BYTES/RECORD

Note: For a 16-channel data set, two (B₂) data sets will be required therefore requiring two physical records.

Figure 3-15. PFC Unload Tape (Sheet 2)